The Dissertation Committee for Katie Ann Clark Certifies that this is the approved version of the following dissertation:

Optoelectronic properties and energy transport processes in cylindrical J-aggregates

Committee:

David A. Vanden Bout, Supervisor

Andrew K. Dunn

Graeme Henkelman

John F. Stanton

Katherine A. Willets

Optoelectronic properties and energy transport processes in cylindrical J-aggregates

by

Katie Ann Clark, B.S.

Dissertation

Presented to the Faculty of the Graduate School of

The University of Texas at Austin

in Partial Fulfillment

of the Requirements

for the Degree of

Doctor of Philosophy

The University of Texas at Austin

August 2014

Dedication

To my parents, for their unwavering support.

To my sisters, Heather and Emily, and brother, Shane.

To my friends.

You all mean the world to me.

Acknowledgements

There are so many people that made this effort possible. Above all, I must thank my advisor, Professor David Vanden Bout, for his guidance, encouragement and expertise. There really are not enough superlatives.

The Vanden Bout group went through a lot of changes during my tenure; the group was 3 people at its smallest and 13 at its largest. I primarily worked with two fellow members of "Team DVB." Dr. Craig Cone and I toiled dutifully to collect polarization-resolved spectra and images of C8S3 J-aggregates. He was my group mentor and remains a dear friend. Leigh Krueger and I collaborated to determine the low-temperature photophysical properties and quantify energy transport in the aggregates. We never published together, but Dr. Micah Glaz was my partner in crime and sounding board. I would like to thank the other members of Team DVB, who provided helpful discussions and presented motivating group meetings over the years: Dr. David Ostrowski, Dr. Taki Adachi, Dr. Johanna Brazard, Dr. Dörthe Eisele, Dr. Matt Traub, Dr. Erin (Katie) Walker, Dr. Zhongjian Hu, Katherine Koen, Beiyue Shao, Marlene Gutierrez, Shauna Ingle, Jonathan Travis, and Andrew Martinez. The quick collaboration with John Brantley (Bielawski group) was fruitful and fun, and I want to thank Dr. Ryan Cheng for lending helpful input (and Adobe Illustrator skills) over the years.

Some of my best graduate school experiences have come in the form of teaching. I would be remiss if I did not acknowledge Dr. David Vanden Bout and Dr. Cynthia LaBrake's lasting impact- they taught me to teach, which is an amazing gift. I would also like to thank a few others I have had the pleasure to work with: Dr. Paul McCord, Dr. John Stanton, and Dr. Robb Wilson. In addition, a shout out to Gregory Browning and

Jordan Johnson for keeping the wheels on the department and making life as a TA so much easier.

My family has served as my ultimate inspiration and motivation. Their support has been instrumental and means so much to me. Finally, I would like to thank my Austin family for all of the dinners, gatherings and adult sodas that we shared throughout the process: Dr. Taki Adachi, Dr. Amy Bonaparte, Dr. Ryan Cheng, Dr. Craig Cone and Courtney Russo, Michelle Fox, Dr. Micah Glaz, Leigh Krueger, Dr. Sai Sriharsha Manoj Konda, Dr. Stephanie Taylor, Rye Terrell, Dr. Zachary Pozun, and Dr. Ting Yan.

Optoelectronic properties and energy transport processes in cylindrical J-aggregates

Katie Ann Clark, Ph.D.

The University of Texas at Austin, 2014

Supervisor: David A. Vanden Bout

The light harvesting systems of photosynthetic organisms harness solar energy by efficient light capture and subsequent transport of the light's energy to a chemical reaction center. Man-made optical devices could benefit by mimicking these naturally occurring light harvesting processes. Supramolecular organic nanostructures, composed of the amphiphilic carbocyanine dye 3,3'-bis- (2-sulfopropyl)-5,5',6,6'-tetrachloro-1,1'-dioctylbenzimida-carbocyanine (C8S3), self assemble in aqueous solution to form tubular, double-walled J-aggregates. These J-aggregates have drawn comparisons to light harvesting systems, owing to their optical and structural similarities to the cylindrical chlorosomes (antenna) from green sulfur bacteria. This research utilizes optical spectroscopy and microscopy to study the supramolecular origins of the exciton transitions and fundamental nature of exciton energy transport in C8S3 artificial light harvesting systems. Two J-aggregate morphologies are investigated: well-separated, double-walled nanotubes and bundles of agglomerated nanotubes.

Linear dichroism spectroscopy of flow-aligned nanotubes is used to generate the first quantitative, polarized model for the complicated C8S3 nanotube excitonic absorption spectrum that is consistent with theoretical predictions. The C8S3 J-aggregate photophysical properties are further explored, as the Stokes shift, quantum yield, and spectral line broadening are measured as a function of temperature from 77 – 298 K. The

temperature-dependent emission ratios of the C8S3 J-aggregate two-band fluorescence spectra reveal that nanotube emission is well described with Boltzmann partitioning between states, while the bundles' is not. Finally, understanding energy transport in these materials is critical for the proposed use of artificial light harvesting systems in optoelectronic devices. The spatial extent of energy transfer in individual C8S3 J-aggregate structures is directly determined using fluorescence imaging. We find that aggregate structural hierarchy greatly influences exciton transport distances: impressive average exciton migration distances of ~ 150 nm are measured along the nanotubes, while these distances increase to over 500 nm in the bundle superstructures.

Table of Contents

List of Tables

List of Figures

Chapter 1: Introduction

1.1 LIGHT HARVESTING SYSTEMS

For centuries, humans have looked to nature for inspiration to solve complex problems, and the diverse field of biomimetics demonstrates the value of this approach.[1-9] Since countless natural phenomena occur on the nanoscale, the intersection of biomimicry and nanotechnology is of particular interest.[10] Photosynthesis, the essential biological process by which light energy is captured and converted to chemical energy, has inspired scientists and engineers to develop materials, devices and technology to capture solar energy for human consumption.[2-3, 11-14] Energy transport (ET) in organic systems is of interest for a variety of applications including light harvesting (LH) for solar energy conversion. One strategy for utilizing organic materials to capture sunlight is to mimic the LH antennae of naturally occurring photosynthetic systems. Green sulfur bacteria (GSB) are well-studied phototrophs that live in low sunlight environments and photosynthesize very efficiently.[15-16] The first step in bacterial photosynthesis is the absorption of sunlight by LH antennae. Directly following light absorption is the rapid (<100 ps) transport of the excitation to a reaction center, where charge separation occurs.[2, 15, 17]

1.2 MOLECULAR AGGREGATES : EXCITONIC SYSTEMS

Chlorosomes, the LH antennae of photosynthetic GSB, are comprised of closely-packed cylindrical molecular aggregates that are ~10 nm in diameter and up to one micron in length.[18-19] These rod-like aggregates are primarily composed of organized bacteriochlorphyll (Bchl) chromophores, which are optimally arranged for efficient light capture and energy transport.[20-21] The cylindrical structure of GSB LH antenna is distinct: molecular aggregation is due solely to Bchl intermolecular interactions. The

chlorosomes' structure is not further supported by integrated proteins, which is the prevalent assembly for other bacteria and higher-order photosynthetic antennae.[17, 20-21] The delocalized nature of the chlorosome's excited states has important consequences for optical and transport properties, which are echoed in the molecular aggregates that form artificial light harvesting systems.

In the 1930s, Jelley and Scheibe independently observed an interesting result of pseudo isocyanine (PIC) dye solutions: at high concentrations, the broad absorption band became very sharp and shifted from 525 nm to 570 nm.[22-25] This new, narrow band, called a J-band, is observed for several dyes above critical concentrations, and the spectral change is ascribed to dye aggregation and excitonic dye coupling.[22-24, 26-29] The spontaneous dye organization is non-covalent and is driven by van der Waal's forces, electrostatic forces, and in some cases, hydrogen bonding. Today, molecular dye aggregates that exhibit characteristically high molar absorptivity, narrowed and red-shifted absorption, and near-resonant fluorescence emission are termed J-aggregates (or Scheibe aggregates), after the co-discoverers. [30-31] The remarkable spectral properties of molecular J-aggregates are attributed to strong dipole-dipole coupling of individual chromophores, which leads to delocalized excitations (excitons) across many dyes. The optical properties of tightly-bound excitons observed in J-aggregates are well-described with the Frenkel exciton model, depicted in Figure 1.1.[29, 32-33] Synthetic advances by Daehne and co-workers has led to morphological control of water soluble J-aggregates via the adjustment of the polarity and identity of substituent groups of the 5,5′6,6′-tetrachlorobenzimidacarbocyanine dye.[34-35] A diverse set of aggregate morphologies, which includes linear chains, rings, cylinders, and ribbons can form based on multiple factors, such as chromophore side chains, solvent choice, and dye concentration. [35-42] While cyanine dye J-aggregates have found extensive technical application as

photographic spectral sensitizers,[43-44] they have recently garnered significant interest as artificial LH systems owing to the discovery of molecular aggregates in photosynthetic bacteria.[15, 45-47]

The amphiphilic carbocyanine dye 3,3'-bis- (2-sulfopropyl)-5,5',6,6'-tetrachloro-1,1'-dioctylbenzimida-carbocyanine (C8S3) self-assembles in aqueous solution to form tubular, double-walled J-aggregates where alkyl chains form the interior and polar sulfate groups comprise the exterior of a bilayer structure. The nanotubes exhibit diameters of ~ 10 nm and lengths ranging from hundreds nanometers to microns. Over many months, the nanotubes agglomerate spontaneously into massive super-structures, termed bundles, with diameters over 500 nm; the aggregate size and geometry were revealed using cryo-TEM.[48-50] A schematic of C8S3 monomer, nanotube, and bundles is given in Figure 1.2.

Cylindrical C8S3 J-aggregates have garnered significant interest as artificial LH systems due to their optical and morphological resemblance to GSB chlorosomes.[37, 51] Monomer dyes in both the Bchl rods of GSB chlorosomes *and* cyanine dye aggregates are highly ordered. Monomer coupling, driven by molecular organization into closely-packed, ordered structures, is a prerequisite for long-range exciton transport in molecular aggregates; as such, determining the bulk and individual photophysical properties of C8S3 J-aggregates is vital.

1.3 CYLINDRICAL J-AGGREGATES: OPTOELECTRONIC PROPERTIES

Self-assembled molecular aggregates exhibit properties arising from electronic states that are delocalized across closely-packed molecules. The structural arrangement of dye molecules determines the type and optical characteristics of the resulting aggregate. When monomer dipoles align in a head-to-tail *(parallel)* geometry, J- *(H-)* aggregates that exhibit red *(blue)* shifted spectra with respect to the monomer are formed. Small

(large) slip angles, defined as the angle between polarization axes and the line of molecule centers, give rise to J- *(H-)* aggregates;[31, 52] these structural arrangements are illustrated in Figure 1.3. Both J- and H-aggregates exhibit extraordinary photophysical properties that differ radically from the individual monomers that comprise them, which can be explained with the Frenkel exciton model.[53-54] The model calculates the energy and transitions that arise from an effective 1-D Hamiltonian. For linear J-aggregates, like the one depicted in Figure 1.1, the transition dipoles of the individual molecules are parallel, and only one exciton state contains effectively all the oscillator strength; thus, a single optical transition is observed.[55]

Knoester and co-workers have developed the prevailing model for tubular C8S3 J-aggregate absorption, which calculates the number, energy, and relative strength of transitions arising from concentric helical cylinders that are treated independently.[56-57] Molecular arrangement is found by wrapping a planar bricklayer structure upon itself, wherein each brick (unit cell) contains one dye molecule that is modeled as a point dipole. Each cylinder shows three transitions: one polarized parallel and, due to cylindrical symmetry, two degenerate transitions polarized perpendicular to the long axis of the tube.[56] Overall, the model for a double-walled cylinder predicts four optical transitions, which is fewer than experimentally observed, but it does well to explain much of what is detected for C8S3 nanotubes. The homogenous model was improved by the of inclusion energetic disorder of monomer excitation energies[57-58] (ε_n in Figure 1.1), which better reproduces dichroism spectra[55, 57] and the asymmetric J-band shape.[59-60] Despite adjustments, the bricklayer exciton model fails to account for experimentally observed high-energy transitions.

C8S3 nanotubes consist of two cylindrical structures: the inner and outer wall. The degree of inner and outer cylinder coupling has been subject to debate, with previous

research indicating both weak[61-63] and very strong[64-68] cylinder interaction. Only recently was the extent of coupling definitively revealed. Eisele et al. demonstrated two techniques to isolate the inner wall spectrum by eliminating outer wall spectral absorption: chemical oxidation and sample dilution.[69] The former is irreversible, while the latter isolation method only decouples the overlapping inner and outer-wall exciton transitions temporarily. Once the outer wall transitions were eliminated, the inner-wall spectrum, which shows four transitions, was compared to the double-walled spectrum. The energies and shape of the remaining four transitions did not change with respect to the unperturbed J-aggregate; therefore, the two cylinders should be treated as weakly coupled, essentially separate aggregate systems. A new structural model, the extended herringbone (EHB),[69] was developed to account for the decoupled experimental spectra, wherein each unit cell contains two non-planar monomer dyes. This results in four (rather than two when there is one molecule per unit cell) optical transitions for each cylinder.

Despite extensive theoretical modeling, open questions regarding the polarization of the exciton transitions remain. While the models predict pure polarization, near-field imaging of nanotubes suggests the polarizations might be mixed.[62] Furthermore, theoretical investigations of aggregate disorder also indicate the possibility of mixed-polarization exciton states.[70] Chapter 2 describes our effort to assign the polarizations of the C8S3 nanotube excitonic absorption transitions, which is critical in establishing the accuracy of the theoretical model. We exploited the simple, yet elegant, chemical oxidation method, combined with reduced linear dichroism (LD^r) spectroscopy, to determine the polarizations and energies of the C8S3 nanotube exciton absorption transitions. Chemical oxidation was utilized to "turn off" outer wall optical absorption and produce stable nanotube samples with a simplified absorption profile associated only with the nanotube inner wall. The oxidized aggregates were aligned in a flow cell to

collect LD^r spectra, which reveal a series of both polarized and isotropic transitions. Four spectral transitions, assigned to be purely parallel or perpendicular to the aggregate long axis, that fit both the experimental LD^r and isotropic spectra were used create a model for oxidized J-aggregate excitonic absorption. The inner wall spectral fit was used as a basis for the more complicated double-walled spectrum. The LD^r spectral study was repeated using pristine, un-oxidized nanotubes, and the spectrum for the full double-walled nanotubes could be fit using six total transitions: four from the oxidized (inner-wall) fit and two additional transitions distinct to the outer wall. A quantitative model that agrees with experimental absorption and emission spectral results and aligns with current theory was constructed wherein the energies and polarizations of excitonic transitions remained consistent for both the unperturbed and chemically oxidized C8S3 J-aggregates. In addition, the polarization studies reveal, in contrast to the strongly polarized transitions that comprise the low-energy region of the excitonic nanotube spectrum, that the high-energy absorption is isotropic and due to highly localized exciton transitions that arise due to disorder. This work represents the first polarized, quantitative model for C8S3 double-walled nanotubes that is consistent with theoretical predictions and experimental results.

After months of aging, the nanotube absorption spectrum changes. It is accepted that even slight changes to J-aggregate morphology can alter their interaction with light.[49, 57] The spectral transformation is caused by the agglomeration of nanotubes into bundles. The presence of bundles, whose diameters can reach well over 500 nm, was first observed via cryo-TEM.[49] In Chapter 3, we investigate the temperature dependence of C8S3 nanotubes and bundles bulk spectral behavior. Previous experiments have examined the role of temperature in the exciton dynamics of J-aggregates and revealed that critical features, including exciton migration distance[71-73], fluorescence lifetime[74-76]

and Stokes shift,[72-73, 77] rely on the available thermal energy. Absorption and emission spectral line broadening and Stokes shift are evaluated in the temperature range from 77–298 K. We found that the relative quantum yield of the nanotubes increased dramatically upon cooling, while the bundles quantum yield exhibited a comparatively muted response over the same temperature range. While aggregate absorption does not change with temperature, which indicates structural stability, the emission spectra vary dramatically. Both J-aggregates exhibit two fluorescence bands, and the high-energy emission decreases systematically as the sample temperature is lowered. The temperature dependence of their emission ratios is determined and, across the measured temperature range, nanotube emission is well described with Boltzmann statistics, while the bundles' is not.

1.4 CYLINDRICAL J-AGGREGATES: EXCITON TRANSPORT

Based on their strong dipole-dipole interactions and delocalized excitons, cylindrical J-aggregates offer the possibility of directed energy transfer (ET) along the aggregate long axis and are treated as artificial light harvesting systems.[37, 78] As such, there is much interest in quantifying the extent of ET in J-aggregates. The mechanism of exciton transport in molecular J-aggregates, which can be wave packet-like coherent motion, incoherent hopping, or even an intermediate combination, is unclear.[79-80]Coherent exciton motion, observed in systems where disorder is low (such as molecular crystals), is modeled as wave packets that propagate with an average velocity.[81] Coherent exciton motion suggests greater transport distances than if excitons scattered more frequently, which is incoherent motion that is described with a diffusive, Förster model. Currently, there is no final answer to the question on physical nature of the ultrafast exciton migration of highly delocalized excitons observed in J-aggregates.

Multiple experimental studies have been conducted to measure the extent of exciton migration within J-aggregates of varying morphologies. While transport can be measured with a number of ensemble methods, these tend to measure lower limits, as they probe multiple environments and configurations in bulk systems. In addition, these difficult experiments are plagued with inconsistent results due to their indirect nature. Exciton mobility has been measured for J-aggregates using exciton-exciton annihilation (EEA), where two excitons collide, one is annihilated, and the other is further excited to a higher energy state. The time it takes for this process to occur and the fluorescence to quench allows for the estimation of exciton diffusion distances. Low temperature EEA studies of PIC J-aggregates provide wide-ranging estimates of exciton delocalization from 20-50000 molecules.[80] In addition, EEA experiments estimate an unreasonably large exciton diffusion distance of 30 μm in cylindrical J-aggregates. The depolarization of aggregate fluorescence at 5K (compared to highly polarized emission at room temperature) suggests rapid energy transfer between aggregates of differing orientations,[82] and quenching studies propose long-range exciton migration distances up to hundreds of nanometers in cylindrical cyanine J-aggregates.[37] Recently, theoretical exciton diffusion lengths of 200 nm[83] have been calculated for cyanine J-aggregate thin films; however, experimental diffusion lengths of 50 nm are reported for these films.[84]

Given the inconsistency of indirect ET quantification results, a direct measure of energy migration is favored. Exciton migration distances in perylene bis-(phenethylimide) thin films and crystals have been determined by comparing far-field collected emission to near-field laser excitation spots.[85] While near-field excitation offers very small excitation regions, it is more practical to utilize far-field excitation and collection, which is the approach used recently to measure energy transport in $MoSe_2$ crystals,[86] organic quantum wires,[87] and Rhodobacter sphaeroides LH2 antenna

complexes.[88] Two-dimensional (2-D) LH2 crystals and patterned linear nano-arrays of the bacterial LH2 complexes exhibit fluorescence emission profiles larger than the excitation spot, indicating energy is moving away from the excitation point. Emission from the large 2-D crystals is isotropic, while fluorescence from the quasi-1D array aligns with the pattern's geometry. Energy propagation distances, measured to be > 1 μm, are far beyond what is necessary for photosynthesis.

In Chapter 4, we take advantage of single-particle spectroscopy techniques to quantify exciton transport lengths in C8S3 J-aggregate nanotubes and bundles by spatially resolving the emission from individual nanostructures after localized excitation. Nanotubes and bundles were deposited on solid substrates at concentrations that allowed for imaging individual aggregates. Fluorescence confocal images of the aggregates were collected, and regions of interest within the sample were identified. These regions were excited with a focused laser spot, and the resulting fluorescence emission was imaged onto an electron multiplying charged coupled device camera. A 2-D Gaussian fitting scheme was used to quantitatively compare the laser excitation beam profile to the broadened aggregate emission profiles. The double-walled tubes exhibit average 1-D energy transport lengths of 140 nm, while energy migration in the bundled nanotubes was found to be both two-dimensional and remarkably long, with distances spanning many hundreds of nanometers. Due to this disparity between the nanotubes and bundles, the role that structural hierarchy plays in exciton transport is explored.

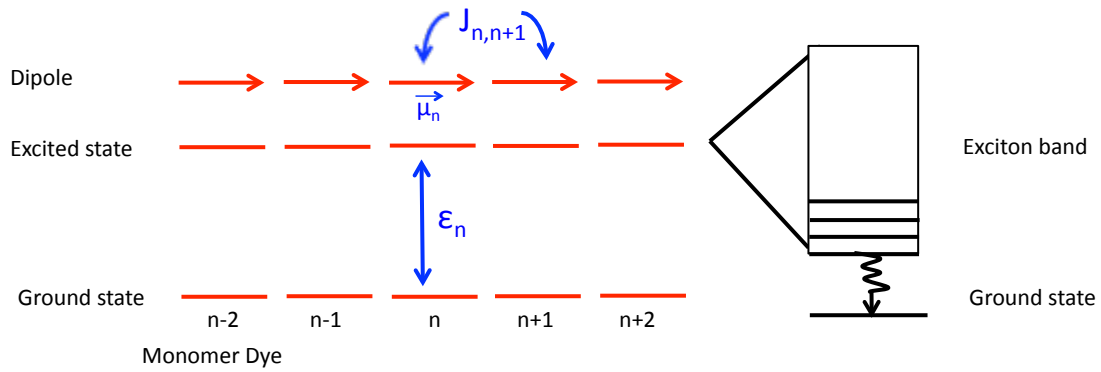

Figure 1.1 Illustration of the Frenkel exciton model for a linear J-aggregate

For a homogenous linear J-aggregate with parallel (head to tail) transition dipoles (μ_n) and equal excitation energies of ε_n. The monomers, modeled as a two-level system, interact with each other via a strong dipole-dipole coupling, J, which leads to the coherent exciton states. The excitonic state with the highest transition dipole moment lays at the lower edge of the exciton band and has a lower absorption energy than the monomer; the absorption band is red-shifted relative to the monomer.
Figure based on Reference 33.

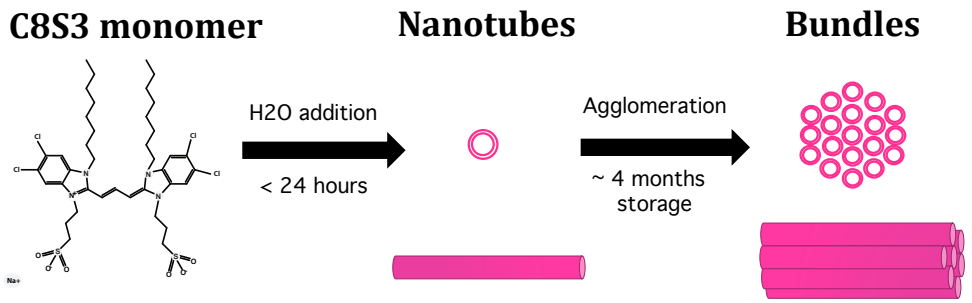

Figure 1.2 Cartoon depicting C8S3 aggregation

The carbocyanine monomer dye is well solvated in methanol. Double walled cylindrical J-aggregates form quickly when water is added to the methanol dye solution. After many months of storage, the nanotubes spontaneously assemble into close-packed cylindrical super-structures (bundles). Cartoons are not to scale.

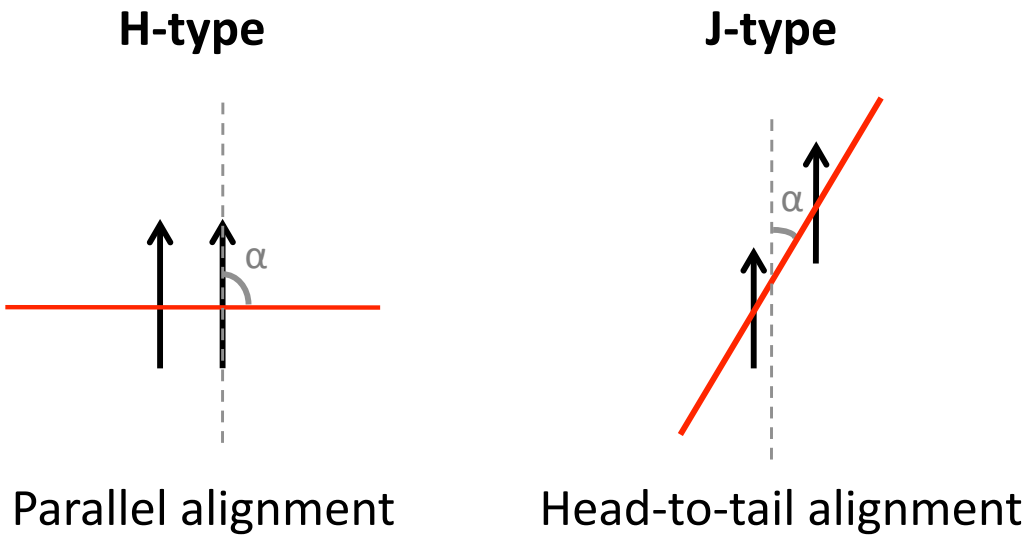

Figure 1.3 Illustrations of slip angles in H- and J-type dimers

The structural arrangement of momomer transition dipoles (depicted as arrows) in aggregates determines their optical properties. The angle between the long axis of a dye molecule and the straight line passing through the dye molecule centers is the slip angle. Large slip angles ($\alpha > 54.7°$) correspond to H-aggregates, while small slip angles ($\alpha < 54.7°$) correspond to J-aggregates. This principle is illustrated above for the simplest aggregates, dimers.

REFERENCES

1. Nathan, F. L.; Paul, V.; Tony, J. P., The State of the Art in Biomimetics. *Bioinspiration & Biomimetics* **2013,** *8*, 013001.
2. Gust, D.; Moore, T. A.; Moore, A. L., Mimicking Photosynthetic Solar Energy Transduction. *Acc. Chem. Res.* **2000,** *34*, 40-48.
3. LaVan, D. A.; Cha, J. N., Approaches for Biological and Biomimetic Energy Conversion. *Proceedings of the National Academy of Sciences* **2006,** *103*, 5251-5255.
4. Ciamician, G., The Photochemistry of the Future. *Science* **1912,** *36*, 385-394.
5. Gust, D.; Moore, T. A., Mimicking Photosynthesis. *Science* **1989,** *244*, 35-41.
6. Sarikaya, M.; Askay, I. A., *Biomimetics: Design and Processing of Materials*. AIP Press: Woodbury, NY, 1995.
7. Bhushan, B., Biomimetics: Lessons from Nature–an Overview. *Philosophical Transactions of the Royal Society A: Mathematical, Physical and Engineering Sciences* **2009,** *367*, 1445-1486.
8. Bar-Cohen, Y., Biomimetics : Biologically Inspired Technologies. Taylor and Francis: Hoboken, 2005.
9. Large, M., *Optical Biomimetics: Materials and Applications*. Woodhead Publishing: Philadelphia, 2012.
10. Nash, M., *Biomimetics. Encyclopedia of Nanoscience and Society. Sage Publications, Inc*. SAGE Publications, Inc.: Thousand Oaks, CA, 2010.
11. Sykora, M.; Maxwell, K. A.; DeSimone, J. M.; Meyer, T. J., Mimicking the Antenna-Electron Transfer Properties of Photosynthesis. *Proceedings of the National Academy of Sciences* **2000,** *97*, 7687-7691.
12. Gratzel, M., Photoelectrochemical Cells. *Nature* **2001,** *414*, 338-334.
13. Rochford, J.; Chu, D.; Hagfeldt, A.; Galoppini, E., Tetrachelate Porphyrin Chromophores for Metal Oxide Semiconductor Sensitization: Effect of the Spacer Length and Anchoring Group Position. *J. Am. Chem. Soc.* **2007,** *129*, 4655-4665.
14. Harriman, A., Unusually Slow Charge Recombination in Molecular Dyads. *Angew. Chem. Int. Ed.* **2004,** *43*, 4985-4987.
15. Orf, G.; Blankenship, R., Chlorosome Antenna Complexes from Green Photosynthetic Bacteria. *Photosynth. Res.* **2013,** *116*, 315-331.

16. Balaban, T. S.; Tamiaki, H.; Holzwarth, A. R., Chlorins Programmed for Self-Assembly. In *Top. Curr. Chem.: Supermolecular Dye Chemistry*, 2005; Vol. 258, pp 1-38.

17. Blankenship, R. E., Matsuura, K., Antenna Complexes from Green Photsynthetica Bacteria. In *Light-Harvesting Antennas in Photosynthesis*, Govindjee, Ed. Kluwer: Dordrecht, 2003; Vol. 13, pp 195-217.

18. Olson, J. M., Chlorophyll Organization in Green Photosynthetic Bacteria. *Biochimica et Biophysica Acta (BBA) - Reviews on Bioenergetics* **1980,** *594*, 33-51.

19. Oostergetel, G. T.; Reus, M.; Chew, A. G. M.; Bryant, D. A.; Boekema, E. J.; Holzwarth, A. R., Long-Range Organization of Bacteriochlorophyll in Chlorosomes of Chlorobium Tepidum Investigated by Cryo-Electron Microscopy. *FEBS Letters* **2007,** *581*, 5435-5439.

20. Renger, T.; May, V.; Kühn, O., Ultrafast Excitation Energy Transfer Dynamics in Photosynthetic Pigment–Protein Complexes. *Physics Reports* **2001,** *343*, 137-254.

21. Psencik, J.; Ikonen, T. P.; Laurinmaki, P.; Merckel, M. C.; Butcher, S. J.; Serimaa, R. E.; Tuma, R., Lamellar Organization of Pigments in Chlorosomes, the Light Harvesting Complexes of Green Photosynthetic Bacteria. *Biophys. J.* **2004,** *87*, 1165-1172.

22. Jelley, E. E., Spectral Absorption and Fluorescence of Dyes in the Molecule State. *Nature* **1936,** *138*, 1009-1010.

23. Jelley, E. E., Molecular, Nematic and Crystal States of I:I'-Diethyl-Psi-Cyanine Chloride. *Nature* **1937,** *139*, 631-632.

24. Scheibe, G., Über Die Veränderlichkeit Der Absorptionsspektren in Lösung Und Die Nebenvalenzen Als Ihre Ursache. *Angew. Chem.* **1937,** *50*, 212-219.

25. Scheibe, G., Variability of the Absorption Spectra of Some Sensitizing Dyes and Its Cause. *Angewandte Chemie* **1936,** *1936*, 563.

26. Franck, J.; Teller, E., Migration and Photochemical Action of Excitation Energy in Crystals. *J. Chem. Phys.* **1938,** *6*, 861-872.

27. Scholes, G. D.; Rumbles, G., Excitons in Nanoscale Systems. *Nature Materials* **2006,** *5*, 683-696.

28. Möbius, D., Scheibe Aggregates. *Advanced Materials* **1995,** *7*, 437-444.

29. Davydov, A. S., *Theory of Molecular Excitons*. Plenum Press: New York, 1971.

30. Würthner, F.; Kaiser, T. E.; Saha-Möller, C. R., J-Aggregates: From Serendipitous Discovery to Supramolecular Engineering of Functional Dye Materials. *Angew. Chem. Int. Ed.* **2011,** *50*, 3376-3410.

31. Kobayashi, T., *J-Aggregates*. World Scientific, Singapore: 1996.

32. Frenkel, J., On the Transformation of Light into Heat in Solids. I. *Phys. Rev.* **1931,** *37*, 17-44.

33. Bloemsma, E. A. Exciton Localization and and Optical Spectroscopy of Linear and Tubular J-Aggregates. Dissertation, University of Groningen, Groningen, 2013.

34. De Rossi, U.; Moll, J.; Spieles, M.; Bach, G.; Dähne, S.; Kriwanek, J.; Lisk, M., Control of the J-Aggregation Phenomenon by Variation of the N-Alkyl-Substituents. *J. Prakt. Chem.* **1995,** *337*, 203-208.

35. Pawlik, A.; Ouart, A.; Kirstein, S.; Abraham, H. W.; Daehne, S., Synthesis and Uv/Vis Spectra of J-Aggregating 5,5 ',6,6 '-Tetrachlorobenzimidacarbocyanine Dyes for Artificial Light-Harvesting Systems and for Asymmetrical Generation of Supramolecular Helices. *Eur. J. Org. Chem.* **2003**, 3065-3080.

36. Mishra, A.; Behera, R. K.; Behera, P. K.; Mishra, B. K.; Behera, G. B., Cyanines During the 1990s: A Review. *Chem. Rev.* **2000,** *100*, 1973-2011.

37. Kirstein, S.; Daehne, S., J-Aggregates of Amphiphilic Cyanine Dyes: Self-Organization of Artificial Light Harvesting Complexes. *Int. J. Photoenergy* **2006**.

38. Hamanaka, Y.; Kawasaki, O.; Yamauchi, T.; Nakamura, A., Morphology of Self-Assembled Merocyanine J-Aggregates in Films Studied by Scanning near-Field Optical Microscope. *Chem. Phys. Lett.* **2003,** *378*, 47-54.

39. von Berlepsch, H.; Kirstein, S.; Hania, R.; Pug≈ælys, A.; B√∂ttcher, C., Modification of the Nanoscale Structure of the J-Aggregate of a Sulfonate-Substituted Amphiphilic Carbocyanine Dye through Incorporation of Surface-Active Additives. *J. Phys. Chem. B* **2007,** *111*, 1701-1711.

40. von Berlepsch, H.; Bottcher, C.; Ouart, A.; Regenbrecht, M.; Akari, S.; Keiderling, U.; Schnablegger, H.; Dahne, S.; Kirstein, S., Surfactant-Induced Changes of Morphology of J-Aggregates: Superhelix-to-Tubule Transformation. *Langmuir* **2000,** *16*, 5908-5916.

41. Vacha, M.; Saeki, M.; Hashizume, K.; Tani, T., Micro-Spectroscopy of Individual Nanostructures of Molecular Aggregates: Relationship between Morphology and Optical Properties. *Chemical Physics* **2002,** *285*, 149-155.

42. Kobayashi, T., Ed., *J-Aggregates (Volume 2)*. World Scientific Publishing Company: Singapore, 2012.

43. Mees, C. E. K., *The Theory of the Photographic Provess*. The MacMillan Company: New York, 1942.

44. Herz, A. H., Aggregation of Sensitizing Dyes in Solution and Their Adsorption onto Silver Halides. *Adv. Colloid Interface Sci.* **1977,** *8*, 237-298.

45. McDermott, G.; Prince, S. M.; Freer, A. A.; Hawthornthwaitelawless, A. M.; Papiz, M. Z.; Cogdell, R. J.; Isaacs, N. W., Crystal-Structure of an Integral Membrane Light-Harvesting Complex from Photosynthetic Bacteria. *Nature* **1995,** *374*, 517-521.

46. Holzwarth, A. R.; Schaffner, K., On the Structure of Bacteriochlorophyll Molecular Aggregates in the Chlorosomes of Green Bacteria - a Molecular Modeling Study. *Photosynth. Res.* **1994,** *41*, 225-233.

47. Knoester, J.; Daehne, S., Prospects of Artificial Light Harvesting Systems: An Introduction. *Int. J. Photoenergy* **2006,** *2006*.

48. von Berlepsch, H.; Bottcher, C.; Ouart, A.; Burger, C.; Dahne, S.; Kirstein, S., Supramolecular Structures of J-Aggregates of Carbocyanine Dyes in Solution. *J. Phys. Chem. B* **2000,** *104*, 5255-5262.

49. von Berlepsch, H.; Kirstein, S.; Hania, R.; Pugzlys, A.; Böttcher, C., Modification of the Nanoscale Structure of the J-Aggregate of a Sulfonate-Substituted Amphiphilic Carbocyanine Dye through Incorporation of Surface-Active Additives. *J. Phys. Chem. B* **2007,** *111*, 1701-1711.

50. Eisele, D. M.; Arias, D. H.; Fu, X.; Bloemsma, E. A.; Steiner, C. P.; Jensen, R. A.; Rebentrost, P.; Eisele, H.; Tokmakoff, A.; Lloyd, S.; Nelson, K. A.; Nicastro, D.; Knoester, J.; Bawendi, M. G., Robust Excitons Inhabit Soft Supra-Molecular Nanotubes. *Proc. Natl. Acad. Sci. USA*, submitted for publication.

51. Saikin, S. K.; Eisfeld, A.; Valleau, S.; Guzik, A. A., Photonics Meets Excitonics: Natural and Artificial Molecular Aggregates. *Nanophotonics* **2013,** *2*, 21-38.

52. Kasha, M.; Rawls, H. R.; Ashraf El-Bayoumi, M., The Exciton Model in Molecular Spectroscopy. *Pure Appl. Chem.* **1965,** *11*, 371-392.

53. Kasha, M., Relation between Exciton Bands and Conduction Bands in Molecular Lamellar Systems. *Reviews of Modern Physics* **1959,** *31*, 162-169.

54. Spano, F. C., The Spectral Signatures of Frenkel Polarons in H- and J-Aggregates. *Acc. Chem. Res.* **2009,** *43*, 429-439.

55. Knoester, J., Modeling the Optical Properties of Excitons in Linear and Tubular J-Aggregates. *Int. J. Photoenergy* **2006**.

56. Didraga, C.; Klugkist, J. A.; Knoester, J., Optical Properties of Helical Cylindrical Molecular Aggregates: The Homogeneous Limit. *J. Phys. Chem. B* **2002,** *106*, 11474-11486.

57. Didraga, C.; Pugzlys, A.; Hania, P. R.; von Berlepsch, H.; Duppen, K.; Knoester, J., Structure, Spectroscopy, and Microscopic Model of Tubular Carbocyanine Dye Aggregates. *J. Phys. Chem. B* **2004,** *108*, 14976-14985.

58. Didraga, C.; Knoester, J., Optical Spectra and Localization of Excitons in Inhomogeneous Helical Cylindrical Aggregates. *J. Chem. Phys.* **2004,** *121*, 10687-10698.

59. Heijs, D. J. Optical Dynamics in Multichromophore Systems. Dissertation, University of Groningen, Groningen, 2006.

60. Fidder, H.; Terpstra, J.; Wiersma, D. A., Dynamics of Frenkel Excitons in Disordered Molecular Aggregates. *J. Chem. Phys.* **1991,** *94*, 6895-6907.

61. Lyon, J. L.; Eisele, D. M.; Kirstein, S.; Rabe, J. P.; Vanden Bout, D. A.; Stevenson, K. J., Spectroelectrochemical Investigation of Double-Walled Tubular J-Aggregates of Amphiphilic Cyanine Dyes. *J. Phys. Chem. C* **2008,** *112*, 1260-1268.

62. Eisele, D. M.; Knoester, J.; Kirstein, S.; Vanden Bout, D. A., Uniform Exciton Fluorescence from Individual Molecular Nanotubes Immobilized on Solid Substrates. *Nat Nano* **2009,** *4*, 658-663.

63. Augulis, R.; Pugžlys, A.; van Loosdrecht, P. H. M., Exciton Dynamics in Molecular Aggregates. *Phys. Status Solidi C* **2006,** *3*, 3400-3403.

64. Milota, F.; Sperling, J.; Nemeth, A.; Kauffmann, H. F., Two-Dimensional Electronic Photon Echoes of a Double Band J-Aggregate: Quantum Oscillatory Motion Versus Exciton Relaxation. *Chemical Physics* **2009,** *357*, 45-53.

65. Milota, F.; Sperling, J.; Nemeth, A.; Abramavicius, D.; Mukamel, S.; Kauffmann, H. F., Excitonic Couplings and Interband Energy Transfer in a Double-Wall Molecular Aggregate Imaged by Coherent Two-Dimensional Electronic Spectroscopy. *J. Chem. Phys.* **2009,** *131*, 054510-23.

66. Sperling, J.; Nemeth, A.; Hauer, J.; Abramavicius, D.; Mukamel, S.; Kauffmann, H. F.; Milota, F., Excitons and Disorder in Molecular Nanotubes: A 2d Electronic Spectroscopy Study and First Comparison to a Microscopic Model. *J. Phys. Chem. A* **2010,** *114*, 8179-8189.

67. Womick, J. M.; Miller, S. A.; Moran, A. M., Correlated Exciton Fluctuations in Cylindrical Molecular Aggregates. *J. Phys. Chem. B* **2009,** *113*, 6630-6639.

68. Womick, J. M.; Miller, S. A.; Moran, A. M., Probing the Dynamics of Intraband Electronic Coherences in Cylindrical Molecular Aggregates. *J. Phys. Chem. A* **2009,** *113*, 6587-6598.

69. Eisele, D. M.; Cone, C. W.; Bloemsma, E. A.; Vlaming, S. M.; van der Kwaak, C. G. F.; Silbey, R. J.; Bawendi, M. G.; Knoester, J.; Rabe, J. P.; Vanden Bout, D. A., Utilizing Redox-Chemistry to Elucidate the Nature of Exciton Transitions in Supramolecular Dye Nanotubes. *Nat Chem* **2012,** *4*, 655-662.

70. Vlaming, S. M.; Bloemsma, E. A.; Nietiadi, M. L.; Knoester, J., Disorder-Induced Exciton Localization and Violation of Optical Selection Rules in Supramolecular Nanotubes. *J. Chem. Phys.* **2011,** *134*, 114507-11.

71. Scheblykin, I. G.; Sliusarenko, O. Y.; Lepnev, L. S.; Vitukhnovsky, A. G.; Van der Auweraer, M., Strong Nonmonotonous Temperature Dependence of Exciton Migration Rate in J Aggregates at Temperatures from 5 to 300 K. *J. Phys. Chem. B* **2000,** *104*, 10949-10951.

72. Kaiser, T. E.; Scheblykin, I. G.; Thomsson, D.; Wu¨rthner, F., Temperature-Dependent Exciton Dynamics in J-Aggregates—When Disorder Plays a Role. *J. Phys. Chem. B* **2009,** *113*, 15836-15842.

73. Scheblykin, I. G.; Sliusarenko, O. Y.; Lepnev, L. S.; Vitukhnovsky, A. G.; Van der Auweraer, M., Excitons in Molecular Aggregates of 3,3‘-Bis-[3-Sulfopropyl]-5,5‘-Dichloro-9- Ethylthiacarbocyanine (Thiats): Temperature Dependent Properties. *J. Phys. Chem. B* **2001,** *105*, 4636-4646.

74. Dorn, H.-P.; Müller, A., Scheibe-Aggregates of Pseudoisocyanine in Solution and in Molecular Monolayers. *Appl. Phys. B* **1987,** *43*, 167-172.

75. Fidder, H.; Knoester, J.; Wiersma, D. A., Superradiant Emission and Optical Dephasing in J-Aggregates. *Chemical Physics Letters* **1990,** *171*, 529-536.

76. Scheblykin, I. G.; Bataiev, M. M.; Van der Auweraer, M.; Vitukhnovsky, A. G., Dimensionality and Temperature Dependence of the Radiative Lifetime of J-Aggregates with Davydov Splitting of the Exciton Band. *Chemical Physics Letters* **2000,** *316*, 37-44.

77. Pugzlys, A.; Augulis, R.; van Loosdrecht, P. H. M.; Didraga, C.; Malyshev, V. A.; Knoester, J., Temperature-Dependent Relaxation of Excitons in Tubular Molecular Aggregates: Fluorescence Decay and Stokes Shift. *J. Phys. Chem. B* **2006,** *110*, 20268-20276.

78. Knoester, J.; Daehne, S., Prospects of Artificial Light Harvesting Systems: An Introduction. *Int. J. Photoenergy* **2006**, 1-3.

79. Knoester, J.; Agranovich, V. M., Frenkel and Charge-Transfer Excitons in Organic Solids. In *Electronic Excitations in Organic Based Nanostructures*, Agranovich, V. M. B., G.F., Ed. Elsevier: Amsterdam, 2003; Vol. 31, pp 1-96.

80. Sundström, V.; Gillbro, T.; Gadonas, R. A.; Piskarskas, A., Annihilation of Singlet Excitons in J Aggregates of Pseudoisocyanine (Pic) Studied by Pico- and Subpicosecond Spectroscopy. *J. Chem. Phys.* **1988,** *89*, 2754-2762.

81. Silinsh, E. A., Capek, V., *Organic Molecular Crystals: Interaction, Localization, and Transport Phenomena*. American Institute of Physics: New York, 1994.

82. Spitz, C.; Knoester, J.; Ouart, A.; Daehne, S., Polarized Absorption and Anomalous Temperature Dependence of Fluorescence Depolarization in Cylindrical J-Aggregates. *Chemical Physics* **2002,** *275*, 271-284.

83. Valleau, S.; Saikin, S. K.; Yung, M.-H.; Guzik, A. A., Exciton Transport in Thin-Film Cyanine Dye J-Aggregates. *J. Chem. Phys.* **2012,** *137*, 034109: 1-13.

84. Akselrod, G. M.; Tischler, Y. R.; Young, E. R.; Nocera, D. G.; Bulovic, V., Exciton-Exciton Annihilation in Organic Polariton Microcavities. *Physical Review B* **2010,** *82*, 113106.

85. Adams, D. M.; Kerimo, J.; O'Connor, D. B.; Barbara, P. F., Spatial Imaging of Singlet Energy Migration in Perylene Bis(Phenethylimide) Thin Films. *J. Phys. Chem. A* **1999,** *103*, 10138-10143.

86. Kumar, N.; Cui, Q.; Ceballos, F.; He, D.; Wang, Y.; Zhao, H., Exciton Diffusion in Monolayer and Bulk Mose2. *Nanoscale* **2014,** *6*, 4915-4919.

87. Dubin, F.; Melet, R.; Barisien, T.; Grousson, R.; Legrand, L.; Schott, M.; Voliotis, V., Macroscopic Coherence of a Single Exciton State in an Organic Quantum Wire. *Nat Phys* **2006,** *2*, 32-35.

88. Escalante, M.; Lenferink, A.; Zhao, Y.; Tas, N.; Huskens, J.; Hunter, C. N.; Subramaniam, V.; Otto, C., Long-Range Energy Propagation in Nanometer Arrays of Light Harvesting Antenna Complexes. *Nano Letters* **2010,** *10*, 1450-1457.

Chapter 2: Quantifying the Polarization of Exciton Transitions in Double-Walled Nanotubular J-Aggregates*

2.1 INTRODUCTION

An interesting class of self-assembled supramolecular materials is nanotubular J-aggregates formed from amphiphilic cyanine dyes in solution[1]. These aggregates assemble through van der Waals and hydrophobic forces[2-4] and form tubular structures in a fashion similar to other self-assembled, one-dimensional nanostructures.[5] The cyanine nanotubes closely resemble the highly efficient, naturally occurring antenna systems of light harvesting complexes of the Green Sulfur Bacteria, which contain multi-layer tubules of aggregated photosynthetic pigments, bacteriochlorophyll.[6-9] This has made the cyanine nanotube J-aggregate systems of interest as artificial, quasi one-dimensional light harvesting systems.[10-22] Recent theoretical work has proposed that the polarizations of the exciton transitions is strongly affected by localization of the exciton within the aggregate structure as a result of energetic disorder.[23-24] However, rigorous comparisons to the theoretical model require quantitative measurements of the polarizations. Previous experiments have only qualitatively examined the polarization of the exciton spectrum.[17] In addition, this analysis has been hindered by the fact that the double-walled spectrum is congested by numerous overlapping transitions.[16] In this paper both issues will be addressed through dichroic absorption experiments on flow aligned tubular aggregates. First, to alleviate the problem of too many overlapping spectral transitions, chemical oxidation is utilized to isolate the exciton transitions that arise only from the inner-wall (IW) of the aggregate.[14, 25] Second, a quantitative polarization model will be developed

* Portions of this chapter were published in Clark, K.A.; Cone, C.W.; Vanden Bout, D.A.; Quantifying the Polarization of Exciton Transitions in Double-Walled Nanotubular J-Aggregates. *J. Phys. Chem. C* **2013**, *117*, 26473-26481. CWC assisted with oxidation and spectral collection; DVB supervised the project.

that is consistent with all of the absorption and emission data by simultaneously fitting both the reduced linear dichroism and isotropic absorption spectra.

While there are multiple varieties of amphiphilic cyanine dyes that form aggregates with diverse morphologies, those that form nanotubular structures are of keen interest and are well studied.[10-22, 25-27] Monomers of the 3,3'-bis(2-sulfopropyl)-5,5',6,6'-tetrachloro-1,1'-dioctylbenzimida-carbocyanine (C8S3) dye self-assemble in a water/methanol solution to form well-defined double-walled nanotubular supramolecular assemblies that are 13 nm in diameter and several microns in length, as characterized by CryoTEM.[16-17] Scheme 2.1a and 2.1b, respectively, illustrate the molecular structure of the cyanine dye monomer and the cylindrical aggregate system. Upon aggregation, the absorption spectrum of the well solvated monomer dye narrows and red shifts, both dramatic spectral changes characteristic of J-aggregate formation. The optical properties of the aggregate system can be generally understood in terms of a Frenkel exciton model, wherein the coupling of transition dipoles of individual dye molecules leads to newly created, delocalized electronic transitions that extend over multiple dye molecules.[28-31] Additionally, C8S3 nanotubes display intense, nearly resonant fluorescence emission that is typical of many J-aggregate systems.[28-29, 32] The predominate theory that describes the absorption of cylindrical J-aggregates, developed by Knoester and coworkers, predicts two transitions for each cylindrical supramolecular system. For a single, double-walled aggregate in the homogeneous limit (where all excitons exhibit cylindrical symmetry), there should be one transition that is polarized parallel to the long axis of each cylinder and a second, degenerate pair of transitions that are polarized perpendicular to the aggregate axis.[16] Thus, this model predicts that the spectrum of a double-walled tubular system would have a total of four transitions. Recently, an extended herringbone model, which consists of eight transitions for the double-walled tubes, has been developed that

better represents the high energy region of the experimental spectrum.[14] Additionally, theoretical work has shown that disorder in cylindrical aggregate systems will lead to exciton localization[33] on segments of the tubular aggregate and a potential breakdown of the cylindrical symmetry selection rules for the polarization.[15-16, 23-24, 34] A quantitative measure of the transitions' polarizations relative to the C8S3 structure is needed for a rigorous comparison to these predictions. This can be accomplished with linear dichroism measurements of physically aligned aggregates.

Linear dichroism is a powerful spectroscopic tool that elucidates valuable information on molecular orientation, structure and transition moments of small and large molecules.[35-37] Linear Dichroism (LD) is the difference in the absorption of light linearly polarized parallel and perpendicular to the orientation axis of an anisotropic sample, with a known alignment, and is given by $LD = A_{\parallel} - A_{\perp}$. LD spectroscopy has previously been used to qualitatively characterize transition polarizations of C8S3 and similar cylindrical J-aggregate systems that were aligned using a streaming flow technique.[17,38-39] These aggregates have a high aspect ratio, and the long axis orients along the flow direction.[37, 40] In our study, the reduced linear dichroism is utilized to not only characterize the direction but also the magnitude of the C8S3 transition polarizations as well. The reduced linear dichroism, LD^r, is the LD normalized by the isotropic absorbance (A_{iso})

$$LD^r = \frac{LD}{A_{iso}} \qquad (1)$$

Thus, the LD^r has no dependence on the path length or sample concentration and is a pure measure of the polarization of the transitions. For cases where the oriented sample is uniaxial, A_{iso} is related to the polarized component spectra:

$$A_{iso} = \frac{A_{\parallel} + 2A_{\perp}}{3} \qquad (2)$$

Furthermore, the reduced linear dichroism is quantitatively related to the angle of the absorption transition dipoles relative to the orientation axis.

$$LD^r = \frac{3}{2} S\left(3\cos^2\alpha - 1\right) \qquad (3)$$

where α is the angle of the orientation of the nanotube absorption transition dipole. S is an orientation factor that depends on θ, the angle that designates the macroscopic alignment of the orientation axis to the laboratory orientation direction (see Scheme 2.2):

$$S = \frac{1}{2}\left(3\langle\cos^2\theta\rangle - 1\right) \qquad (4)$$

The orientation factor S, has a maximum value of 1 for perfectly aligned uniaxial samples; for isotropic, un-oriented samples, S equals zero. Positive LD and LD^r amplitudes indicate absorption transitions parallel to the molecular orientation axis of the sample, while negative values indicate perpendicularly polarized transitions to the orientation direction. One challenge with interpreting LD^r magnitude is that the quantity depends both on the polarization of the transition relative to the long axis of the object and the macroscopic alignment of the object. As it is generally difficult (if not impossible) to perfectly align a sample in the flow cell geometry, the orientation factor S is unknown. Thus, for any transition both the orientation factor and its polarization are unknown. However, any model of the reduced linear dichroism must assume the same S

factor for the entire spectrum. This means that polarization knowledge of any single peak in the spectrum is sufficient to calibrate the alignment of the entire sample.

Since the full double-walled nanotube spectrum is comprised of several overlapping transitions, linear dichroism experiments are performed on both the full double-walled system and on the inner wall-only aggregates (isolated with chemical oxidation). Based on these two experiments a comprehensive, self-consistent model is developed that characterizes the polarizations of the exciton transitions in the C8S3 J-aggregate nanotube system.

2.2 EXPERIMENTAL

2.2.1 J-aggregate Solution Preparation

C8S3 Nanotube solutions were prepared via the alcoholic route as previously reported.[17, 25] C8S3 monomer dye powder (dye S0440, MW= 902.8 g mol-1, FEW Chemicals, Germany) was dissolved in methanol (Fisher scientific, spectroscopic grade) and stirred for 20 minutes to make a solution of approximately 8mM. This solution was further diluted with methanol to create a monomer stock solution of 2.32 mM, which was refrigerated.

C8S3 J-aggregate solutions were prepared by adding 260 μL of 2.32 mM stock to 1 mL of high purity water (18MΩ cm, Barnstead); upon this aqueous addition, a characteristic solution color change from red (monomer) to bright pink (J-aggregates) was observed. The solution was agitated lightly, then capped and allowed to aggregate in the dark for time periods between 5 and 24 hours. After this variable time step, an additional 1 mL of high purity water was added to the solution to halt the aggregation process. Steady-state absorption spectra were measured to verify the aggregation process; samples were stored at room temperature in the dark.

2.2.2 Isotropic and Polarized Absorption measurements

All absorption spectra were acquired at room temperature using a Hewlett Packard UV-Vis 8453 spectrophotometer. Steady state, isotropic absorption spectra of C8S3 solutions (monomer, oxidized C8S3 nanotubes and pure C8S3 nanotube) were measured using a 0.1 mm path length quartz cuvette (Starna, 40 μL).

Polarized flow-aligned absorption spectra of the double-walled aggregates were obtained by placing a linear polarizer in the path between the spectrophotometer's lamp source and the sample chamber at either 0° or 90° (which corresponds to parallel or perpendicular to direction of aligned nanotubes, respectively), and sampling after flow was begun (Scheme 2.2). The instrument was blanked after the polarizer was placed in the path or rotated to eliminate spectral background issues. A Cole-Parmer Masterflex peristaltic pump (Easy-Load II pump head, L/S 14 peroxide cured silicone tubing) was used to pump the J-aggregate solution through a 0.1 mm path length quartz flow cell (Agilent Technologies, 6.2 μL) at a flow rate of 75 mL min^{-1}. To ensure sample integrity remained intact throughout the flow experiments, isotropic J-aggregate absorption spectra collected before and after flow were compared and found to be unchanged.

2.2.3 Chemical Oxidation of C8S3 J-Aggregates

To prepare chemically oxidized nanotube samples, 150 μL of 22 mM aqueous $AgNO_3$ (Sigma Aldrich) was added to 10 mL of J-aggregate solution. The J-aggregate and $AgNO_3$ mixture was illuminated with white light for 60 seconds then flowed once through silicone tubing using the Masterflex peristaltic pump to thoroughly mix the two solutions. After approximately 100 minutes, when no further change in the absorption profile shape was observed, polarized flow-aligned spectra of the oxidized sample were collected. To ensure further spectral changes due to oxidation did not occur during the

flow experiments, isotropic absorption spectra before and after flow were collected and found to be unchanged.

2.2.4 Fluorescence Emission of C8S3 J-aggregates

Fluorescence spectra of oxidized and pure J-aggregate solutions were acquired with a Horiba Scientific FluoroLog®-3 spectrofluorometer in a 0.1 mm quartz cell (Starna) using an excitation wavelength of 532 nm.

2.3 Results and Discussion

2.3.1 C8S3 Monomer and J-aggregate Absorption Spectroscopy

Figure 2.1 shows the absorption spectrum of C8S3 monomer dye in methanol along with the spectrum of the double-walled cylindrical J-aggregates in a mixture of methanol and water. The broad absorption of C8S3 monomer is peaked around 520 nm, while sharp, red-shifted features define C8S3 J-aggregate absorption. The two prominent J-bands centered at 589 and 599 nm are respectively attributed to the outer and inner aggregate wall [13, 16, 25, 41] and have been previously observed to be predominately polarized parallel to the aggregate long axis. [16-17] The shoulder near 585 nm has previously been assigned to the two predicted (overlapping) perpendicular transitions for each wall. [16]

2.3.2 Inner-wall Isolation

The individual transitions of the C8S3 nanotube absorption are difficult to characterize as a result of numerous overlapping transitions. One approach to simplify this spectrum is to isolate a subset of peaks that arise from only one of the aggregate walls; recent experimental studies reveal that it is possible to isolate the spectral contribution of the inner-wall of the C8S3 J-aggregate through both chemical oxidation and dilution.[14, 25] While controlled dilution results in a temporary loss of outer wall

spectral contribution (and eventual return of the full J-aggregate spectrum), chemical oxidation of the aggregates is irreversible.[14] Both methods result in a simpler absorption profile singularly attributed to the inner wall**.** The difference in oxidation rates between the inner and outer wall during oxidation has been observed previously, with the outer wall oxidizing faster the inner wall.[41] Oxidation of dye molecules in the outer wall can be accomplished by adding silver ions to the solution and illuminating with white light; as the dye molecules are oxidized and silver ions reduced, silver nanoparticles form.[10, 13] The chemical oxidation also causes distinct change in the optical absorbance of the cylindrical aggregates while cryoTEM studies reveal the double-walled aggregate morphology is unchanged.[14] Previous experiments revealed the oxidation depends on the silver ion concentration and that the methanol in the solution also acted as a mild oxidizing agent.[13] The polarization experiments require the aggregates to be pumped through a flow cell at a fast streaming flow rate in order to gain macroscopic alignment. When previously published oxidation conditions[13] were utilized in conjunction with the flow cell alignment technique, there was a rapid acceleration of the oxidation kinetics, which resulted in complete (inner *and* outer wall) aggregate oxidation in less than one minute. Generating stable aggregate solutions where only inner wall contributions remain requires a careful balance of oxidation kinetics such that the outer wall has completely oxidized before the entire aggregate has been oxidized. We define inner wall isolation as complete when normalized spectral profiles of the oxidized J-aggregate solution are unchanging. This was achieved, despite the vigorous mixing by pumping through the flow cell, by greatly reducing the amount of silver ion added to initiate the oxidation process. Over half of the total monomer dye is located in the larger outer wall cylinder, and the complete dye oxidation is a two electron process.[25] A rough calculation yields a 2:1 ratio of total C8S3 monomer dye to silver ion in our oxidation scheme. By introducing fewer silver ions than

C8S3 dye molecules comprising the outer wall and then thoroughly mixing the $AgNO_3$ and J-aggregate solutions before the flow cell experiments were performed, we were able to generate an inner wall isolated aggregate sample that was kinetically stable for over 30 minutes.

The oxidation results are shown in Figure 2.2a, which depicts the time decay of the full C8S3 nanotube spectrum to the final inner wall spectrum after addition of $AgNO_3$. The absolute absorption of both aggregate J-bands decrease. The chemical oxidation of the nanotubes was monitored via steady state absorption spectroscopy by tracking the decline of the high energy J-band absorption that is attributed to outer wall dye molecules. After ~ 90 minutes the shape of the spectrum stops changing, with the final spectrum retaining only the inner wall peak at 599 nm. With stable oxidized aggregates in the flow cell, the polarizations of the transitions could be quantified using reduced linear dichroism spectroscopy.

2.3.3 Spectral Characterization: Polarization and Energy Assignment

a. C8S3 J-aggregate inner wall spectral model

All spectra, models and transitions are presented in energy space rather than versus wavelength. Figure 2.2b shows the polarized flow-aligned absorption spectra of the chemically oxidized C8S3 J-aggregate nanotubes. It is clear from the parallel and perpendicular spectra that at least four polarized transitions make up the spectrum of the inner wall. The sharp prominent J-band centered at 16722 cm^{-1}, and the broader transition band at 17620 cm^{-1}, appear to be polarized predominately parallel to the aggregate long axis as they dominate the spectrum polarized parallel to the flow direction ($A_{\parallel}$). Similarly, the flow-aligned spectrum acquired with the polarizer at 90° ($A_{\perp}$) reveals two perpendicular polarized transitions, centered at 17241 and 17981 cm^{-1}. The parallel and

perpendicular spectra can be combined as in equations 1 and 2 to generate an experimental reduced linear dichroism spectrum, which contains only polarization information. The LD^r spectrum exhibits five distinct regions that are marked in Figure 2.2d. Regions I and III have positive LD^r amplitudes, meaning the combined transitions in these energy ranges are largely dominated by absorption transitions parallel to the orientation (long) axis of the aggregates. Regions II and IV have negative LD^r amplitudes, which designates the collective exciton transitions in these regions are overall perpendicular to the long axis of the aggregates. The high-energy absorption, Region V, is isotropic. Importantly, the inner wall experimental LD^r spectrum (Figure 2.2d), exhibits three clear positions where the reduced linear dichroism equals zero, signifying equal parallel and perpendicular absorption contributions at these energies. These unique positions are essential in the exact determination of the transition energies and widths for the inner wall isotropic excitonic spectral fit. There is no ambiguity regarding the parallel and perpendicular contributions where $LD^r = 0$ because they are exactly the same regardless of the effective nanotube alignment.

For a sample that is perfectly aligned parallel to the flow direction, we would expect transitions polarized parallel to the object's long axis to exhibit an $LD^r = 3$. In contrast, transitions polarized exactly perpendicular to the long axis should yield an $LD^r = -1.5$. The C8S3 J-aggregate experimental LD^r maximum is 1.5 for the transition centered at 16722 cm^{-1}. This could be a result of that transition being only partially polarized along the parallel direction. More likely, $LD^r < 3$ is the result of imperfect macroscopic nanotube alignment, which practically prevents the observation of theoretical LD^r extremes.

A model that reproduces both the isotropic absorption spectrum and the reduced linear dichroism spectrum was constructed using purely polarized transitions. The inner-

wall spectrum has been previously modeled with four transitions[14] that exhibit the polarizations observed here. The inner wall absorption model consists of four Lorentz functions. These four transitions, depicted in Figure 2.2c, are numbered from lowest energy (peak 1) to highest energy (peak 4). Each is classified by having either purely parallel or perpendicular contribution to the inner wall J-aggregate exciton spectrum (i.e. $\alpha = 0°$ or $\alpha = 90°$ for all transitions). The polarizations are assigned based on polarized flow-absorption results with peaks 1 and 3 assigned as parallel to the long axis, while peaks 2 and 4 are assigned perpendicular polarization.

The preliminary inner wall LD^r fit was then compared with the experimentally determined inner wall LD^r spectrum, and the Lorentz functions of the fit (peaks 1-4) were optimized by modulating positions, widths and areas until both the calculated and experimental LD^r spectra were in good agreement *and* the isotropic inner wall exciton spectrum was well represented. It was possible to generate a self-consistent model that fit both the isotropic absorption spectrum and the reduced linear dichroism spectrum with only four peaks. Figure 2.2c shows the experimental inner wall isotropic absorption of C8S3 nanotubes overlaid with the absorption model that is composed of four purely polarized transitions. Agreement between the isotropic spectrum and model is excellent up to ~18200 cm^{-1}. The high-energy tail (Region V, Figure 2.2d) of the isotropic spectrum was not well represented in this model and was omitted during optimization. This was predominantly a result of spectral Region V exhibiting purely isotropic absorbance and thereby yielding no signatures in the dichroism spectra. The experimental and model inner wall LD^r spectra are plotted in Figure 2.2d. It should be noted that the calculated inner wall LD^r fit is scaled by a factor of ~0.6 in order to overlay the experimental inner wall LD^r spectrum; this scalar can be considered the wavelength-independent scaling factor S, noted earlier, that specifies the laboratory-system

alignment. The value S depends on the angle θ between the aggregate long axis and the macroscopic orientation direction; $S_{IW} = 0.6$ maps to a distribution of angles with an $\theta_{avg} = 31°$, a reasonable value considering the large size of the rod-like J-aggregates[37].

b. C8S3 J-aggregate double-walled spectral model

With a consistent model developed for isotropic and LD^r spectra of chemically oxidized J-aggregates, an analogous experimental and analysis approach was used to expand this model to the pure, un-oxidized C8S3 J-aggregate excitonic absorption spectrum. The full spectrum was assumed to contain the same transitions found in the IW spectral model along with four more transitions associated with the outer wall.[14] Figure 2.3a gives the polarized spectra for the double-walled aggregates obtained in the flow cell scheme. It is apparent that the lowest energy J-bands are predominately parallel polarized while the higher energy transitions have more perpendicular character. The parallel spectrum ($A_{||}$) exhibits three clear transitions: the two transitions identified in the inner wall spectrum (peaks 1 and 3) and the outer wall's high-energy, sharp J-band centered at 16995 cm^{-1}. The perpendicular absorption ($A_{\perp}$) seemingly reveals only the two inner wall transitions (peaks 2 and 4) that are orthogonally polarized to the aggregate long axis. As done for the oxidized aggregates, the polarized spectra were combined according to equations 1 and 2 to obtain an experimental reduced linear dichroism spectrum, fullexp LD^r, seen in Figure 2.3c. The double-walled LD^r spectrum has three distinct regions that are designated in Figure 2.3c; Regions I and II are dominated by transitions parallel and perpendicular, respectively, to the aggregate long axis. Region III, which maps to the high-energy component of the spectrum, has an effective LD^r value of zero, indicating isotropic spectral absorption.

Assuming similar supramolecular structures, with two molecules per unit cell, for the inner and outer cylinders, would result in a spectrum with a total of eight transitions,[14]

comprised of the four transitions identified in the inner wall plus four new transitions for the outer wall. However, because the higher energy region of the spectrum is composed of fairly broad and overlapping transitions, this portion of the spectrum was modeled with only two transitions (rather than four): peak 3 (parallel) and peak 4 (perpendicular). The energies of peaks 1 and 2 vary marginally (to align with experimental results), but were kept close to the values that fit the inner wall spectrum. Peaks 3 and 4 were retained from the inner wall model and fixed in position, width, and magnitude. Finally, the full model contains two 'new' peaks that correspond to the lowest energy transitions for the outer wall. The prominent outer wall J-band centered at 16995 cm^{-1} was fit as the parallel-polarized peak 5. A small perpendicular transition, peak 6, was included to account for the corresponding perpendicular transition. While small in magnitude, this perpendicular transition was essential to best model the LD^r and the isotropic C8S3 J-aggregate spectra.

This full absorption model is comprised of the three parallel transitions and three perpendicular transitions. Inner wall transitions (peaks 1-4) and two transitions that uniquely belong to the full, double-walled spectrum (peaks 5 and 6) are found in Figure 2.3b. The LD^r spectrum for the pure C8S3 nanotubes is calculated from the six polarization-assigned transitions. The outer wall transitions, fit with peaks 5 and 6, were adjusted until both the calculated spectra simultaneously reproduced both the experimental LD^r and isotropic absorption spectra. The full absorption model was constructed with minimal adjustment to the inner wall transitions (peaks 1-4). Figures 2.3b and 2.3c illustrate the ability of six purely polarized transitions to model C8S3 J-aggregate absorption and LD^r spectra, respectively. Again, the calculated full LD^r is scaled to account for imperfect laboratory alignment, with $S_{full} = 0.51$. This S value

corresponds to a distribution of alignment angles that average ~ 35° and agrees nicely with inner wall results ($S_{IW} = 0.6$, $\theta_{avg} = 31°$).

There are obvious differences between the LD^r spectra of the oxidized and pure J-aggregate samples, which are overlaid in Figure 2.4. Most notably, the full LD^r spectrum has a single position (17900 cm^{-1}) where the reduced linear dichroism equals zero, designating equal parallel and perpendicular absorption contributions at this energy, whereas the LD^r spectrum of the oxidized sample crosses zero three times. Of the three points where the inner wall LD^r spectrum crosses zero, the two with lowest energy do not appear in full LD^r spectrum. This indicates the absence of peaks 5 and 6 absorption (assigned parallel and perpendicular polarizations, respectively) in the inner wall C8S3 J-aggregate spectrum. Centered at 16995 cm^{-1}, peak 5 has a sizeable contribution to the overall full isotropic spectrum (Figure 2.3b), but is not present in the inner wall spectrum (Figure 2.2c) due to the preferential chemical oxidation of the nanotubular J-aggregates outer wall spectroscopic contribution.

Theoretical models[17,16,32] predict that peaks 1 and 5 (the lowest energy J-bands) of the isotropic C8S3 J-aggregate absorption are polarized parallel and belong to the inner and outer walls, respectively, of the aggregate system. Our LD^r spectral results for the double-walled aggregate system are consistent with this theory. Non-overlapping transitions of the same polarization should exhibit the same LD^r amplitude;[37] this is verified experimentally and can be seen in Figure 2.4, where the transitions centered at 16722 cm^{-1} and 16995 cm^{-1} both have experimental LD^r values of 1.3, indicating these transitions exhibit equal parallel polarization to the aggregate long axis.

Overall, care was taken to shift peak positions and modulate peak ratios minimally from the inner wall to the full spectral model, although some flexibility was required. A shift of the lowest energy J-band (peak 1) to a slightly higher energy when the nanotubular

aggregates are chemically oxidized is measured. This small blue shift, observed in both the reduced linear dichroism and isotropic absorption spectra could be due to slight coupling between the inner and outer walls or even environmental factors arising from the chemical oxidation of the sample.[13, 16, 41] Table 2.1 lists details of transition energies, polarization designation, widths, and peak area ratios for the full and inner wall spectral fits.

Knoester and coworkers have shown that the exciton transition bandwidths of cylindrical molecular aggregates are associated with static molecular energetic disorder as well as homogenous[16, 42] and inhomogeneous broadening.[15] In this work, the FWHM of each peak was chosen to align with experimental spectral data. The isotropic inner wall and full C8S3 J-aggregate spectra were modeled up to ~18200 cm^{-1} in the spectrum. The spectral and dichroism models do not account for absorbance at higher energies ($\nu >$ 18200 cm^{-1}). It was possible to account for the absorption in this region by adding two isotropic peaks to the full and inner wall spectral fits. While these peaks bettered the isotropic spectral fits, there was little improvement in the agreement with the dichroism data for either the pure or oxidized sample, as the transitions in this region are not strongly polarized. The high energy region of the spectrum is not explained by the prevailing theoretical model,[16] which predicts four lower energy transitions that exhibit pure polarization. The LD^r spectra reveal that the absorbance is essentially isotropic rather than strongly polarized at energies greater than 18200 cm^{-1}. Thus, these transitions are likely the result of highly localized exciton transitions that arise from disorder within the aggregate system.[24, 43] This disorder causes weaker coupling, which reduces coherence length and leads to higher-energy exciton transitions,[23-24, 44-46] Moreover, the disorder causes many different exciton transitions that are localized in different patches of the tubes, creating an isotropic continuum of transitions.[45, 47]

2.3.4 C8S3 J-aggregate Fluorescence Spectroscopy

The fluorescent properties of C8S3 nanotube solutions display noteworthy features including superradiance,[34] extremely narrow Stokes shift[32, 43] and two fluorescence emission bands.[16] The negligible Stokes shift can be seen in Figure 2.1, where the J-aggregate emission spectrum almost perfectly overlays the lowest energy absorption transition at 599 nm. The two peaks in the spectrum were previously believed to thermalize in population on an ultrafast timescale such that the relative intensity of the two lowest energy J-bands in the emission spectrum reflected the Boltzmann distribution of population.[48] This idea was probed by applying a Boltzmann distribution to the inner wall and full spectral models of the absorption to simulate a thermal emission spectrum. Figures 2.5a and 2.5b show the normalized calculated emission that results from applying the Boltzmann distribution to the inner wall and full absorption models, respectively. While the pure C8S3 J-aggregate emission displays two fluorescence bands, the oxidized J-aggregate solution emission exhibits only one; this is due to the preferential 'turning off' of the outer wall dye molecule absorption via aqueous silver ion addition. For both solutions there is excellent agreement between the experimental and calculated C8S3 J-aggregate emission spectra, suggesting both that the model is consistent and the emission is thermalized. The Boltzmann calculated emission indicates that the overwhelming majority of emission (> 95% of integrated spectral area) emanates from states parallel to the aggregate long axis. While the amount of fluorescence stemming from parallel states is greater than what is observed in polarization measurements on individual aggregates,[49] the results agree qualitatively.

2.4 CONCLUSIONS

The class of tubular aggregates prepared from amphiphilic cyanine dyes is of increasing importance and interest due to their novel optical properties and outstanding

energy transfer. While there is no direct imaging method capable of determining dye arrangement within the structurally uniform, double-walled C8S3 J-aggregates, this information is necessary to improve understanding of these one-dimensional model light harvesting systems. Due to the complexity of the excitonic absorption spectrum, previous theoretical models for C8S3 J-aggregate nanotube absorption vary in the number and energy of proposed transitions.

Here, the complicated J-aggregate spectrum was simplified by selectively "turning off" the absorption attributed to outer wall dye molecules. Polarized absorption spectra were collected for chemically oxidized and pure aggregate samples aligned via streaming flow. The polarized component spectra were manipulated to create reduced linear dichroism spectra for both samples. The LD^r spectra were used to construct a robust, quantitative fit for the inner wall absorption using perfectly polarized transitions. Results indicate that four transitions (2 each parallel and perpendicular) characterize the chemically oxidized (inner wall) aggregate spectrum. Once a fit for inner wall absorption was produced, it was extended to account for the full isotropic excitonic absorption of C8S3 nanotubes. Six purely polarized transitions, 3 each parallel and perpendicular to the aggregate long axis, were necessary to accurately model the aggregate spectrum. By requiring the transitions to reconstruct both the reduced linear dichroism (LD^r) and isotropic absorption spectra, we ultimately arrived at a consistent model for both the isolated inner wall and the full, double-wall C8S3 J-aggregate excitonic absorption. The results reveal that the spectrum of the inner wall is dominated by two lower energy J-bands that are purely polarized parallel and perpendicular to the long axis of the cylinder. In addition, the spectrum has a series of higher energy peaks that are strongly overlapping in energy. While the model treats these as independent transitions, they clearly represent a broad distribution of transitions to excitonic states that have less well-defined

polarization. This trend continues to the higher energy end of the spectrum where the disorder in the cylinder leads to transitions similar in energy to monomer dye with completely isotropic polarization character. The outer wall spectrum deduced from the full, double-walled spectrum reveals that the as the diameter of the tube increases the characteristic J-bands at low energy begin to merge. In contrast to the inner wall, the two lowest energy J-bands for the outer wall are nearly degenerate. This is consistent with the theoretical prediction that as the diameter of the tube increases, disorder will lead to a localization of the exciton on patches of the cylinder and a break down of the selections rule that lead to distinct transitions with orthogonal polarizations.[24] A major question that remains is the spatial correlation of the disorder in the systems.[44] The current results suggest that the aggregates are composed of regions of well-coupled monomers that lead to the strongly polarized J-bands as well as disordered regions that result in the higher energy isotropic transitions. The polarizations of the J-bands, particularly for the inner wall, indicate that these states maintain their cylindrical symmetry despite the disorder present in the system. The question remains how are these two types of domains integrated along the nanotube. One possibility is that these two types of excitons arise from distinct spatial regions on the aggregates whose segregation is on a shorter length scale than probed in the previous measurements.[49] Well-ordered regions give rise to states delocalized around the tube, and regions of disorder responsible for the higher energy transitions occur in other larger domains along the tube. However, previous results have shown that the nanotubes are uniform on length scales greater than 50 nm,[49] indicating that if such segregation existed it would need to be uniform on this length scale. An alternate explanation is that these exciton states arise from nearly identical spatial regions within the nanotube structure. Small patches of dye with energetic and/or position disorder lead to the higher energy isotropic transitions. Despite this disorder, the lower

energy exciton states maintain their cylindrical symmetry by delocalizing around these patches. This later perspective suggests that the 2-D nature of the excitons in cylindrical systems may make them less prone to regions of disorder, thereby allowing their electronic and spectral properties to be less vulnerable to subtle changes in supramolecular structure.

2.5 APPENDIX

Modeling C8S3 J-aggregate excitonic absorption using reduced linear dichroism spectroscopy

2.5.1 Inner-wall fit

Four perfectly polarized transitions (peaks 1-4) were used to fit the isolated inner-wall C8S3 J-aggregate absorption (IW model, Equation 5).

$$\text{IW model} = \sum_{i=1}^{4} peak\, i = \frac{IW_{II} + 2IW_{\perp}}{3} \qquad (5)$$

The parallel and perpendicular spectral fit components are noted by IW_{II} and $IW_{\perp}$ and expressed in Equations 6 and 7.

$$IW_{II} = 3(\text{peak } 1 + \text{peak } 3) \qquad (6)$$

$$IW_{\perp} = \frac{3}{2}(\text{peak } 2 + \text{peak } 4) \qquad (7)$$

A reduced linear dichroism (IWfit LD^r, Equation 8) spectrum was calculated from the inner-wall model by taking the difference in parallel and perpendicular absorption and normalizing by the calculated isotropic absorbance.

$$\text{calculated IWfit } LD^r = 3\left(\frac{IW_{\parallel} - IW_{\perp}}{IW_{\parallel} + 2IW_{\perp}}\right) \qquad (8)$$

2.5.2 Double-walled fit

Six transitions were necessary to fit pure, un-oxidized C8S3 J-aggregate isotropic absorption (full model, Equation 9) at energies less than ~18200 cm^{-1}.

$$\text{full model} = \sum_{i=1}^{6} peak\, i = \frac{full_{\parallel} + 2full_{\perp}}{3} \qquad (9)$$

The transitions are assumed to be purely polarized either parallel to the long axis of the aggregate or perpendicular; the parallel and perpendicular spectral fit components are noted by $full_{\parallel}$ and $full_{\perp}$ and expressed in Equations 10 and 11.

$$full_{\parallel} = 3(peak\,1 + peak\,3 + peak\,5) \qquad (10)$$

$$full_{\perp} = \frac{3}{2}(peak\,2 + peak\,4 + peak\,6) \qquad (11)$$

The reduced linear dichroism spectrum for the pure C8S3 J-aggregates (calculated full LD^r, Equation 12) is calculated from the six polarization-assigned transitions.

$$\text{calculated full } LD^r = 3\left(\frac{full_{\parallel} - full_{\perp}}{full_{\parallel} + 2full_{\perp}}\right) \qquad (12)$$

2.6 FIGURES

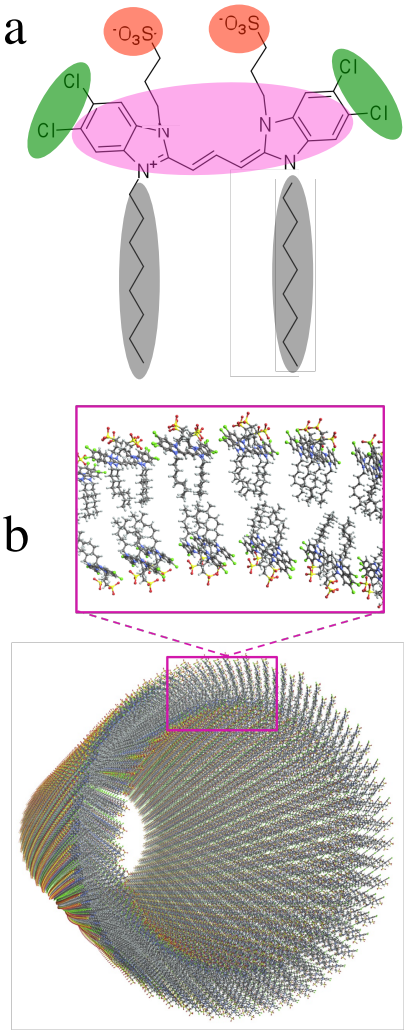

Scheme 2.1 C8S3 Structure

(a) Schematic representation of C8S3 monomer dye and (b) double walled, self-assembled J-aggregates. When water is added to monomer dye solvated in methanol, hydrophobic interactions cause monomer aggregation where non-polar alkyl chains form the interior and polar sulfate groups comprise the exterior of a bilayer structure.

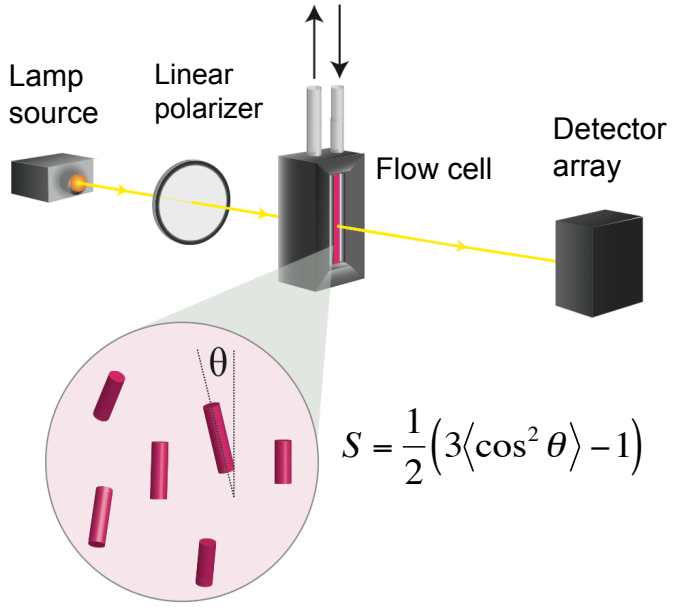

Scheme 2.2 Linear Dichroism Spectral Collection Apparatus

Schematic of modified UV-Vis experiment utilized to acquire polarized absorption spectra of flow-aligned C8S3 J-aggregate samples. C8S3 J-aggregate solution was flowed at 75 mL min^{-1}, which gave maximum alignment without compromising the integrity of the aggregate structure (as indicated by absorption spectra taken after flow experiment). The macroscopic orientation factor, S , is defined by the angle θ of the cylindrical aggregates to the laboratory "vertical."

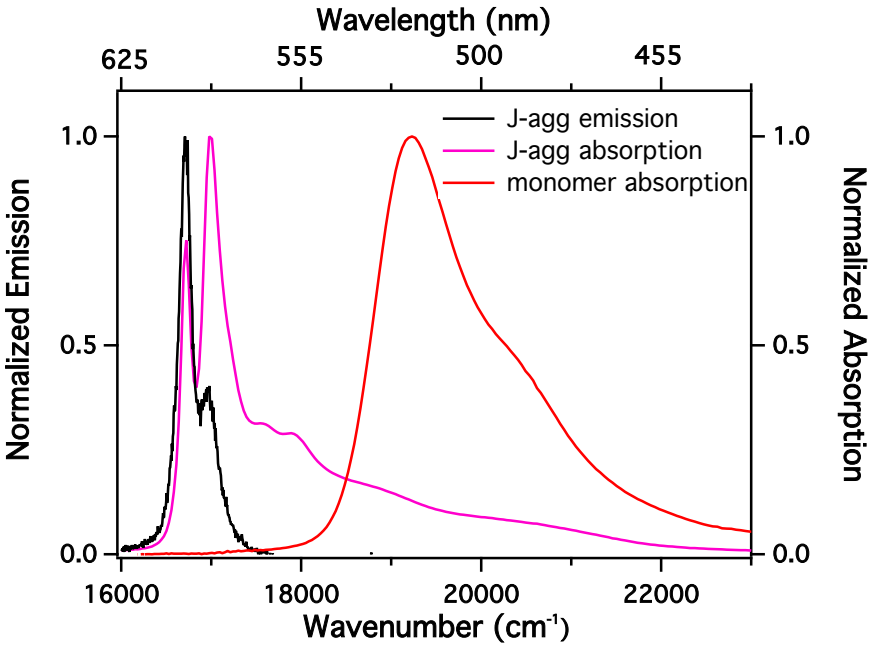

Figure 2.1 C8S3 Absorption Spectra

Optical absorption spectrum of C8S3 monomer (in methanol, red) and C8S3 J-aggregate solution absorption (pink) and fluorescence emission (black) spectra, both in methanol/water. The broad monomer dye absorption red-shifts and splits into narrowed J-bands upon dye molecule aggregation. The two-band J-aggregate fluorescence emission exhibits a very narrow (< 1 nm) Stokes shift.

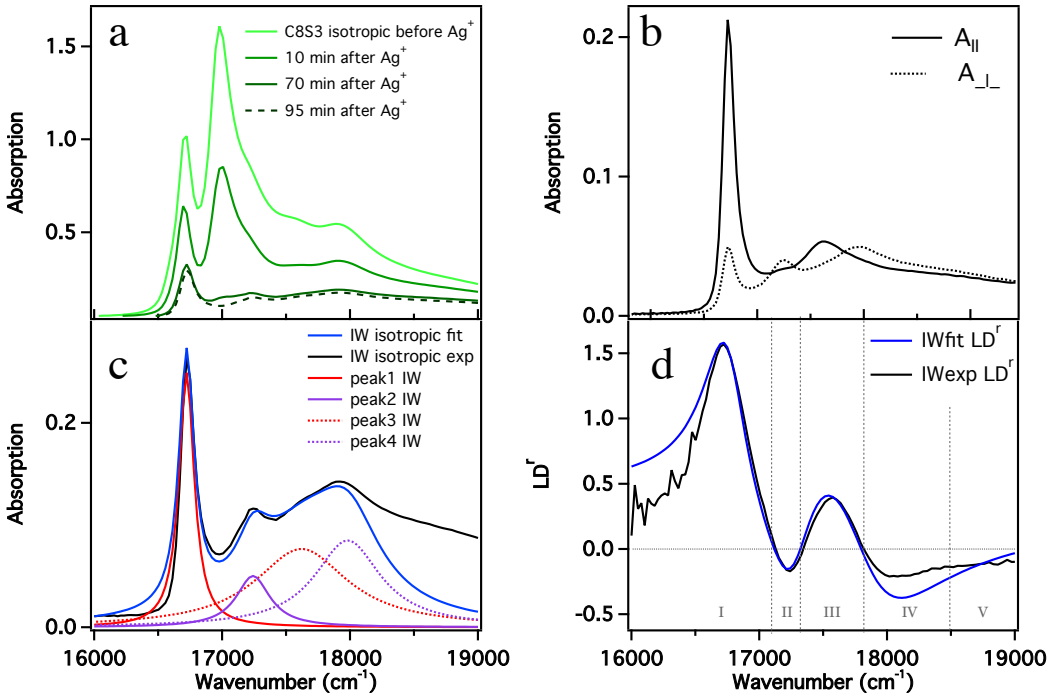

Figure 2.2 C8S3 nanotubes: oxidation and spectral model

(a) C8S3 J-aggregate absorption spectra. Black: absorption spectrum before addition of Ag+ oxidizing agent. Green solid: absorption spectra taken 10, 70 minutes after addition of $AgNO_3$ (aq) and subsequent illumination and flow. Dashed- absorption spectrum taken 95 minutes after $AgNO_3$ (aq) addition. (b) Parallel (solid line, polarizer at 0°) and perpendicular (dotted line, polarizer at 90°) absorption spectra of flow-aligned chemically oxidized C8S3 J-aggregates. (c) Steady state isotropic absorption spectrum (black- experimentally measured, blue-fit) of chemically oxidized C8S3 J-aggregates. The fit is comprised of four purely polarized transitions; peaks 1 and 3 (red) are parallel and peaks 2 and 4 (purple) are perpendicular to the long axis of the doubled walled nanotubular aggregates. (d) Fit (blue) and experimental (black) reduced linear dichroism spectra of chemically oxidized C8S3 J-aggregates. Dashed lines qualitatively indicate spectral regions where excitonic transitions are overall parallel ($LD^r > 0$) or perpendicular ($LD^r < 0$) to the aggregate long axis.

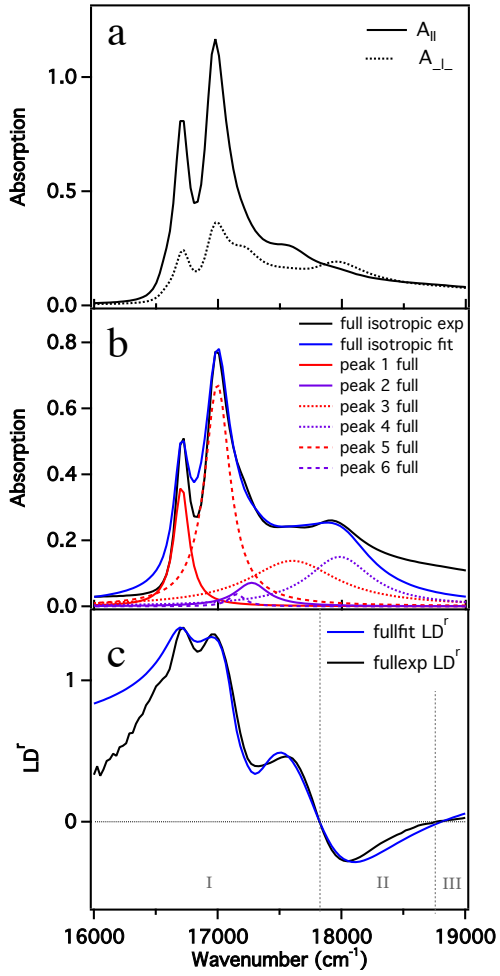

Figure 2.3 C8S3 Nanotubes: full spectral model

(a) Parallel (polarizer at 0°, solid line) and perpendicular (polarizer at 90°, dotted line) absorption spectra of flow-aligned C8S3 J-aggregates. (b) Steady state isotropic absorption spectrum (black- experimentally measured, blue-fit) of C8S3 J-aggregates. The fit is comprised of six purely polarized transitions; peaks 1 and 3 and 5 (red) are parallel and peaks 2, 4 and 6 (purple) are perpendicular to the long axis of the J-aggregates. (c) Fit (blue) and experimental (black) reduced linear dichroism spectra of C8S3 J-aggregates. Dashed lines qualitatively guide where transitions are overall parallel ($LD^r > 0$) or perpendicular ($LD^r < 0$) to the aggregate long axis.

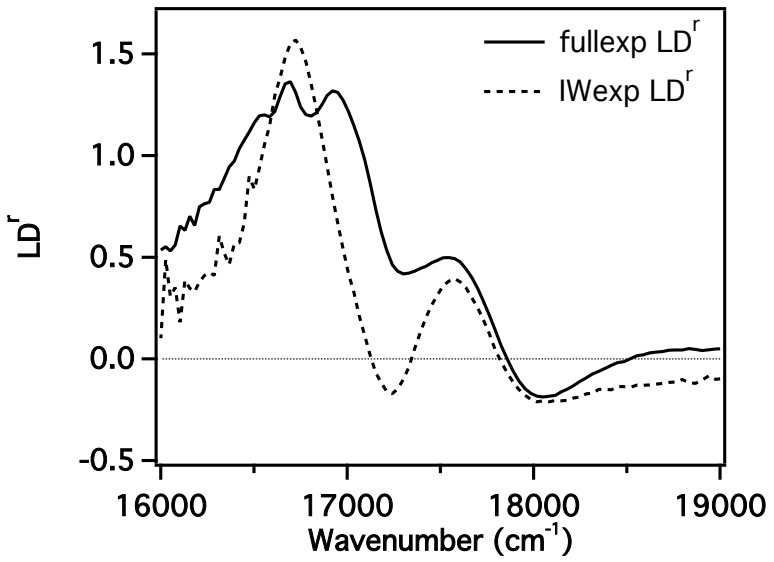

Figure 2.4 C8S3 IW and full LD^r comparison

Reduced linear dichroism spectra for chemically oxidized (Iwexp LD^r, dashed line) and pure (fullexp LD^r, solid line) C8S3 J-aggregates calculated from experimentally obtained polarized absorption spectra. The LD^r spectra and orientation factor values, S(IW) = 0.58 and S(full) = 0.5, indicate slightly better vertical alignment of chemically oxidized nanotubes.

Peak (Polarization)	IW center (ν,cm^{-1})	Full center (ν,cm^{-1})	IW and full FWHM (cm^{-1})	IW peak area ratio	Full peak area ratio
1(‖)	16722	16705	145	Peak 1:2 = 2.24	Peak 1:2 = 2.47
2 (⊥)	17241	17271	320		
3 (‖)	17620	17620	885	Peak 3:4 = 1.27	Peak 3:4 = 1.29
4 (⊥)	17981	17981	630		
5 (‖)	----	16995	245	-----	
6 (⊥)	---	17175	155		

Table 2.1 C8S3 J-aggregate isotropic spectral fit details

This table gives detailed information regarding the newly determined model for double-walled C8S3 J-aggregate solution absorption. Peaks 1-4 are present in both the full and chemically oxidized (IW) C8S3 J-aggregate absorption spectra while peaks 5 and 6, attributed to outer wall contribution, are exclusive to the full, un-oxidized spectrum. The center wavenumber of peaks 1 and 2 varied marginally from the IW to the full model. The full width half maximum (FWHM) of each transition was held constant for both the IW and full models, while the peak ratios were allowed minor variance.

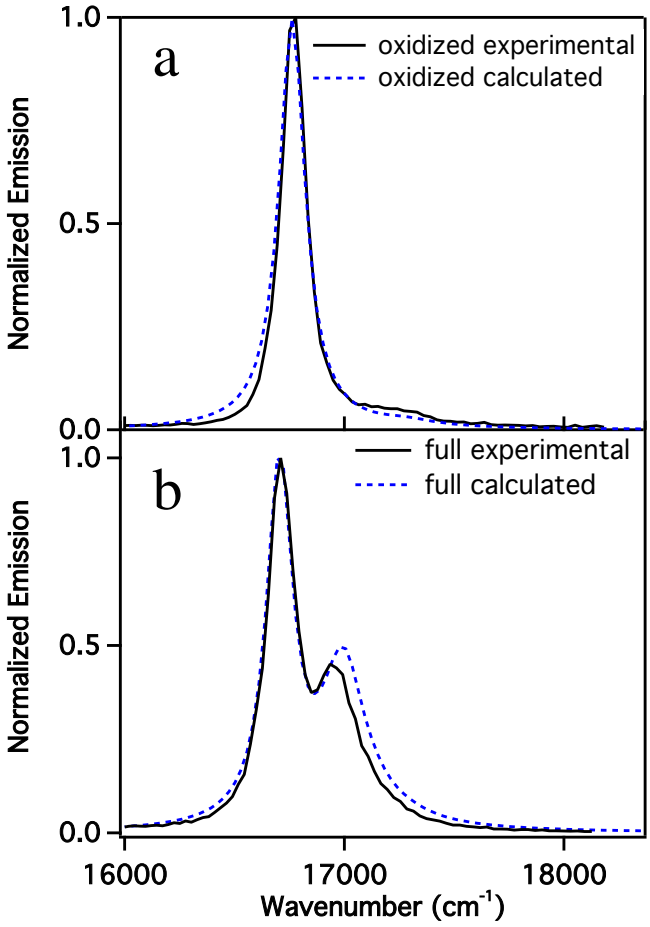

Figure 2.5 C8S3 emission spectra

Experimentally collected and Boltzmann calculated C8S3 J-aggregate (a) chemically oxidized (b) pure bulk fluorescence emission spectra. By applying the Boltzmann distribution to the inner wall and full aggregate spectral fits and comparing to experimentally collected emission, the models are further verified.

2.7 REFERENCES

1. De Rossi, U.; Moll, J.; Spieles, M.; Bach, G.; Dähne, S.; Kriwanek, J.; Lisk, M., Control of the J-Aggregation Phenomenon by Variation of the N-Alkyl-Substituents. *J. Prakt. Chem.* **1995,** *337*, 203-208.

2. von Berlepsch, H.; Bottcher, C.; Ouart, A.; Burger, C.; Dahne, S.; Kirstein, S., Supramolecular Structures of J-Aggregates of Carbocyanine Dyes in Solution. *J. Phys. Chem. B* **2000,** *104*, 5255-5262.

3. Pawlik, A.; Kirstein, S.; DeRossi, U.; Daehne, S., Structural Conditions for Spontaneous Generation of Optical Activity in J-Aggregates. *J. Phys. Chem. B* **1997,** *101*, 5646-5651.

4. Pawlik, A.; Ouart, A.; Kirstein, S.; Abraham, H. W.; Daehne, S., Synthesis and Uv/Vis Spectra of J-Aggregating 5,5 ',6,6 '-Tetrachlorobenzimidacarbocyanine Dyes for Artificial Light-Harvesting Systems and for Asymmetrical Generation of Supramolecular Helices. *Eur. J. Org. Chem.* **2003**, 3065-3080.

5. Aida, T.; Meijer, E. W.; Stupp, S. I., Functional Supramolecular Polymers. *Science* **2012,** *335*, 813-817.

6. Linnanto, J. M.; Korppi-Tommola, J. E. I., Investigation on Chlorosomal Antenna Geometries: Tube, Lamella and Spiral-Type Self-Aggregates. *Photosynth. Res.* **2008,** *96*, 227-245.

7. Balaban, T. S., Tailoring Porphyrins and Chlorins for Self-Assembly in Biomimetic Artificial Antenna Systems. *Acc. Chem. Res.* **2005,** *38*, 612-623.

8. Oostergetel, G. T.; Reus, M.; Chew, A. G. M.; Bryant, D. A.; Boekema, E. J.; Holzwarth, A. R., Long-Range Organization of Bacteriochlorophyll in Chlorosomes of Chlorobium Tepidum Investigated by Cryo-Electron Microscopy. *FEBS Letters* **2007,** *581*, 5435-5439.

9. Psencik, J.; Ma, Y.-Z.; Arellano, J. B.; Hala, J.; Gillbro, T., Excitation Energy Transfer Dynamics and Excited-State Structure in Chlorosomes of Chlorobium Phaeobacteroides. *Biophys. J.* **2003,** *84*, 1161-1179.

10. Kirstein, S.; Daehne, S., J-Aggregates of Amphiphilic Cyanine Dyes: Self-Organization of Artificial Light Harvesting Complexes. *Int. J. Photoenergy* **2006**.

11. Milota, F.; Prokhorenko, V. I.; Mancal, T.; von Berlepsch, H.; Bixner, O.; Kauffmann, H. F.; Hauer, J., Vibronic and Vibrational Coherences in Two-Dimensional Electronic Spectra of Supramolecular J-Aggregates. *J. Phys. Chem. A* **2013,** *117*, 6007-6014.

12. Würthner, F.; Kaiser, T. E.; Saha-Möller, C. R., J-Aggregates: From Serendipitous Discovery to Supramolecular Engineering of Functional Dye Materials. *Angew. Chem. Int. Ed.* **2011,** *50*, 3376-3410.

13. Eisele, D. M.; von Berlepsch, H.; Bottcher, C.; Stevenson, K. J.; Vanden Bout, D. A.; Kirstein, S.; Rabe, J. P., Photoinitiated Growth of Sub-7 Nm Silver Nanowires within a Chemically Active Organic Nanotubular Template. *J. Am. Chem. Soc.* **2010,** *132*, 2104-2105.

14. Eisele, D. M.; Cone, C. W.; Bloemsma, E. A.; Vlaming, S. M.; van der Kwaak, C. G. F.; Silbey, R. J.; Bawendi, M. G.; Knoester, J.; Rabe, J. P.; Vanden Bout, D. A., Utilizing Redox-Chemistry to Elucidate the Nature of Exciton Transitions in Supramolecular Dye Nanotubes. *Nat Chem* **2012,** *4*, 655-662.

15. Didraga, C.; Knoester, J., Optical Spectra and Localization of Excitons in Inhomogeneous Helical Cylindrical Aggregates. *J. Chem. Phys.* **2004,** *121*, 10687-10698.

16. Didraga, C.; Pugzlys, A.; Hania, P. R.; von Berlepsch, H.; Duppen, K.; Knoester, J., Structure, Spectroscopy, and Microscopic Model of Tubular Carbocyanine Dye Aggregates. *J. Phys. Chem. B* **2004,** *108*, 14976-14985.

17. von Berlepsch, H.; Kirstein, S.; Hania, R.; Pugzlys, A.; Böttcher, C., Modification of the Nanoscale Structure of the J-Aggregate of a Sulfonate-Substituted Amphiphilic Carbocyanine Dye through Incorporation of Surface-Active Additives. *J. Phys. Chem. B* **2007,** *111*, 1701-1711.

18. Sperling, J.; Nemeth, A.; Hauer, J.; Abramavicius, D.; Mukamel, S.; Kauffmann, H. F.; Milota, F., Excitons and Disorder in Molecular Nanotubes: A 2d Electronic Spectroscopy Study and First Comparison to a Microscopic Model. *J. Phys. Chem. A* **2010,** *114*, 8179-8189.

19. von Berlepsch, H.; Kirstein, S.; Bottcher, C., Effect of Alcohols on J-Aggregation of a Carbocyanine Dye. *Langmuir* **2002,** *18*, 7699-7705.

20. Milota, F.; Sperling, J.; Nemeth, A.; Abramavicius, D.; Mukamel, S.; Kauffmann, H. F., Excitonic Couplings and Interband Energy Transfer in a Double-Wall Molecular Aggregate Imaged by Coherent Two-Dimensional Electronic Spectroscopy. *J. Chem. Phys.* **2009,** *131*, 054510-23.

21. Womick, J. M.; Miller, S. A.; Moran, A. M., Correlated Exciton Fluctuations in Cylindrical Molecular Aggregates. *J. Phys. Chem. B* **2009,** *113*, 6630-6639.

22. Womick, J. M.; Miller, S. A.; Moran, A. M., Probing the Dynamics of Intraband Electronic Coherences in Cylindrical Molecular Aggregates. *J. Phys. Chem. A* **2009,** *113*, 6587-6598.

23. Spano, F. C., Modeling Disorder in Polymer Aggregates: The Optical Spectroscopy of Regioregular Poly(3-Hexylthiophene) Thin Films. *J. Chem. Phys.* **2005,** *122*, 234701-15.

24. Vlaming, S. M.; Bloemsma, E. A.; Nietiadi, M. L.; Knoester, J., Disorder-Induced Exciton Localization and Violation of Optical Selection Rules in Supramolecular Nanotubes. *J. Chem. Phys.* **2011,** *134*, 114507-11.

25. Lyon, J. L.; Eisele, D. M.; Kirstein, S.; Rabe, J. P.; Vanden Bout, D. A.; Stevenson, K. J., Spectroelectrochemical Investigation of Double-Walled Tubular J-Aggregates of Amphiphilic Cyanine Dyes. *J. Phys. Chem. C* **2008,** *112*, 1260-1268.

26. von Berlepsch, H.; Bottcher, C.; Ouart, A.; Regenbrecht, M.; Akari, S.; Keiderling, U.; Schnablegger, H.; Dahne, S.; Kirstein, S., Surfactant-Induced Changes of Morphology of J-Aggregates: Superhelix-to-Tubule Transformation. *Langmuir* **2000,** *16*, 5908-5916.

27. Milota, F.; Sperling, J.; Nemeth, A.; Kauffmann, H. F., Two-Dimensional Electronic Photon Echoes of a Double Band J-Aggregate: Quantum Oscillatory Motion Versus Exciton Relaxation. *Chemical Physics* **2009,** *357*, 45-53.

28. Jelley, E. E., Spectral Absorption and Fluorescence of Dyes in the Molecule State. *Nature* **1936,** *138*, 1009-1010.

29. Scheibe, G., Über Die Veränderlichkeit Der Absorptionsspektren in Lösung Und Die Nebenvalenzen Als Ihre Ursache. *Angew. Chem.* **1937,** *50*, 212-219.

30. Frenkel, J., On the Transformation of Light into Heat in Solids. I. *Phys. Rev.* **1931,** *37*, 17-44.

31. Scholes, G. D.; Rumbles, G., Excitons in Nanoscale Systems. *Nat Mater* **2006,** *5*, 683-696.

32. Spano, F. C., The Spectral Signatures of Frenkel Polarons in H- and J-Aggregates. *Acc. Chem. Res.* **2009,** *43*, 429-439.

33. Abrahams, E.; Anderson, P. W.; Licciardello, D. C.; Ramakrishnan, T. V., Scaling Theory of Localization: Absence of Quantum Diffusion in Two Dimensions. *Phys. Rev. Lett.* **1979,** *42*, 673-676.

34. Knoester, J., Modeling the Optical Properties of Excitons in Linear and Tubular J-Aggregates. *Int. J. Photoenergy* **2006**.

35. Hofrichter, J.; Eaton, W. A., Linear Dichroism of Biological Chromophores. *Annu. Rev. Biophys. Bio.* **1976,** *5*, 511-560.

36. Nordén, B., Applications of Linear Dichroism Spectroscopy. *Appl. Spectrosc. Rev.* **1978,** *14*, 157-248.

37. Nordén, B.; Rodger, A.; Dafforn, T., *Linear Dichroism and Circular Dichroism: A Textbook on Polarized-Light Spectroscopy*. Royal Society of Chemistry: Cambridge, 2010.

38. von Berlepsch, H.; Kirstein, S.; Hania, R.; Didraga, C.; Pugzlys, A.; Bottcher, C., Stabilization of Individual Tubular J-Aggregates by Poly(Vinyl Alcohol). *J. Phys. Chem. B* **2003,** *107*, 14176-14184.

39. v. Berlepsch, H.; Böttcher, C., Supramolecular Structure of Ttbc J-Aggregates in Solution and on Surface. *Langmuir* **2013,** *29*, 4948-4958.

40. Dafforn, T. R.; Rodger, A., Linear Dichroism of Biomolecules: Which Way Is Up? *Curr. Opin. Struc. Biol.* **2004,** *14*, 541-546.

41. Cone, C. W.; Cho, S.; Lyon, J. L.; Eisele, D. r. M.; Rabe, J. r. P.; Stevenson, K. J.; Rossky, P. J.; Vanden Bout, D. A., Singular Value Decomposition Analysis of Spectroelectrochemical Redox Chemistry in Supramolecular Dye Nanotubes. *J. Phys. Chem. C* **2011,** *115*, 14978-14987.

42. Didraga, C.; Klugkist, J. A.; Knoester, J., Optical Properties of Helical Cylindrical Molecular Aggregates: The Homogeneous Limit. *J. Phys. Chem. B* **2002,** *106*, 11474-11486.

43. Kobayashi, T., Ed., *J-Aggregates (Volume 2)*. World Scientific Publishing Company: Singapore, 2012.

44. Spano, F. C.; Clark, J.; Silva, C.; Friend, R. H., Determining Exciton Coherence from the Photoluminescence Spectral Line Shape in Poly(3-Hexylthiophene) Thin Films. *J. Chem. Phys.* **2009,** *130*, 074904-16.

45. Spano, F. C.; Yamagata, H., Vibronic Coupling in J-Aggregates and Beyond: A Direct Means of Determining the Exciton Coherence Length from the Photoluminescence Spectrum. *J. Phys. Chem. B* **2011,** *115*, 5133-5143.

46. Eisfeld, A.; Schulz, G.; Briggs, J., The Influence of Geometry on the Vibronic Spectra of Quantum Aggregates. *J. Lumin.* **2011,** *131*, 2555-2564.

47. Bednarz, M.; Knoester, J., The Linear Absorption and Pump-Probe Spectra of Cylindrical Molecular Aggregates. *J. Phys. Chem. B* **2001,** *105*, 12913-12923.

48. Pugzlys, A.; Augulis, R.; van Loosdrecht, P. H. M.; Didraga, C.; Malyshev, V. A.; Knoester, J., Temperature-Dependent Relaxation of Excitons in Tubular Molecular Aggregates: Fluorescence Decay and Stokes Shift. *J. Phys. Chem. B* **2006,** *110*, 20268-20276.

49. Eisele, D. M.; Knoester, J.; Kirstein, S.; Vanden Bout, D. A., Uniform Exciton Fluorescence from Individual Molecular Nanotubes Immobilized on Solid Substrates. *Nat Nano* **2009,** *4*, 658-663.

Chapter 3: Temperature-dependent exciton properties of C8S3 J-aggregates

3.1 INTRODUCTION

Molecular cyanine dye J-aggregates have been the target of intense experimental and theoretical investigation since their discovery in the 1930s.[1-6] The collective properties of J-aggregates are fundamentally different from the individual constituent dyes of which they are comprised. Strong dye dipole-dipole interactions give rise to excitons, new electronic transitions that extend across many dye molecules that are described according to the Frenkel exciton model.[7-10] Upon aggregation, the system's optical properties change dramatically, with the resulting aggregate absorption spectrum revealing narrowed and red-shifted excitonic J-bands as compared to the monomer.[1-2] Furthermore, J-aggregates exhibit a high absorption cross-section and small Stokes shift.[11-12] A diverse set of aggregate morphologies, which include linear chains, rings, and ribbons can form based on multiple factors such as chromophore side chains, solvent choice, and dye concentration.[8, 11, 13-17] Certain derivatives of the 5,5′,6,6′-tetrachloro-1,1′-dioctylbenzimidacarbocyanine (TBC) chromophore form aggregates with tubular geometries,[18] which are of interest as artificial light harvesting systems, energy transport materials and use in organic photovoltaic devices.[4, 11, 19-20]

This report will focus on the two J-aggregate structures formed from the TBC derivative, amphiphilic dye 3,3′-bis(2-sulfopropyl)-5,5′,6,6′-tetrachloro-1,1′-dioctylbenzimidacarbocyanine (C8S3). When C8S3 monomer solvated in methanol is introduced to water, double-walled nanotubes with diameters of ~ 15 nm form in under 24 hours.[16, 20] After months of aging, the nanotubes agglomerate into massive super-structures, termed bundles, with diameters over 500 nm observed via cryo-TEM and AFM. [16, 21-22] Self-assembly of C8S3 double-walled nanotubes is due to strong π-π

coupling between the chromophores as well hydrophobic interaction of the aliphatic side chains with the polar aqueous solvent.[8, 18, 23-24] The structure and optoelectronic properties of cylindrical cyanine dye J-aggregate nanotubes resemble those of rod-shaped bacteriochlorphyll aggregates, the light harvesting complexes of green photosynthetic bacteria.[25-28] As a result, the CSS3 nanotubes, which absorb in the visible region, are seen as potential candidates for utilization in artificial light harvesting systems.[3, 11] While significant theoretical and experimental efforts have resulted in a consistent structural model for the nanotubes,[20, 29] C8S3 bundles have not received the same level of attention. This is likely in part due to the somewhat unpredictable structural arrangement of the chromophores that comprise the bundles. In contrast to the remarkable C8S3 nanotube structural uniformity,[16, 19] the bundle diameter is based on solution age and is largely irregular.[16] Although little is known about bundle formation, all C8S3 nanotube solutions eventually bundle and exhibit the same absorption spectrum, suggesting this is the thermodynamically favored structure. Increased stability, combined with the recent report that energy migration distances in bundles greatly exceed what is measured in the isolated nanotubes,[21] clearly motivates the further investigation of the bundles' photophysical properties.

Because these aggregate systems interact strongly with light, spectroscopy provides a window with which to probe the excited states in these artificial light-harvesting materials. Previous experiments have examined the role of temperature in the exciton dynamics of J-aggregates, and revealed that critical characteristics including exciton migration distance,[30-32]fluorescence lifetime[33-35]and Stokes shift [31-32, 36] hinge on the available thermal energy. While the nanotubes have been investigated at 5 K,[36] the temperature dependent spectral features of the bundles has not been examined. We study

the effect of temperature on the excitonic absorption and emission of C8S3 nanotubes and bundles from 77-298 K.

The fluorescence quantum yield, Stokes shift, and exciton bandwidth and thermalization are investigated for both structures. C8S3 nanotubes emit from two states, which have previously been described as independent exciton transitions from the inner and outer cylinders.[20, 37] The extent of cylinder coupling has been debated and reported to range from weak[19, 29, 37-38] to strong.[39-43] While the structural arrangement of chomophores that comprise the bundles is uncertain, these super-structures also exhibit two emission bands. In order to determine if the aggregate emission in each system is better described by coupled states or independent exciton states in thermal equilibrium, he temperature-dependence of the two-band exciton emission is explored in both the nanotubes and bundles. In addition, we present experimental approaches for forming stable aggregate glasses at low temperatures and demonstrate that solvent effects have an unexpected consequence on the energy of C8S3 J-aggregate spectra.

3.2 EXPERIMENTAL

3.2.1 C8S3 nanotube and bundles solutions

C8S3 monomer dye powder (dye S0440, MW = 902.8 g mol^{-1}, FEW Chemicals, Germany) was stirred for 20 minutes in methanol (Fisher scientific, spectroscopic grade) to make a 2.32 mM C8S3 monomer stock solution. C8S3 J-aggregate nanotube solutions were prepared by adding 130 μL of the stock solution to 500 μL of high purity water (18MΩ cm, Barnstead). The solution was capped and stored in darkness. To stop the dye aggregation, an additional 500 μL of water was added to the solution after 5 to 24 hours. Bundling of the J-aggregate solutions was spectrally verified after a minimum of 3 months of room temperature storage in darkness. Ethylene glycol C8S3 nanotube

solutions were prepared by adding 50 μL of ethylene glycol (EM Science, 100%) to the nanotube solution after aggregation was complete. 'Half-route' nanotube solutions, which contain half the water as typical nanotube solutions, were prepared as described above, except the final 500 μL water addition was eliminated.

3.2.2 C8S3 J-aggregate spectroscopy

All steady state absorption spectra of C8S3 monomer, nanotubes and bundles were collected with a Hewlett Packard UV-Vis 8453 spectrophotometer using a 0.1 mm path length demountable quartz cuvette (Starna). Bulk fluorescence spectra of solutions were collected at 532 nm excitation using a Horiba Scientific FluoroLog®-3 spectrofluorometer; a 0.01 mm path length cell was used to avoid inner-filter effects (see appendix). In order to attain the correct sample height, a house-designed stand was machined so the UV-Vis and fluorometer could accommodate the cryostat. For low temperature absorption and fluorescence measurements, the C8S3 samples were either cooled rapidly in the cryostat (Janis Supertran 330) or flash-frozen in liquid nitrogen (LN2) then immediately placed in the cryostat equipped with a Lakeshore 330 temperature controller set to 77 K. Two sensors (one attached to the cryostat cold finger, the second directly to the sample cuvette) were used to monitor the sample temperature. Once the sample sensor reached 77 K, a minimum of 30 minutes was allotted for equilibration before a spectrum was acquired. The temperature was increased in increments of 30-50 K (30 minute equilibration for each temperature step) until the sample reached room temperature.

3.3 RESULTS AND DISCUSSION

3.3.1 C8S3 J-aggregates: formation and spectral signatures

C8S3 monomers, shown in Scheme 3.1, self-assemble in aqueous solution to form isolated double-walled tubular aggregates; the spontaneous dye organization is driven by π-π chromophore coupling and aided by the interaction of hydrophobic and hydrophilic side chains.[24] Solution preparation affects nanotube size, an effect detected by cryoTEM: when C8S3 monomer is directly dissolved in water, the tubes have 15 nm diameters (direct-route); if the monomer is first dissolved in methanol and then added to water, the tubes have 13 nm diameters (alcoholic-route).[16] Morphology clearly plays an important role in determining the characteristic absorption features for the C8S3 J-aggregates– each structure has a unique spectral signature. The alcoholic and direct-route nanotubes exhibit distinct absorption spectra with differing number and energies of transitions.[16]

Scheme 3.1 illustrates the structure of nanotubes and bundles. Bundling of tubules into super-structures comprised of the nanotubular building blocks occurs over a long time scale that can exceed six months.[16] All results presented herein are for alcoholic route nanotubes and bundles. Steady state, normalized room temperature C8S3 monomer, nanotube and bundle absorption spectra are shown in Figure 3.1. In contrast to the broad monomer dye absorption (in methanol, centered at 520 nm), C8S3 J-aggregate absorption is narrowed and red-shifted. The complex, but well-studied, double-walled nanotube absorption exhibits at least six excitonic bands,[29, 44] and is readily identified by the two sharp, lowest energy J-bands centered at 589 and 599 nm. The lowest energy band is attributed to transitions to nanotube's inner wall (IW) states, while the higher energy (589 nm) absorption is due to outer wall (OW) transitions.[20, 29, 45] The bundle absorption spectrum is defined by a broad transition at 575 nm and a sharp transition at 602 nm. A decrease in absolute absorption (relative to the nanotubes) upon bundling is observed,[16]

which is likely the result of the physical size of the bundles exceeding the skin depth of the excitation light in the absorption experiment.

3.3.2 C8S3 J-aggregates: temperature dependent steady state spectroscopy

a. Absorption

Previous attempts at collecting direct-route (solvated in only water) C8S3 nanotube absorption spectra at low temperatures were unsuccessful due to noisy spectra caused by light scatter; only peak positions were observed.[36] Figure 3.2a shows the alcoholic-route C8S3 nanotube excitonic absorption spectra for temperatures ranging from 77-298 K; the corresponding bundle spectra are given in Figure 3.2b. Absorption spectra were collected at 298 K, and the room temperature sample was placed into the cryostat and cooled rapidly to 77 K. Although the spectra are slightly noisy, again due to light scatter, the absorption profiles are unchanged with temperature; however, the absorption maxima shift to higher energy at lower temperature for both aggregate structures. The spectral shift is monotonic in this temperature range, ~ 1 nm per 50 K temperature step.

Forming stable aggregate glasses at low temperatures was integral to this spectral study. The aggregate solutions are primarily water; as the solution rapidly cools and forms a glass, the water expands and tends to shatter. In order to collect low-noise nanotube absorption spectra, we adjusted the typical nanotube solution preparation. The first solution modification was the addition of ethylene glycol (EG) to form a more stable glass upon sample cooling, a method introduced by Cooper[46] and utilized in numerous low temperature J-aggregate studies.[35, 46-50] Figure 3.3a shows the absorption spectra at varying temperatures for the EG nanotubes; the pristine EG absorption profiles show excellent signal to noise and there is minimal variance (< 5 %) in exciton J-band widths

as the temperature is modulated from 77-298 K. A second method used to collect low noise spectra was to decrease the fraction of water in the J-aggregate sample by preparing 'half-route' nanotubes. Half-route aggregate solutions, which were flash-frozen before being placed in the cryostat, were used immediately after aggregation verification with steady state absorption measurements. Figure 3.3b displays half-route nanotube absorption spectra at varying temperatures. Like the ethylene glycol (EG) nanotube solutions, the half-route nanotube absorption profiles show improved signal to noise.

Although the EG and half route nanotube absorption profiles are pristine, the EG and half-route nanotubes' absorption energy does not vary with sample temperature. It should be noted that the EG and half route nanotube solutions were flash-frozen (by immersion in LN2) before being placed in the cryostat, and we do not observe the same systematic blue spectral shift noted above for the regularly prepared solutions (that were not flash-frozen but rapidly cooled in the cryostat). It was previously reported that LN2 flash-frozen, direct-route C8S3 nanotube absorption maximum blue shifted ~ 6 nm upon cooling to 5 K,[36] but the low temperature spectral profiles were not fully resolved. The magnitude of the reported direct-route nanotube shift agrees well with what we clearly measured for the alcoholic-route nanotubes, seen in Figure 3.2a. The low temperature spectral blue shift appears for both flash-frozen and rapidly cooled nanotube samples, which suggests that sample preparation, rather than cooling rate, is the cause of the spectral shift. The aggregate structures, and therefore spectra, are extremely sensitive to solvent and surfactant effects;[16, 20] thus, it follows that altering the solvent conditions via the addition of EG (or by decreasing the water:methanol ratio, as in the half-route nanotubes) prevents the blue shift that is observed for the conventionally prepared nanotube samples.

To determine the origin of the J-aggregate spectral blue shift, absorption spectra of C8S3 monomer in only methanol and in a methanol/EG solution were collected at 77 K (flash-frozen) and 298 K; these four monomer spectra are overlaid in Figure 3.4. The absorption profile of monomer solvated in only methanol exhibits a blue shift of 2 nm at 77 K as compared to room temperature, while no spectral shift is observed for the monomer in a mixture of methanol/EG, which confirms the theory that the solvent rather than cooling method, influences whether or not a spectral blue shift is observed for the molecular aggregates at low temperature.

b. Total Emission and Relative Quantum Yield

Bulk fluorescence emission spectra were collected for C8S3 nanotubes and bundles; all aggregate solutions were flash-frozen in LN2 before emission spectra were acquired. C8S3 nanotube and bundle emission spectra from 77 to 298 K are displayed in Figures 3.5a and 3.5b, respectively. For both structures, the total emission decreases monotonically as the temperature is stepped back to room temperature. The total nanotube fluorescence intensity varies greatly with temperature, while the measured change in total bundle emission is less significant. Since the absorption profiles do not vary with temperature and the absorption is steady at the excitation wavelength (λ_{ex} = 532 nm ≈ 18880 cm^{-1}) across the temperature range, the relative fluorescence quantum yield was determined for the both J-aggregate structures by integrating the emission spectra and normalizing by the respective room temperature intensity. Figure 3.5c displays the relative quantum yield for C8S3 nanotubes and bundles. At 77 K, the nanotubes are roughly twelve times brighter than at room temperature. The quantum yield (Φ_{QY}) of C8S3 nanotubes is taken to be equivalent to the structurally similar tubular C8O3 J-aggregates, which is 0.035 at room temperature[51-52] and the nanotube fluorescence

lifetime, ~100 ps at 298 K[52] decreases as the temperature is lowered;[36] both results support the notable increase in nanotube Φ_{QY} at low temperature. Conversely, the bundles show a subtler response to varying temperature than the nanotubes: the relative Φ_{QY} increased by less than a factor of 2 when the temperature was modulated from 298 K to 77 K, as seen in Figure 3.5c.

C8S3 nanotubes and bundles have nearly equal absorption at 532 nm, the chosen excitation wavelength. Nanotube and bundle emission were each measured three times, and for every trial (equal integration times, slit widths, and same sample cell), the bundles exhibit a total intensity that is essentially 1 order of magnitude greater than the nanotubes (Figures 3.5a and 3.5b). It is possible that the bundles' absolute Φ_{QY} is much higher than the nanotubes, which could explain the comparatively muted fluorescence increase at low temperature. Another scenario accounts for the system's structural hierarchy: the Φ_{QY} decreases when the monomer dye aggregates into double-walled nanotubes, which is attributed to an increase in non-radiative relaxation pathways.[51] By the same logic, it does not follow that a dramatic increase in QY would accompany the further agglomeration of C8S3 nanotubes into bundles.

It is well known that J-aggregate fluorescence lifetime decreases with decreasing temperature.[35, 53-55] At room temperature, C8S3 nanotubes have a fluorescence lifetime of ~ 100 ps,[52] and C8S3 bundle lifetime is two exponential, with slower decay constants of 200 ps (88% relative amplitude) and 2 ns.[21] Aggregate dimensionality is known to influence the temperature dependence of the radiative lifetime;[35, 56] previous work indicates that excitons migrate in two dimensions (2-D) across the bundles,[21] while the nanotubes are assumed to be quasi one-dimensional (1-D) exciton systems.[19] Theoretical analysis predicts that the temperature dependence of the radiative lifetime is stronger for 2-D excitons than for 1-D excitons,[35, 53] but many cyanine J-aggregates, including PIC[55]

and TDBC,[57] show a much stronger dependence of QY and radiative lifetime on temperature than predicted. Even if the bundles and nanotubes respective radiative lifetimes exhibited identical response to temperature, it does not account for the sensitivity of their relative non-radiative rates to temperature.

c. Normalized emission and thermalization

Normalized emission spectra of C8S3 nanotubes at temperatures ranging from 77 K to 298 K are displayed in Figure 3.6a. At room temperature, the nanotubes display no Stokes shift, and emit from exciton states centered at 16694 and 16977 cm^{-1} (599 and 589 nm). The systematic blue shift of the spectrum at low temperature, noted above for the absorption, is clearly evident in the nanotube fluorescence spectra. The spectra demonstrate that the nanotubes emit from two exciton states: the low-intensity upper (energy) band corresponds to the OW, while the majority of emission emanates from IW (lower energy band) exciton states.[20, 45] As the sample temperature is decreased, the OW emission is depressed. If the two cylinders are in thermal equilibrium before emission occurs, the emission population ratio P_{IW}/P_{OW} should follow the Boltzmann factor:

$$\frac{P_{OW}}{P_{IW}} = \frac{g_{OW}\exp^{-E_{OW}/k_B T}}{g_{IW}\exp^{-E_{IW}/k_B T}} = \frac{g_{OW}}{g_{IW}}\exp^{-\Delta E/k_B T} \qquad (1)$$

where g_{OW}/g_{IW} represents density of states from the absorption profile. The linear form of this relationship is given by:

$$\ln\left(\frac{P_{OW}}{P_{IW}}\right) = \ln\left(\frac{g_{OW}}{g_{IW}}\right) - \frac{\Delta E}{k_B T} \qquad (2)$$

Nanotube emission spectra were fit using two Lorentzian functions to determine this experimental emission ratio at all temperature steps; a representative fit is shown for the 127 K spectrum in the inset of Figure 3.6a. The Lorentzian areas were calculated, and the natural log of the peak area ratios was plotted vs $1/k_BT$, as shown in Figure 3.6c. Data points were fit with a simple linear regression; the slope of the line gives the experimental $\Delta E_{FIT} = 245 \pm 17$ cm^{-1}, which is very close to the expected $\Delta E = 280$ cm^{-1}, that is based on the fits to the nanotube absorption spectrum.

To determine how ΔE_{FIT} varied from the predicted energy difference across the temperature range, experimental and Boltzmann calculated spectra were compared at each temperature. An overlay of these spectra for each temperature step, as well as the calculation method, is presented in the appendix. According to Boltzmann statistics, if the energy transfer (ET) from the OW to the IW is thermalized, OW emission should decrease as the temperature is lowered and until none is observed at 77 K. Generally, there is excellent agreement between the calculated and experimental nanotube emission and the trend is observed (shown in Figure 3.6a), but we observe slightly more upper band (OW) emission than predicted by Boltzmann statistics across the temperature range. The nanotube OW absorption is stronger than the IW absorption, but the majority of nanotube emission is from the IW, which suggests that significant ET occurs between the nanotubes IW and OW cylinders before emission takes place.[36] Nanotube absorption population ratios do not change with temperature (Figures 3.2a, 3.3a, and 3.3b); thus, we can definitively state that the ET between the cylinders does not diminish even as thermal energy is removed from the system. At 77 K, some OW excitation cannot transfer to the IW, likely due to thermalization occurring on roughly the same time scale as the fast fluorescence emission (< 100 ps at 5 K).[36]

Normalized emission spectra for C8S3 bundles at temperatures ranging from 77 K to room temperature are displayed in Figure 3.6b. At room temperature, the bundles exhibit two-band emission, centered at 16610 and 16992 cm^{-1} (602 and 589 nm), and like the nanotubes display no Stokes shift. Unlike the nanotubes, the high-energy bundle emission maximum does not directly correspond to a resolved absorption transition. Interestingly, the 589 nm bundle emission energy corresponds to the strongest nanotube OW absorption band, which suggests that that state is preserved upon bundling, and that relaxation to that state occurs on the bundles emission time scale. Alternatively, the high-energy bundle emission could be attributed to unbundled nanotubes that remain in solution. However, Eisele et al. have recently presented 3-D visualization of the bundles' structure using Cryo-EM tomography, where inter-cylinder distances suggest that only IW cylinders comprise the bundle super-structure and OW dye molecules rearrange to form a protective bundle envelope.[22] This bundle structural determination indicates that the 589 nm bundle emission is unrelated to the nanotube OW, and instead corresponds to an excitonic state unique to the bundle aggregate morphology. Furthermore, the 589 nm bundle emission is not diminished at 77 K, which we would expect if it were due to residual, un-bundled nanotubes in solution.

Similar to the nanotubes, as the temperature of the bundle sample is decreased, the high-energy emission declines; this is shown in Figure 3.6b. As such, an analogous analysis approach was utilized to characterize the bundle emission, even though the bundle emission ratio change is visibly less dramatic than observed for the nanotubes (Figure 3.6a). The bundle spectra were fit using two Lorentzian functions; the bundle spectrum at 188 K and resulting fit are given in the inset of Figure 3.6b. The natural log of bundle area ratios vs $1/k_BT$ is plotted in Figure 3.6c. The slope of the linear fit gives $\Delta E_{FIT,\ BUNDLES} = 60 \pm 8\ cm^{-1}$, which is considerably less than the predicted energy

difference. We observe significantly more high-energy bundle emission at all temperatures than is predicted by Boltzmann statistics; experimental and Boltzmann calculated bundle spectra are compared at 77 K and 298 K in Figures 3.7a and 3.7b. Boltzmann statistics predicts emission resonant with the lowest energy J-band at any temperature, but we observe higher energy fluorescence at each temperature step. This result indicates that exciton thermalization does not occur for the bundles on the timescale of emission at any temperature between 77 and 298 K, and even suggests that two unique bundle structures may exist.

3.3.3 Stokes shift and FWHM

The absorption and emission maxima for both C8S3 nanotubes and bundle solutions are sensitive to temperature changes, which is qualitatively shown in Figures 3.2 and 3.5. The exact nanotube absorption and emission maxima (red open and filled squares, respectively) are displayed in Figure 3.8a. The bundle absorption and emission maxima (black open and filled circles) are shown on the same plot. The magnitude of the aforementioned spectral blue shift is nearly identical for both the nanotubes and bundles (~ 100 cm^{-1} over the measured temperature range). The calculated Stokes shifts for both aggregate structures at each temperature are shown in Figure 3.8b; neither structure exhibits a Stokes shift at room temperature. While the nanotubes Stokes shift hovers around zero across the entire temperature range, a steady increase to ~ 35 cm^{-1} (~1 nm) is observed for the bundles. Time resolved experiments have already revealed that direct-route C8S3 nanotubes exhibit a dynamic Stokes shift only at temperatures below 60 K[36], which agrees well with our measured results above 77 K. However, we detect a growing Stokes shift for bundles at much higher temperatures than necessary to observe the nanotubes' Stokes shift. For linear, 1-D J-aggregates the Stokes shift is attributed to

excitation migration to low energy segments before emission.[58] The bundles, comprised of multiple agglomerated nanotubes, might exhibit increased accessibility to lower energy exciton states due to stabilization provided by the outer layers of the bundle system that is unavailable to the isolated nanotubes.

Two low-dimensional J-aggregates exhibit a noteworthy temperature dependence of the relative Stokes shift (Stokes shift normalized to the fluorescence FWHM), which was categorized into three temperature regimes and further related to density of states accessibility.[31-32] It was suggested by the authors that the phenomenon was generic and could be extended to other low-dimensional aggregate systems. When a similar analysis was attempted for the C8S3 J-aggregates, the same trend was not observed. We attribute this inconsistency to fundamental differences in disorder between the aggregate systems: the J-aggregates that are well described by this method, PIB and THIATS, are very disordered (exhibit ~10X greater spectral bandwidths) and show a much stronger temperature dependence on Stokes shift as compared to the C8S3 J-aggregates.

The temperature dependence of absorption and emission exciton bandwidths was investigated for C8S3 nanotubes and bundles from 77 K to 298 K. The absorption and emission spectra were fit using Lorentzian functions. The absorption and emission full width at half maxima (FWHM) of the lowest energy J-band at each temperature step are presented in Figures 3.9a and 3.9b, respectively. The nanotubes (red squares) and bundles (black circles) both exhibit very narrow absorption and emission FWHM at room temperature, with bundles being slightly larger. For both C8S3 J-aggregates structures, the fluorescence band is narrower than the absorption band at all temperature steps and the narrowing is more pronounced for the emission. At 77 K, the bundle *(nanotube)* absorption FWHM is ~ 80% *(95%)* of the spectral width at 298 K; at 77 K, the bundle *(nanotube)* emission FWHM is ~ 70% *(90%)* of the spectral width at 298 K. This is likely

due to fast relaxation to a more narrow exciton distribution before emission occurs. For both nanotubes and bundles, the ΔFWHM (absorption - emission) increases as the temperature is lowered. Overall, bundle emission narrowing is more pronounced than for the nanotubes (average $\Delta FWHM_{NANOTUBES}$ = 6 cm^{-1} and $\Delta FWHM_{BUNDLES}$ = 12 cm^{-1}); this could be explained by the bundles' longer emission lifetime, which would allow for increased relaxation before emission. Furthermore, C8S3 nanotubes show remarkable uniformity and have a complicated, but well characterized, absorption spectrum comprised of multiple sharp transitions.[20, 29, 44] Conversely, the bundle spectrum is not well understood, but includes a broad higher energy J-band, indicating a higher degree of disorder. The disorder difference between the two aggregate structures likely contributes to the difference in observed narrowing: the nanotubes might exhibit such structural uniformity that considerable narrowing will not be noticed until very low temperature (5 K).[36]

The considerable narrowing of bundle emission is depicted in Figure 3.10b by overlaying the spectra at 77 K and 298 K. In contrast, the nanotube emission band narrowing, displayed in Figure 3.10a, is very minor. It is reasonable to expect the nanotubes and bundles spectra to exhibit both homogenous and inhomogeneous broadening.[59-60] We hypothesize that spectral narrowing at low temperature is in part due to relaxation to lower exciton states before emission. Assuming the $FWHM_{fl}$ is reflective of the homogenous linewidth, the excess width in the absorption should reflect an inhomogeneous distribution of transitions. Relaxation of this distribution to the lowest energy state would lead to a small Stokes shift. To assess if the bundle spectral narrowing is exclusively related to the observed Stokes shift, we compared the calculated absorption FWHM, $FWHM_{abs}$ (calculated) = $FWHM_{fl}$ + Stokes Shift, to the experimental absorption FWHM. The $FWHM_{fl}$ is reflective of the homogenous line width. At T < 200 K, the

magnitude of the measured Stokes shift is not enough to account for the narrowing upon emission (appendix), which suggests that inhomogeneous broadening contributes to the observed spectral widths.

3.4 CONCLUSIONS

The temperature dependent relative quantum yield, absorption and emission line widths, and Stokes shift are presented for two J-aggregate structures of the amphiphilic cyanine dye C8S3: double-walled nanotubes and bundled nanotube superstructures. Steady-state absorption and emission spectra were collected from 77 – 298 K. This work represents the first temperature-dependent spectral study of C8S3 bundles, which (along with the nanotubes) are promising materials for use in optical devices;[21-22] a thorough time-resolved examination of direct-route C8S3 nanotube emission from 5–100 K is found in reference 37.

Previous attempts at determining low temperature C8S3 nanotube absorption were marred by light scatter.[36] The J-aggregates' absorption spectral structure varies subtly as the temperature is modulated. Both aggregate structures exhibit a monotonic blue spectral shift as the temperature is lowered that is reproduced in the fluorescence emission. The magnitude of the shift is nearly identical for both the nanotubes and bundles. To collect low-noise aggregate absorption spectra, two alternate methods of solution preparation were utilized. While the EG and half-route absorption profile shapes are equivalent to the typically prepared nanotube solutions, the spectral blue shift at low temperature was not observed for the alternatively prepared solutions. Further investigation of low temperature monomer spectral behavior revealed that the monomer absorption maximum is sensitive to solvent effects. We conclude that the blue shift measured for the typically prepared J-aggregates is not exclusively a temperature effect,

and instead depends on how the solvent matrix affects the energy of the monomer transition.

Since the absorption spectral profiles do not change from 77 – 298 K, the temperature dependence of relative quantum yield was elucidated for both J-aggregate structures. Both structures show an increase as the temperature was lowered, but the nanotubes' relative quantum yield was almost 5 times more sensitive to temperature than the bundles. The nanotubes show no dependence of the Stokes shift on temperature, an outcome that aligns well with results from time resolved emission experiments,[36] whereas a small bundles Stokes shift steadily grows in as the temperature is lowered. The absorption and emission linewidths varied more across the temperature range for the bundles than the nanotubes. The bundle spectral narrowing as the temperature was lowered cannot be completely accounted for by the Stokes shift, which is likely do to relaxation to lower exciton states before emission. The bundle (and nanotube) steady state spectral properties will be investigated in future experiments at the 5–100 K temperature range. While there is minimal spectral narrowing and no Stokes shift for alcoholic-route C8S3 nanotubes at 77 K, substantial emission narrowing is expected at extremely low temperature.[36] Of particular interest is the aggregates' spectral widths and Stokes shift at very low temperature, in order to assign the extent of spectral broadening to homogeneous or heterogeneous disorder. The bundles, which show a ~ 1 nm Stokes shift at 77 K, should have an increased number of environments compared to well separated nanotubes, and expect to observe a comparatively larger Stokes shift and more narrowing at 5 K.

Both studied aggregates exhibit two emission bands, where the high-energy band decreases as thermal energy is removed. Normalized emission spectra were fit with Lorentz functions and compared to Boltzmann calculated spectra, which revealed that the

nanotube emission is well described using a Boltzmann model while the bundles' is not. As such, we find that the nanotubes inner and outer cylinder walls are in thermal equilibrium and that energy transfer between the two cylinders occurs before or on the timescale of emission. Furthermore, the emission band ratios could be used as a spectral thermometer for the J-aggregate systems.

Recent imaging of exciton transport in C8S3 nanotubes and bundles shows impressive, but varying, extents of exciton migration in the two J-aggregate structures; low temperature imaging should help elucidate the transport mechanism.[9, 21, 61] The determination of the nanotubes and bundles spectral behavior, presented here from 77-298 K temperature range, is critical for the verification of aggregate morphology at low temperature, a result that is significant for future low-temperature aggregate investigations. The aggregate structures are delicate, and our results indicate that both nanotubes and bundles remain intact over the interrogated temperature range, even when subjected to solvent modification and multiple cooling methods.

3.5 APPENDIX

3.5.1 Boltzmann calculated and experimental C8S3 nanotube emission

a. C8S3 nanotubes

Boltzmann-calculated C8S3 nanotube emission spectra were calculated over the temperature range from 77 - 298 K. The nanotube absorption spectrum has been modeled using six transitions, labeled peaks 1-6.[44] These transitions were used to calculate nanotube emission spectra, at each temperature step, using the following method:

$$\text{Boltzmann emission} = \text{peak1} + \sum_{\text{j=2}}^{6} B_j * peak_j$$

$$\text{where } B_j = exp^{-\Delta E_j / k_B T} \text{ and } \Delta E_j\left(cm^{-1}\right) = E_{max}\left(peak\ 1\right) - E_{max}\left(peak\ j\right)$$

The calculated and experimental spectra are overlaid at various temperatures in Figure 3.11. While there is good agreement between the two, slightly more high-energy emission is observed than is predicted by Boltzmann statistics.

b. C8S3 bundles

There is no well-defined, published model for C8S3 bundle absorption, so a slightly different method was used to calculate the Boltzmann predicted emission spectra:

$$\text{Boltzmann emission (bundles)} = exp^{-E/k_BT} * A(E, cm^{-1})$$

where $A(E, cm^{-1})$ is the experimental bundle absorption spectrum.

3.5.2 Comparison of experimental and calculated C8S3 bundle absorption FWHM

To assess if the bundle spectral narrowing is exclusively due to the Stokes shift, we compared the calculated absorption FWHM to the experimental absorption FWHM, shown as a function of temperature in Figure 3.12.

$$\text{calculated FWHM}_{\text{absorption}} = \text{experimental FWHM}_{\text{fluorescence}} + \text{Stokes shift}$$

Across the measured temperature range, the magnitude of the measured Stokes shift is not enough to account for the narrowing upon emission, which suggests that inhomogeneous broadening contributes to the observed spectral widths.

3.5.3 C8S3 J-aggregate self-absorption effect

C8S3 J-aggregates exhibit almost no Stokes shift, and self-absorption affects fluorescence measurements by depressing the high-energy emission band. Rather than diluting the J-aggregate solutions, self-absorption effects were eliminated by using a very short path length (0.01 mm) demountable cuvette (Starna). The nanotube solutions were prepared as described above (3.3×10^{-4} M), then diluted with a methanol/water (10% methanol by volume) solution. Dilution factors are 1:1, 1:15, and 1:30. Undiluted and

1:1 solution emission spectra in two cells (0.10 mm and 0.01 mm) are compared in Figure 3.13. The undiluted and 1:1 spectra collected in the 0.10 mm cell show more blue edge signal attenuation than the same solutions in the 0.01 mm cell. Any dilution greater than 1:15 did not further reduce the aggregate self-absorption, which can be seen in Figure 3.13; normalized undiluted and 1:30 nanotube spectra taken in the short path cell overlay perfectly with 1:15 and 1:30 nanotube spectra taken in the longer path length cell.

3.6 FIGURES

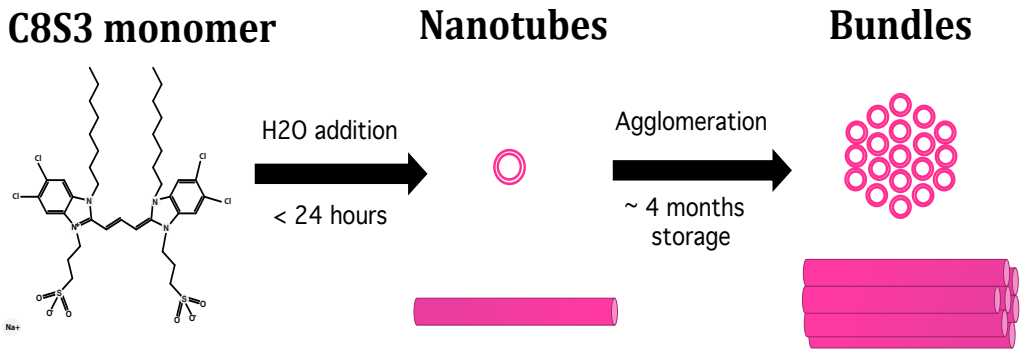

Scheme 3.1 Cartoon depicting C8S3 aggregation

The carbocyanine monomer dye is well solvated in methanol. Double-walled cylindrical J-aggregates form quickly when water is added to the methanol dye solution. Dipole-dipole coupling between the monomers and interactions between water and the hydrophilic sulfonate and hydrophobic octyl side chains drive the aggregation. After many months of storage, the nanotubes spontaneously assemble into close-packed super-structures composed of nanotubular building blocks. Cartoons

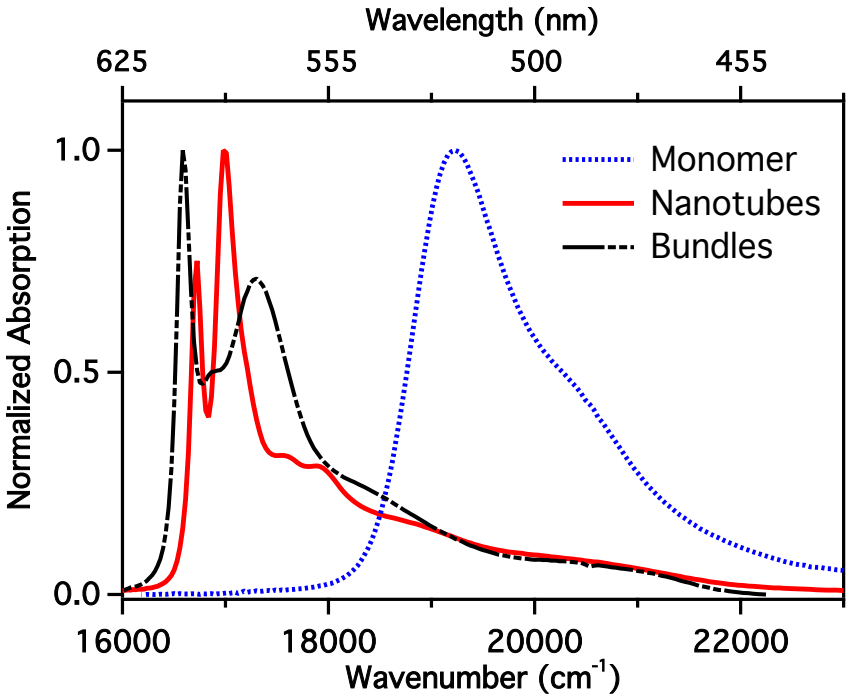

Figure 3.1 C8S3 optical absorption spectra

Optical absorption of C8S3 monomer (blue dashed line, methanol solution), nanotubes (red solid line, H_2O/methanol solution) and bundles (black dash/dot line, H_2O/methanol solution). The nanotubes and bundles exhibit narrowed and red-shifted excitonic absorption bands when compared to the well solvated monomer, both spectral signatures of J-aggregates. \

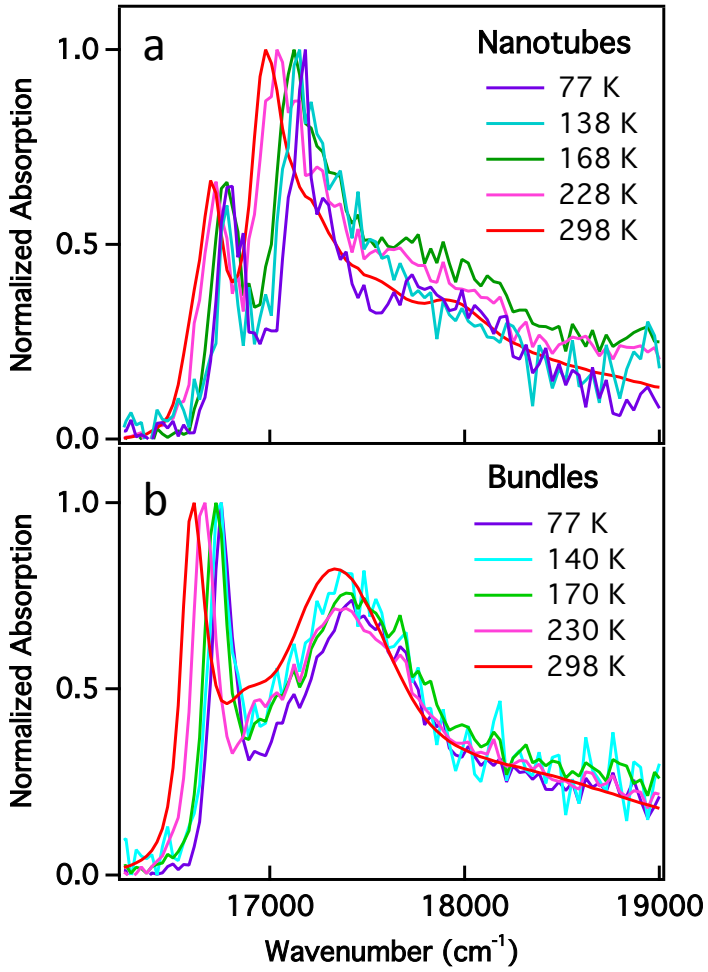

Figure 3.2 Temperature-dependent C8S3 J-aggregate absorption

Absorption spectra of C8S3 J-aggregate (a) nanotubes and (b) bundles from 77 –298 K. For both J-aggregate structures, a systematic blue shift of the spectrum is observed as the sample temperature is lowered.

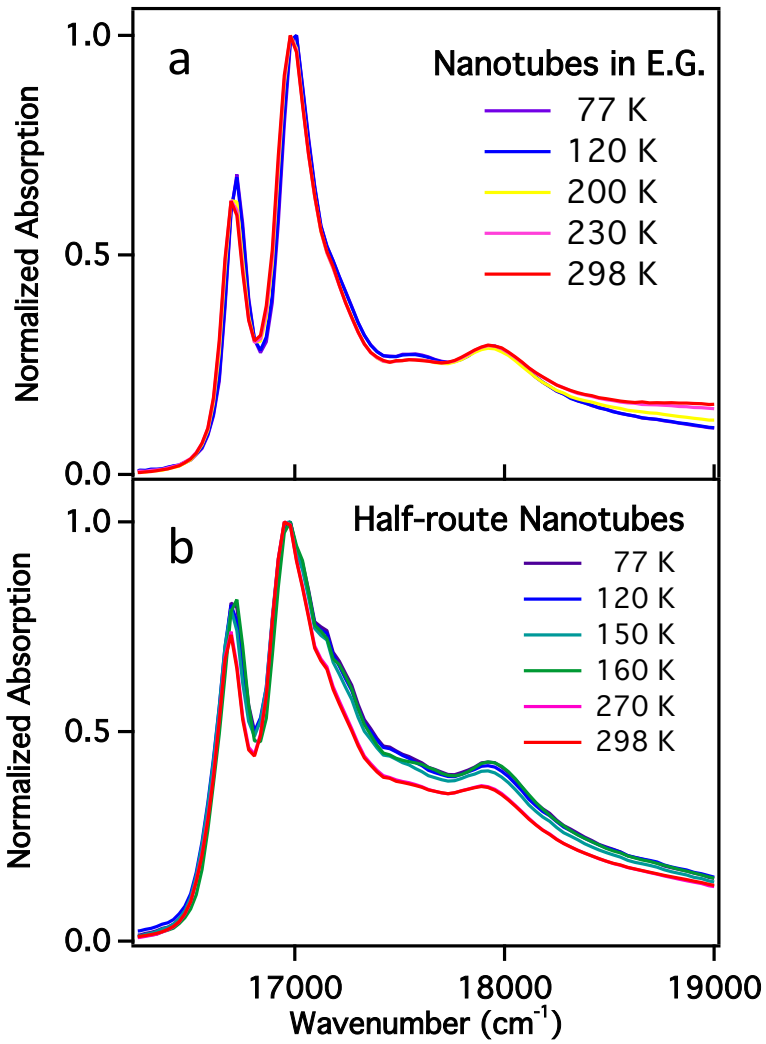

Figure 3.3 C8S3 nanotube absorption: solvent effects

Two methods were utilized to collect high signal to noise spectra, which are plotted from 77–298 K. (a) Absorption spectra of C8S3 J-aggregate nanotubes solvated in a mixture of methanol and ethylene glycol (EG). (b) 'Half-route' nanotubes are solvated in only methanol/water, but contain half of the water as compared to typically prepared nanotube solutions. The solvent adjustments greatly decreased scatter, and also suppressed the spectral blue shift observed for typically prepared nanotubes at low temperature.

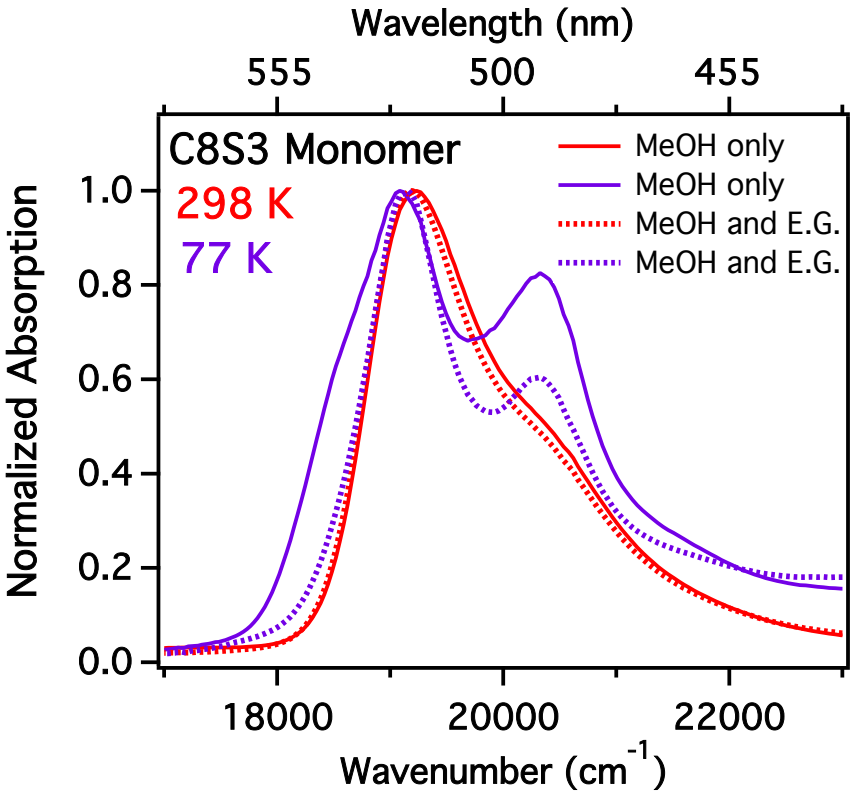

Figure 3.4 Temperature-dependent C8S3 monomer absorption

Absorption spectra of C8S3 monomer solvated in methanol (the typical solvent) at 298 K (red solid) and 77 K (purple solid); the spectrum blue shifts ~2 nm upon cooling. In contrast, C8S3 monomer in methanol/ethylene glycol solution does not shift when the temperature is lowered from 298 K (red, dotted) to 77 K (purple, dotted).

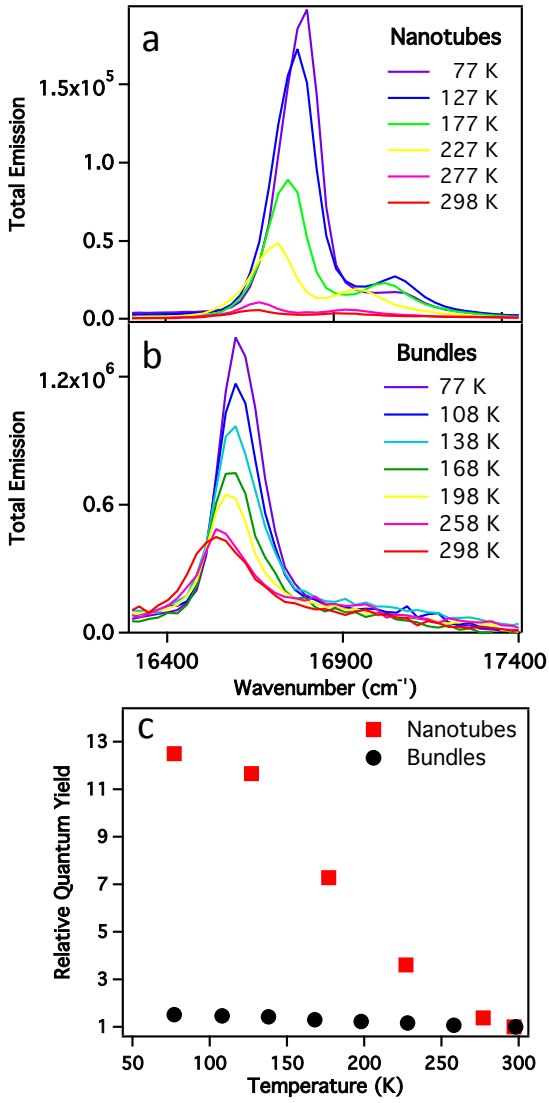

Figure 3.5 Temperature-dependent C8S3 emission and quantum yield

Emission spectra (total) of C8S3 J-aggregate (a) nanotubes and (b) bundles. (c) Temperature dependent relative quantum yield of nanotubes (red squares) and bundles (black circles) from 77 K – 298 K. was determined by integrating over the emission band and normalizing to room temperature.

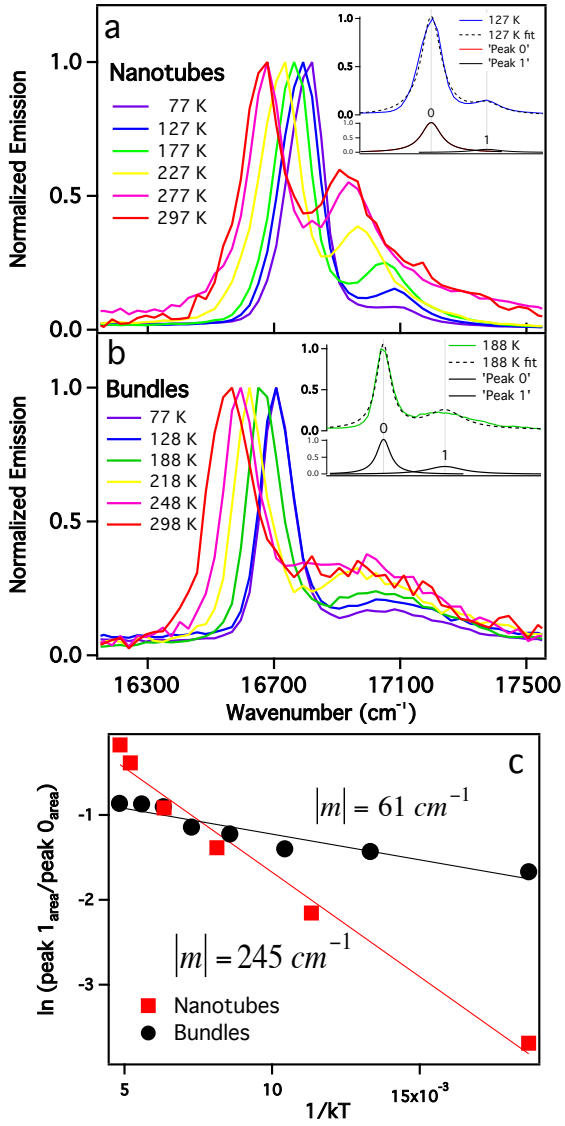

Figure 3.6 Boltzmann analysis of C8S3 J-aggregate emission

Normalized emission spectra of C8S3 (a) nanotubes and (b) bundles from 77 K to room temperature. Each spectrum was fit using two Lorentzians, peak 0 (low energy) and peak 1 (high energy); representative fits are shown in the insets. (c) The peak ratios were used to determine if the spectra fit to the Boltzmann distribution distribution by relating the slope to the experimentally known ΔE.

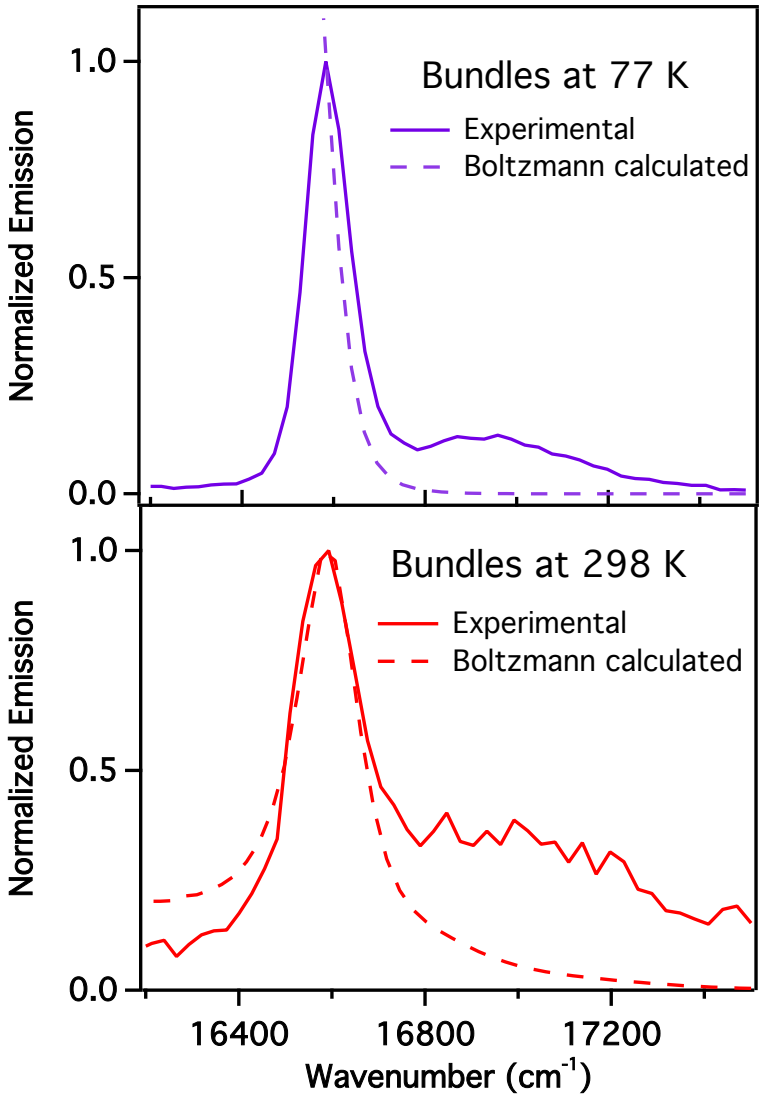

Figure 3.7 C8S3 bundle experimental and calculated emission

Experimental and Boltzmann calculated C8S3 bundle fluorescence emission spectra at (a) 77 K and (b) 298 K. At both temperatures, more high-energy emission is observed than is predicted by the model.

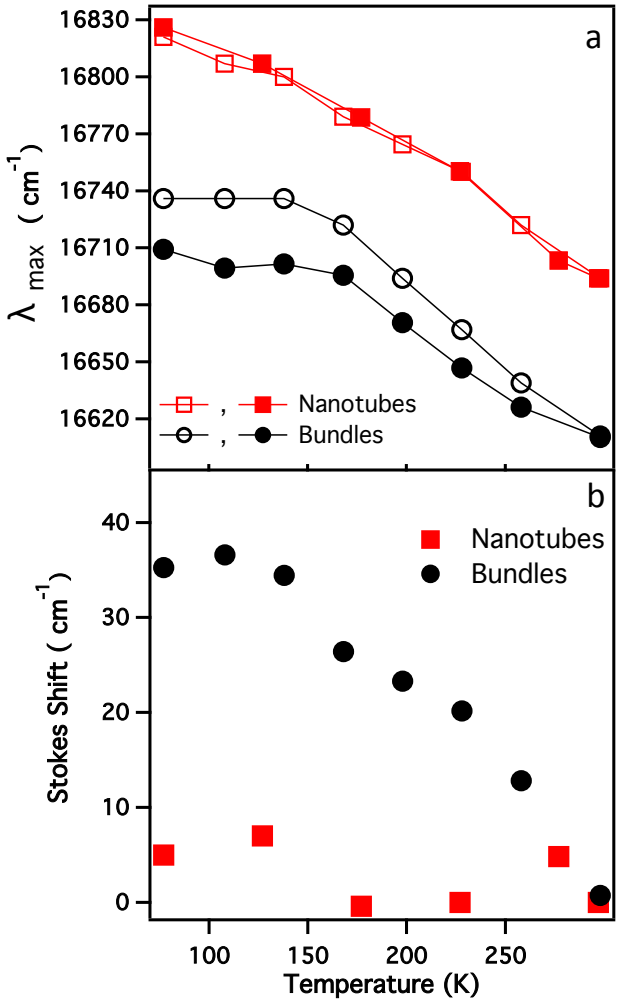

Figure 3.8 C8S3 J-aggregate temperature-dependent Stokes shift

(a) Absorption (open shapes) and emission (filled shapes) maxima for the lowest energy C8S3 nanotube (red square) and bundle (black circle) J-bands. The lines are not fits to the data points, and are present to guide the reader's eye. (b) Temperature dependent Stokes shift for C8S3 nanotubes (red squares) and bundles (black circles). The nanotubes show no Stokes shift over the measured range.

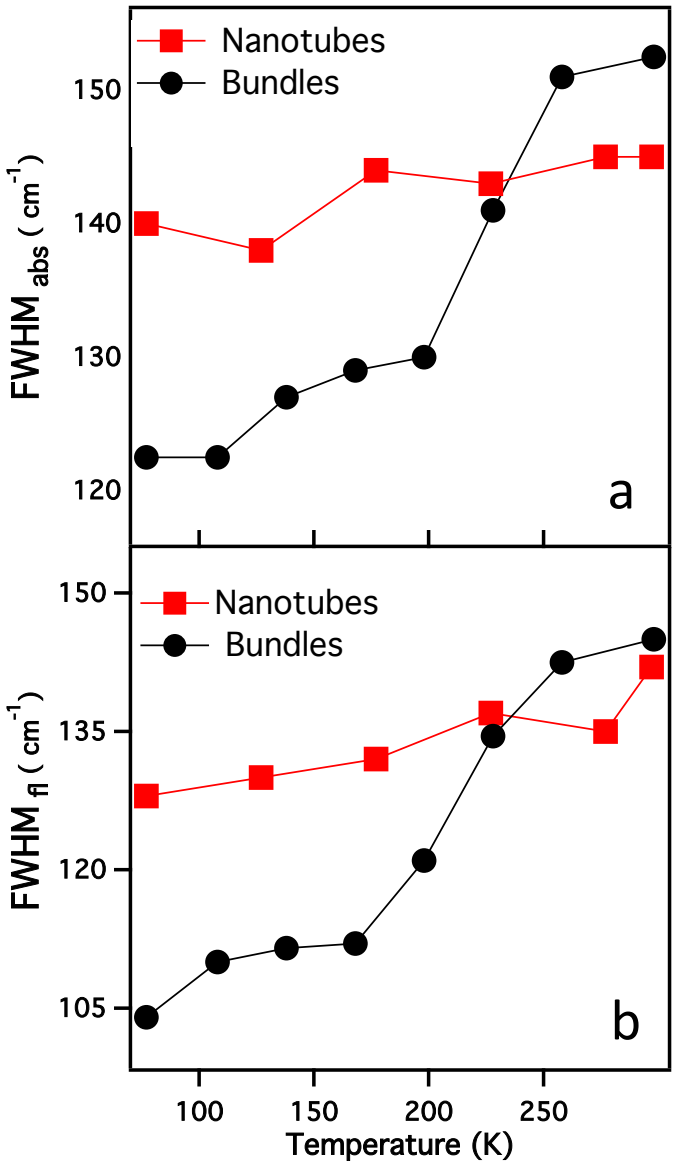

Figure 3.9 C8S3 J-aggregate temperature-dependent FWHM

Temperature dependent (a) absorption and (b) emission FWHM for the lowest energy C8S3 nanotube (red square) and bundle (black circle) J-bands. The lines are not fits and are present to guide the eye.

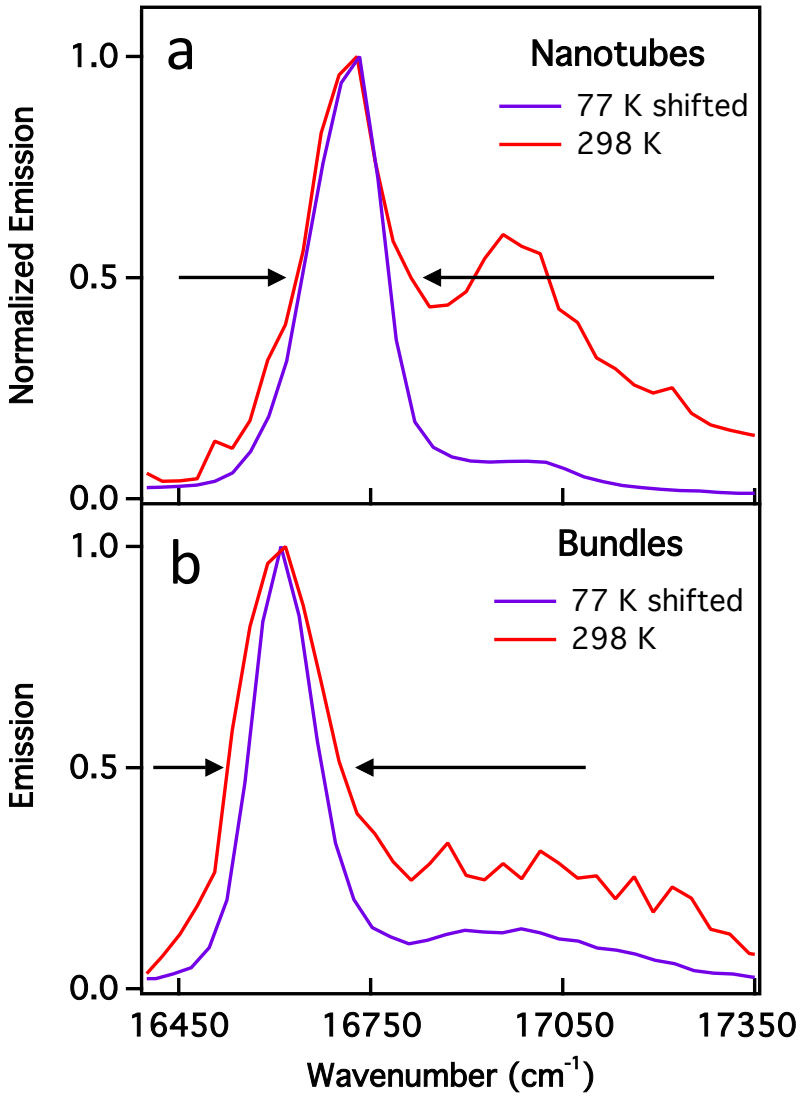

Figure 3.10 C8S3 J-aggregate temperature-dependent spectral narrowing

Overlay of normalized C8S3 (a) nanotube and (b) bundles emission spectra at 298 K (red) and 77 K (purple). At 77 K, bundle emission narrows considerably when compared to room temperature (RT), while nanotube emission width changes only slightly. The 77 K spectrum is shifted to lower energy in order to overlay with the room temperature spectrum.

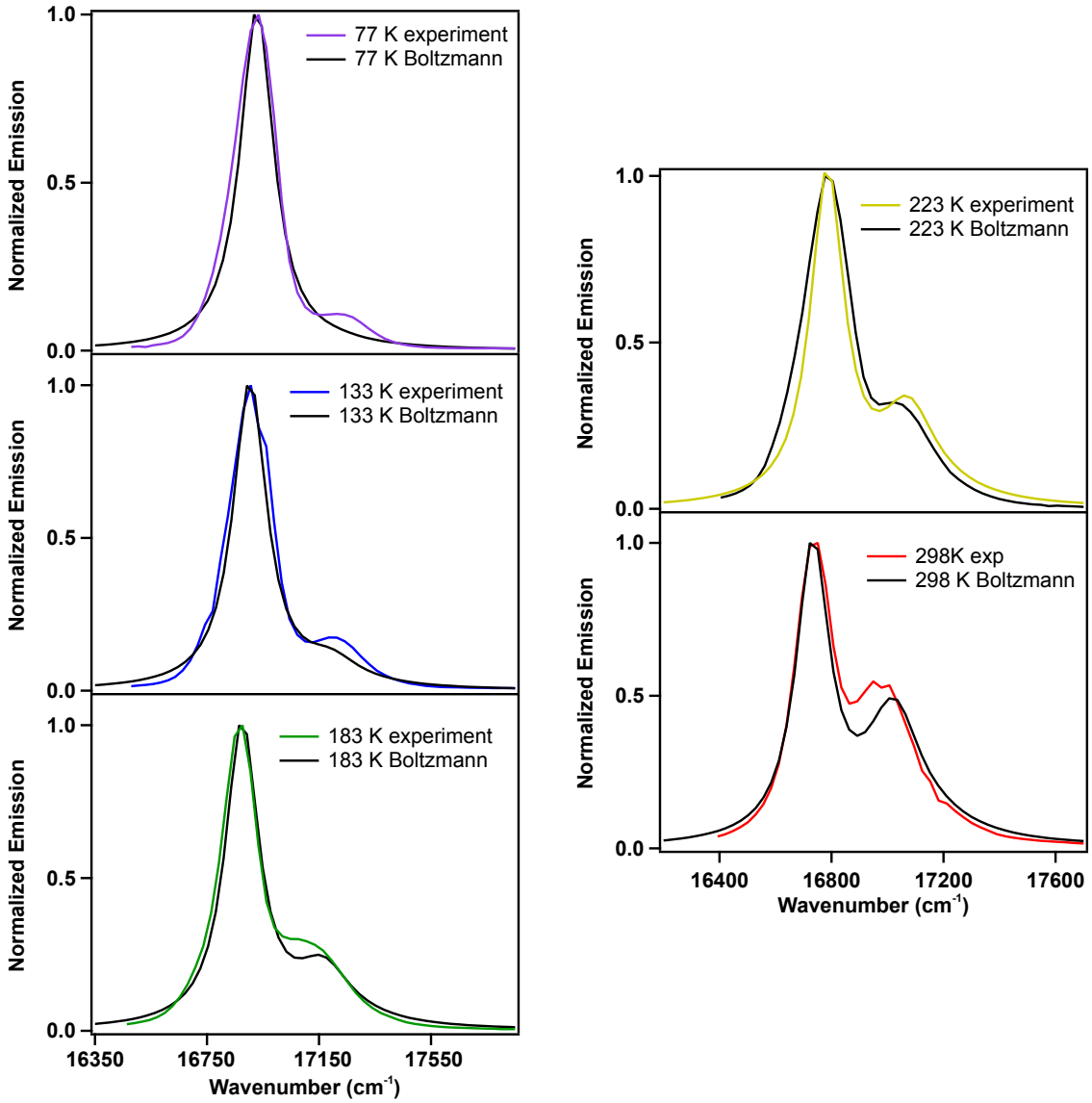

Figure 3.11 C8S3 nanotube emission: Boltzmann calculated vs. experimental

Comparison of Boltzmann calculated (black) and experimentally collected C8S3 nanotube spectra at 77 K (purple), 133 K (blue), 183 K (green), 223 K (yellow) and 298 K (red). Excellent agreement is shown across the measured temperature range.

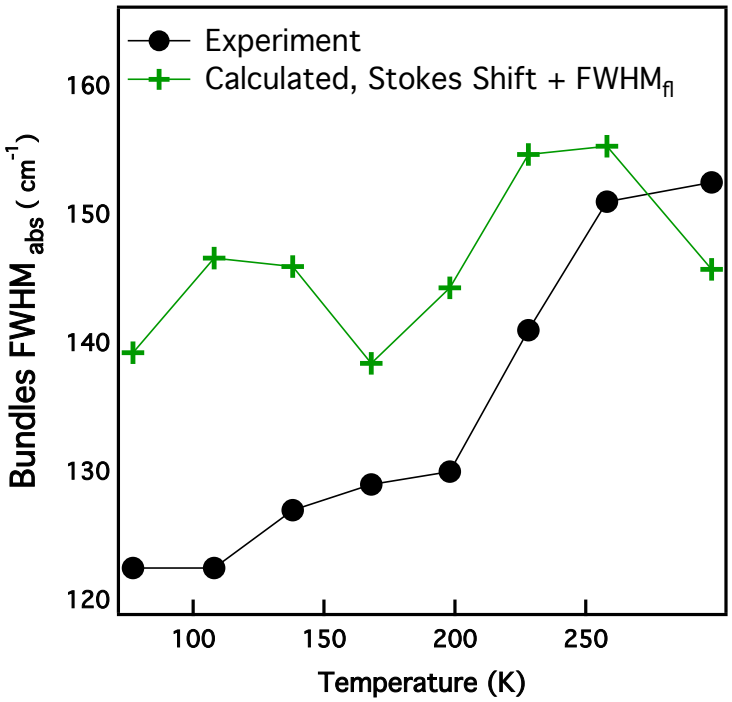

Figure 3.12 C8S3 bundles temperature-dependent FWHM

Comparison of C8S3 bundle experimental (black circles) and 'calculated' (green crosses) absorption FWHM. The lines are not a fit, and are to help guide the eyes.

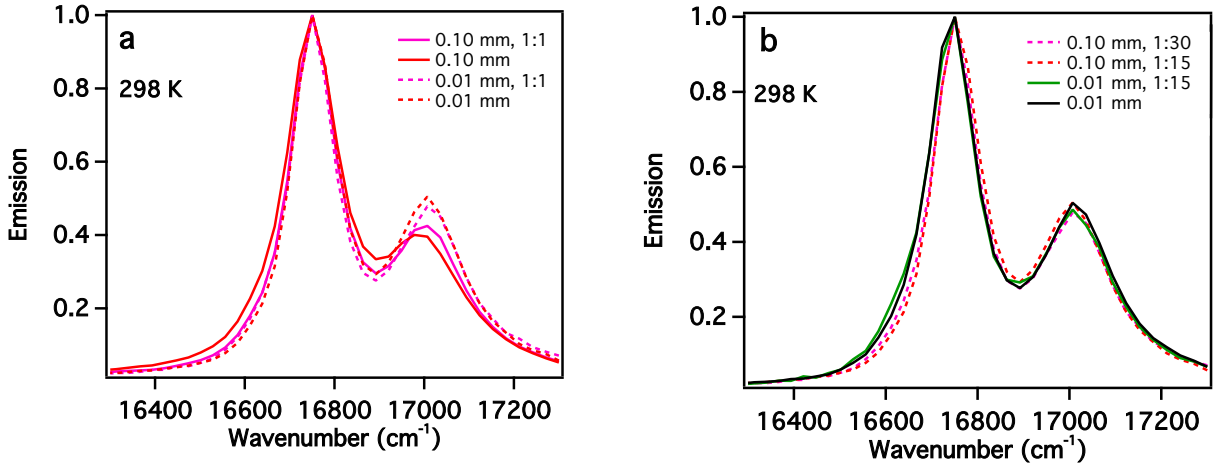

Figure 3.13 C8S3 nanotube emission: eliminating self-absorption

Due to significant absorption and emission spectral overlap, C8S3 J-aggregates exhibit reabsorption that results in depression of the high-energy emission exciton band. It is possible to eliminate this effect using dilution or a very thin sample cell. All emission spectra for the temperature dependent experiments were collected using undiluted nanotube and bundle solutions in the 0.01 mm cell. (a) Solid lines: undiluted (red) and 1:1 diluted (pink) emission spectra in the 0.10 mm cell. Dotted lines: undiluted (red) and 1:1 diluted (pink) emission spectra in the 0.01 mm cell. (b) Solid lines: undiluted (black) and 1:15 diluted (green) emission spectra in the 0.01 mm cell. Dotted lines: 1:15 (red) and 1:30 diluted (pink) emission spectra in the 0.10 mm cell.

3.7 REFERENCES

1. Jelley, E. E., Spectral Absorption and Fluorescence of Dyes in the Molecule State. *Nature* **1936,** *138*, 1009-1010.
2. Scheibe, G., Über Die Veränderlichkeit Der Absorptionsspektren in Lösung Und Die Nebenvalenzen Als Ihre Ursache. *Angew. Chem.* **1937,** *50*, 212-219.
3. Kobayashi, T., *J-Aggregates*. World Scientific, Singapore: 1996.
4. Würthner, F.; Kaiser, T. E.; Saha-Möller, C. R., J-Aggregates: From Serendipitous Discovery to Supramolecular Engineering of Functional Dye Materials. *Angew. Chem. Int. Ed.* **2011,** *50*, 3376-3410.
5. Knoester, J., Modeling the Optical Properties of Excitons in Linear and Tubular J-Aggregates. *Int. J. Photoenergy* **2006**.
6. Saikin, S. K.; Eisfeld, A.; Valleau, S.; Guzik, A. A., Photonics Meets Excitonics: Natural and Artificial Molecular Aggregates. *Nanophotonics* **2013,** *2*, 21-38.
7. Davydov, A. S., *Theory of Molecular Excitons*. Plenum Press: New York, 1971.
8. Kobayashi, T., Ed., *J-Aggregates (Volume 2)*. World Scientific Publishing Company: Singapore, 2012.
9. Knoester, J.; Agranovich, V. M., Frenkel and Charge-Transfer Excitons in Organic Solids. In *Electronic Excitations in Organic Based Nanostructures*, Agranovich, V. M. B., G.F., Ed. Elsevier: Amsterdam, 2003; Vol. 31, pp 1-96.
10. Spano, F. C., The Spectral Signatures of Frenkel Polarons in H- and J-Aggregates. *Acc. Chem. Res.* **2009,** *43*, 429-439.
11. Kirstein, S.; Daehne, S., J-Aggregates of Amphiphilic Cyanine Dyes: Self-Organization of Artificial Light Harvesting Complexes. *Int. J. Photoenergy* **2006**.
12. Würthner, F.; Kaiser, T. E.; Saha-Möller, C. R., J-Aggregates: From Serendipitous Discovery to Supramolecular Engineering of Functional Dye Materials. *Angew. Chem. Int. Ed. 50*, 3376-3410.
13. Mishra, A.; Behera, R. K.; Behera, P. K.; Mishra, B. K.; Behera, G. B., Cyanines During the 1990s: A Review. *Chem. Rev.* **2000,** *100*, 1973-2011.
14. Hamanaka, Y.; Kawasaki, O.; Yamauchi, T.; Nakamura, A., Morphology of Self-Assembled Merocyanine J-Aggregates in Films Studied by Scanning near-Field Optical Microscope. *Chem. Phys. Lett.* **2003,** *378*, 47-54.
15. von Berlepsch, H.; Bottcher, C.; Ouart, A.; Regenbrecht, M.; Akari, S.; Keiderling, U.; Schnablegger, H.; Dahne, S.; Kirstein, S., Surfactant-Induced Changes of Morphology of J-Aggregates: Superhelix-to-Tubule Transformation. *Langmuir* **2000,** *16*, 5908-5916.

16. von Berlepsch, H.; Kirstein, S.; Hania, R.; Pugzlys, A.; Böttcher, C., Modification of the Nanoscale Structure of the J-Aggregate of a Sulfonate-Substituted Amphiphilic Carbocyanine Dye through Incorporation of Surface-Active Additives. *J. Phys. Chem. B* **2007,** *111*, 1701-1711.

17. Vacha, M.; Saeki, M.; Hashizume, K.; Tani, T., Micro-Spectroscopy of Individual Nanostructures of Molecular Aggregates: Relationship between Morphology and Optical Properties. *Chemical Physics* **2002,** *285*, 149-155.

18. von Berlepsch, H.; Bottcher, C., The Morphologies of Molecular Cyanine Dye Aggregates as Revealed by Cryogenic Transmission Electron Microscopy. In *J-Aggregates (Volume 2)*, Kobayashi, T., Ed. World Scientific Publishing Co. : Singapore, 2012.

19. Eisele, D. M.; Knoester, J.; Kirstein, S.; Vanden Bout, D. A., Uniform Exciton Fluorescence from Individual Molecular Nanotubes Immobilized on Solid Substrates. *Nat Nano* **2009,** *4*, 658-663.

20. Didraga, C.; Pugzlys, A.; Hania, P. R.; von Berlepsch, H.; Duppen, K.; Knoester, J., Structure, Spectroscopy, and Microscopic Model of Tubular Carbocyanine Dye Aggregates. *J. Phys. Chem. B* **2004,** *108*, 14976-14985.

21. Clark, K. A.; Krueger, E. L.; Vanden Bout, D. A., Direct Measurement of Energy Migration in Supramolecular Carbocyanine Dye Nanotubes. *J. Phys. Chem. Lett.***2014**, *5*, 2274-2282.

22. Eisele, D. M.; Arias, D. H.; Fu, X.; Bloemsma, E. A.; Steiner, C. P.; Jensen, R. A.; Rebentrost, P.; Eisele, H.; Tokmakoff, A.; Lloyd, S.; Nelson, K. A.; Nicastro, D.; Knoester, J.; Bawendi, M. G., Robust Excitons Inhabit Soft Supra-Molecular Nanotubes. *Proc. Natl. Acad. Sci. USA*, submitted for publication.

23. Makio, S.; Kanamaru, N.; Tanaka, J., The J-Aggregate 5,5″,6,6″-Tetrachloro-1,1″-Diethyl-3,3″-Bis(4-Sulfobutyl)Benzimidazolocarbocyanine Sodium Salt in Aqueous Solution. *Bull. Chem. Soc. Jpn.* **1980,** *53*, 3120-3124.

24. Pawlik, A.; Ouart, A.; Kirstein, S.; Abraham, H. W.; Daehne, S., Synthesis and Uv/Vis Spectra of J-Aggregating 5,5 ',6,6 '-Tetrachlorobenzimidacarbocyanine Dyes for Artificial Light-Harvesting Systems and for Asymmetrical Generation of Supramolecular Helices. *Eur. J. Org. Chem.* **2003**, 3065-3080.

25. Saga, Y.; Tamiaki, H., Transmission Electron Microscopic Study on Supramolecular Nanostructures of Bacteriochlorophyll Self-Aggregates in Chlorosomes of Green Photosynthetic Bacteria. *Journal of Bioscience and Bioengineering* **2006,** *102*, 118-123.

26. Linnanto, J. M.; Korppi-Tommola, J. E. I., Investigation on Chlorosomal Antenna Geometries: Tube, Lamella and Spiral-Type Self-Aggregates. *Photosynth. Res.* **2008,** *96*, 227-245.

27. Balaban, T. S., Tailoring Porphyrins and Chlorins for Self-Assembly in Biomimetic Artificial Antenna Systems. *Acc. Chem. Res.* **2005,** *38*, 612-623.

28. Oostergetel, G. T.; Reus, M.; Chew, A. G. M.; Bryant, D. A.; Boekema, E. J.; Holzwarth, A. R., Long-Range Organization of Bacteriochlorophyll in Chlorosomes of Chlorobium Tepidum Investigated by Cryo-Electron Microscopy. *FEBS Letters* **2007,** *581*, 5435-5439.

29. Eisele, D. M.; Cone, C. W.; Bloemsma, E. A.; Vlaming, S. M.; van der Kwaak, C. G. F.; Silbey, R. J.; Bawendi, M. G.; Knoester, J.; Rabe, J. P.; Vanden Bout, D. A., Utilizing Redox-Chemistry to Elucidate the Nature of Exciton Transitions in Supramolecular Dye Nanotubes. *Nat Chem* **2012,** *4*, 655-662.

30. Scheblykin, I. G.; Sliusarenko, O. Y.; Lepnev, L. S.; Vitukhnovsky, A. G.; Van der Auweraer, M., Strong Nonmonotonous Temperature Dependence of Exciton Migration Rate in J Aggregates at Temperatures from 5 to 300 K. *J. Phys. Chem. B* **2000,** *104*, 10949-10951.

31. Kaiser, T. E.; Scheblykin, I. G.; Thomsson, D.; Wu¨rthner, F., Temperature-Dependent Exciton Dynamics in J-Aggregates—When Disorder Plays a Role. *J. Phys. Chem. B* **2009,** *113*, 15836-15842.

32. Scheblykin, I. G.; Sliusarenko, O. Y.; Lepnev, L. S.; Vitukhnovsky, A. G.; Van der Auweraer, M., Excitons in Molecular Aggregates of 3,3‘-Bis-[3-Sulfopropyl]-5,5‘-Dichloro-9- Ethylthiacarbocyanine (Thiats): Temperature Dependent Properties. *J. Phys. Chem. B* **2001,** *105*, 4636-4646.

33. Dorn, H.-P.; Müller, A., Scheibe-Aggregates of Pseudoisocyanine in Solution and in Molecular Monolayers. *Appl. Phys. B* **1987,** *43*, 167-172.

34. Fidder, H.; Knoester, J.; Wiersma, D. A., Superradiant Emission and Optical Dephasing in J-Aggregates. *Chemical Physics Letters* **1990,** *171*, 529-536.

35. Scheblykin, I. G.; Bataiev, M. M.; Van der Auweraer, M.; Vitukhnovsky, A. G., Dimensionality and Temperature Dependence of the Radiative Lifetime of J-Aggregates with Davydov Splitting of the Exciton Band. *Chemical Physics Letters* **2000,** *316*, 37-44.

36. Pugzlys, A.; Augulis, R.; van Loosdrecht, P. H. M.; Didraga, C.; Malyshev, V. A.; Knoester, J., Temperature-Dependent Relaxation of Excitons in Tubular Molecular Aggregates: Fluorescence Decay and Stokes Shift. *J. Phys. Chem. B* **2006,** *110*, 20268-20276.

37. Lyon, J. L.; Eisele, D. M.; Kirstein, S.; Rabe, J. P.; Vanden Bout, D. A.; Stevenson, K. J., Spectroelectrochemical Investigation of Double-Walled Tubular J-Aggregates of Amphiphilic Cyanine Dyes. *J. Phys. Chem. C* **2008,** *112*, 1260-1268.

38. Augulis, R.; Pugžlys, A.; van Loosdrecht, P. H. M., Exciton Dynamics in Molecular Aggregates. *Phys. Status Solidi C* **2006,** *3*, 3400-3403.

39. Milota, F.; Sperling, J.; Nemeth, A.; Kauffmann, H. F., Two-Dimensional Electronic Photon Echoes of a Double Band J-Aggregate: Quantum Oscillatory Motion Versus Exciton Relaxation. *Chemical Physics* **2009,** *357*, 45-53.

40. Milota, F.; Sperling, J.; Nemeth, A.; Abramavicius, D.; Mukamel, S.; Kauffmann, H. F., Excitonic Couplings and Interband Energy Transfer in a Double-Wall Molecular Aggregate Imaged by Coherent Two-Dimensional Electronic Spectroscopy. *J. Chem. Phys.* **2009,** *131*, 054510-23.

41. Sperling, J.; Nemeth, A.; Hauer, J.; Abramavicius, D.; Mukamel, S.; Kauffmann, H. F.; Milota, F., Excitons and Disorder in Molecular Nanotubes: A 2d Electronic Spectroscopy Study and First Comparison to a Microscopic Model. *J. Phys. Chem. A* **2010,** *114*, 8179-8189.

42. Womick, J. M.; Miller, S. A.; Moran, A. M., Correlated Exciton Fluctuations in Cylindrical Molecular Aggregates. *J. Phys. Chem. B* **2009,** *113*, 6630-6639.

43. Womick, J. M.; Miller, S. A.; Moran, A. M., Probing the Dynamics of Intraband Electronic Coherences in Cylindrical Molecular Aggregates. *J. Phys. Chem. A* **2009,** *113*, 6587-6598.

44. Clark, K. A.; Cone, C. W.; Vanden Bout, D. A., Quantifying the Polarization of Exciton Transitions in Double-Walled Nanotubular J-Aggregates. *J. Phys. Chem. C* **2013,** *117*, 26473-26481.

45. Lyon, J. L.; Eisele, D. M.; Kirstein, S.; Rabe, J. P.; Vanden Bout, D. A.; Stevenson, K. J., Spectroelectrochemical Investigation of Double-Walled Tubular J-Aggregates of Amphiphilic Cyanine Dyes. *J. Phys. Chem. C* **2008,** *112*, 1260-1268.

46. Cooper, W., Multiplet Structure of Aggregated States in 1,1′-Diethyl-2,2′-Cyanine Dye. *Chemical Physics Letters* **1970,** *7*, 73-77.

47. Murata, S., On the Stability of the J Aggregates of Pseudoisocyanine Formed in Low Temperature Glasses. *J. Soc. Photogr. Sci. Technol. Japan* **1989,** *52*, 24-26.

48. Fidder, H.; Terpstra, J.; Wiersma, D. A., Dynamics of Frenkel Excitons in Disordered Molecular Aggregates. *J. Chem. Phys.* **1991,** *94*, 6895-6907.

49. Drobizhev, M. A.; Sapozhnikov, M. N.; Scheblykin, I. G.; Varnavsky, O. P.; Auweraer, M. V. d.; Vitukhnovsky, A. G., Exciton Dynamics and Trapping in J-Aggregates of Carbocyanine Dyes. *Pure and Applied Optics: Journal of the European Optical Society Part A* **1996,** *5*, 569.

50. de Boer, S.; Vink, K. J.; Wiersma, D. A., Optical Dynamics of Condensed Molecular Aggregates: An Accumulated Photon-Echo and Hole-Burning Study of the J-Aggregate. *Chemical Physics Letters* **1987,** *137*, 99-106.

51. Pugzlys, A.; Hania, P. R.; Augulis, R.; Duppen, K.; van Loosdrecht, P. H. M., Cylindrical Aggregates of 5,5 ',6,6 '-Tetrachlorobenzimidacarbocyanine

Amphiphilic Derivatives: Structure-Related Optical Properties and Exciton Dynamics. *Int. J. Photoenergy* **2006**.

52. Al-Khatib, O. Structure and Optical Properties of Complex Aggregate-Structures of Amphiphilic Dye Systems. Ph.D. Dissertation, Humboldt University of Berlin, Berlin, 2012.

53. Potma, E. O.; Wiersma, D. A., Exciton Superradiance in Aggregates: The Effect of Disorder, Higher Order Exciton-Phonon Coupling and Dimensionality. *J. Chem. Phys.* **1998,** *108*, 4894-4903.

54. Kamalov, V. F.; Struganova, I. A.; Yoshihara, K., Temperature Dependent Radiative Lifetime of J-Aggregates. *The Journal of Physical Chemistry* **1996,** *100*, 8640-8644.

55. Fidder, H.; Wiersma, D. A., Collective Optical Response of Molecular Aggregates. *physica status solidi (b)* **1995,** *188*, 285-295.

56. Feldmann, J.; Peter, G.; Göbel, E. O.; Dawson, P.; Moore, K.; Foxon, C.; Elliott, R. J., Linewidth Dependence of Radiative Exciton Lifetimes in Quantum Wells. *Phys. Rev. Lett.* **1987,** *59*, 2337-2340.

57. Moll, J.; Daehne, S.; Durrant, J. R.; Wiersma, D. A., Optical Dynamics of Excitons in J Aggregates of a Carbocyanine Dye. *J. Chem. Phys.* **1995,** *102*, 6362-6370.

58. Bednarz, M.; Malyshev, V. A.; Knoester, J., Temperature Dependent Fluorescence in Disordered Frenkel Chains: Interplay of Equilibration and Local Band-Edge Level Structure. *Phys. Rev. Lett.* **2003,** *91*, 217401.

59. Didraga, C.; Klugkist, J. A.; Knoester, J., Optical Properties of Helical Cylindrical Molecular Aggregates: The Homogeneous Limit. *J. Phys. Chem. B* **2002,** *106*, 11474-11486.

60. Didraga, C.; Knoester, J., Optical Spectra and Localization of Excitons in Inhomogeneous Helical Cylindrical Aggregates. *J. Chem. Phys.* **2004,** *121*, 10687-10698.

61. Kenkre, V. M., Reineker, P., *Exciton Dynamics in Molecular Crystals and Aggregates*. Springer-Verlag: Berlin, 1982.

Chapter 4: Direct measure of energy migration in supramolecular carbocyanine dye nanotubes†

4.1 INTRODUCTION

The capability of light harvesting (LH) assemblies of naturally occurring photosynthetic systems to capture and efficiently transport energy to reaction centers makes them the subject of extensive experimental and theoretical interrogation.[1-12] While energy transfer (ET) across long distances (> 25 nm) is not required for photosynthesis, there is interest in the ultimate limit that such systems can transport energy, particularly for use in artificial assemblies. Recent investigations of patterned nano-arrays of bacterial LH2 complexes reveal energy propagation distances greater than 1 μm, a distance far beyond what is necessary for photosynthesis.[13-14] While natural light harvesting systems consist of arrays of dye molecules held together in a protein scaffold, an alternative approach is to assemble artificial LH systems using only dye molecules. Self-assembled nanotubular J-aggregates of amphiphilic cyanine dyes[15-17] are an example of such an artificial LH system, and they have garnered interest owing to their similarity to the cylindrical chlorosomes from Green Sulfur Bacteria.[3, 6, 10, 18-19]

In these systems, the tight packing of the dyes in the nanotubes leads to highly delocalized excited states described as Frenkel excitons.[20-23] The delocalized nature of the excitons on the cylindrical nanotube suggest these systems should facilitate long-range energy transfer[24] and makes them candidates for use as light harvesting materials in artificial systems.[17, 25-26] Moreover, the quasi-one dimensional structure of the nanotubes offers the possibilities of directed energy transfer along the aggregates. Previous exciton-exciton annihilation (EEA) studies of cyanine J-aggregates provide wide-ranging

† Portions of this chapter were published in Clark, K. A.; Krueger, E. L.; Vanden Bout, D. A., *J. Phys. Chem. Lett.* **2014**, *5*, 2274-2282. ELK assisted with image collection; DVB supervised the project.

estimates of exciton delocalization from 20-50000 molecules at room temperature.[27] Recently, theoretical exciton diffusion lengths of 200 nm[28] have been calculated for cyanine J-aggregate thin films; however, experimental diffusion lengths of 50 nm are reported for these films.[29] Other experiments on nanotubular aggregates estimate enormous exciton migration distances, up to 30 μm, at low temperature.[30] Results of fluorescence depolarization[31] and quenching studies[17] of cylindrical cyanine J-aggregates both propose long range exciton migration distances, up to hundreds of nanometers, in cylindrical cyanine J-aggregates. Given the huge variability of indirect ET quantification experiments, a direct measure of energy migration in the systems is preferred.

This report focuses on two J-aggregate structures of the cyanine dye 3,3‘-bis(2-sulfopropyl)-5,5‘,6,6‘-tetrachloro-1,1‘-dioctylbenzimidacarbocyanine (C8S3): nanotubes and bundled nanotube super-structures (hereafter referred to as bundles). Double-walled C8S3 nanotubes, with diameters of 13 nm and lengths up to several microns can be formed in aqueous solution.[32-33] The majority of C8S3 aggregate research tends to focus on well-separated nanotubes in fresh solutions, largely due to their structural uniformity.[17, 32-34] The agglomeration of C8S3 J-aggregate nanotubes into bundles has been observed in solutions via high-resolution electron microscopy. [33-34] When solutions are stored for many months, only bundles or fragments of bundles, rather than isolated nanotubes, are detected in cryo-TEM micrographs.[33] After months of storage, giant bundles with diameters greater than 500 nm are observed.[33] C8S3 bundles are not as well characterized as the nanotubes, but as materials the bundles offer the advantage of thermodynamic stability. To this point, no exciton transport lengths for C8S3 bundles have been reported, but closely packed PIC J-aggregates are known to participate in inter-aggregate ET.[27] In this report, we will address the spatial extent of energy migration in both individual double-walled nanotubes and close-packed bundle super-structures using

fluorescence optical microscopy. We have quantified exciton transport in C8S3 J-aggregates by spatially resolving the emission from individual nanostructures after localized excitation. This method has been demonstrated using near-field microscopy to localize the excitation spot;[35] however, it is more practical to simply utilize far-field excitation,[13, 36] which is the approach recently used to measure energy transport in the nano-patterned array of LH2 complexes.[13] Results for the C8S3 J-aggregates demonstrate the energy transfer in both systems is sufficiently large to be directly observed via microscopy, with the bundled system showing remarkably long-ranged transport approaching distances of a micron.

4.2 Experimental Methods

4.2.1 Preparation of J-aggregate solutions

Solutions of alcoholic-route C8S3 J-aggregate nanotubes were prepared as previously described in Chapter 2. Some J-aggregate solutions were stored for approximately 4 months before bundling of the nanotubes was spectrally verified. All steady state, room temperature absorption spectra of C8S3 monomer, nanotubes and bundles were collected with a Hewlett Packard UV-Vis 8453 spectrophotometer using a 0.1 mm path length demountable quartz cuvette (Starna). Bulk fluorescence spectra of solutions were collected at 532 nm excitation using a Horiba Scientific FluoroLog®-3 spectrofluorometer; a 0.01 mm path length cell was used to avoid inner-filter effects.

4.2.2 Immobilization of aggregate structures

Glass coverslips were cleaned with a 1:1:2 ratio of H_20_2 (30%):NH_4OH:H_20, then rinsed and stored in high purity H_20. A small volume (2-5 μL) of C8S3 J-aggregate solution (fresh or bundled) was pipetted onto a 25x25mm coverslip tilted ~45° relative to the lab bench; this immobilization method does not disrupt the delicate nanotube

structures.[34] The sample was allowed to dry in the dark before confocal images were collected.

4.2.3 Confocal imaging

A home built sample scanning inverted confocal microscope was used to collect fluorescence images of C8S3 aggregates immobilized on a glass substrate. A 532 nm Coherent Compass 215M continuous wave laser was used for excitation; powers into the microscope ranged from 100 to 1000 nW. A piezoelectrically driven sample stage (Queensgate Instruments) was used to raster scan the sample over a fixed, focused laser spot formed using a 100X, 1.30 N.A. oil immersion objective (Olympus). The same objective collected the emitted fluorescence. A holographic notch filter (Kaiser Optical) and a 550 nm long pass filter removed residual excitation light. A mirror (in a flipper mount) directed the emission through a lens and onto the active area of a single photon counting avalanche photodiode (Perkin-Elmer) and images were created pixel by pixel.

4.2.4 CCD imaging

To image energy transfer along the aggregates, the mirror was folded down and removed from the emission path. Regions of interest, which included well-separated bundles/nanotubes and passive areas of the sample, were located from confocal images; the coordinates of these spots were recorded, and these points placed directly in the focal volume of the laser spot. To collect the focused beam profile, the piezo stage was used to adjust the placement of a passive region of the sample onto the fixed laser spot. After removing excitation filters from the emission path, the focused beam profile was passed through an optical density filter and then imaged onto an electron multiplying charged coupled device (EMCCD) camera (Andor). The same method was used to image the exciton transport within the aggregates. Interesting emitting regions in the confocal image

were moved into the focal volume of the laser. After passing through the excitation filters, the C8S3 emission was imaged onto the EMCCD, where collection times ranged from 5-10s. The optical system was set up where one square CCD pixel (8 μm x 8 μm) corresponds to 57 nm x 57 nm in space. The magnification at the CCD was determined by imaging a USAF test target. Multiple laser beam broadening and energy transfer control experiments were performed; discussion and results of these tests are included in the appendix.

4.3 RESULTS AND DISCUSSION

4.3.1 C8S3 J-aggregate spectral properties

Both C8S3 nanotubes and bundles were first assembled in solution before isolating them on substrates for imaging. The C8S3 monomer dye is strongly soluble in methanol. However, when this solution is introduced into to water, the amphiphilic C8S3 molecules self-assemble into double walled supramolecular nanotubes. After time, these nanotubes assemble to form the aggregate bundles. The close packing and coupling of individual dye molecules result in excitons, excitations that extend over multiple molecules, which dramatically alters the optical properties of the system.[20, 24] Figures 4.1a and 4.1b display absorption and emission spectra for C8S3 monomer, nanotube and bundle solutions; both J-aggregate structures exhibit red-shifted and narrowed bands compared with the monomer, which has an absorption maximum of 520 nm. C8S3 nanotube absorption (Figure 4.1a) is defined by sharp features at 589 and 599 nm, and is well characterized experimentally and theoretically.[22, 32-33, 37-38] The nanotubes emit from two states (corresponding to the inner and outer cylinders)[32] and display no Stokes shift.

The characteristic optical properties of the C8S3 nanotubes change when agglomeration into bundle super-structures occurs. Bundle absorption is characterized by

two transitions: one broad and one sharp, centered at 575 nm and 603 nm respectively. Figure 4.1b shows that C8S3 bundles primarily emit from the lowest energy band and, like the nanotubes, exhibit a negligible Stokes shift. A decrease in the absolute absorbance of the bundles relative to the nanotubes[33] suggests that the bundles are thicker than the penetration depth of the light.

4.3.2 Imaging exciton migration in C8S3 J-aggregate bundles and nanotubes

Representative confocal fluorescence images of C8S3 bundles and nanotubes are shown in Figures 4.2a/b and 4.3. Confocal imaging of immobilized C8S3 bundles revealed structures with diameters ranging from approximately 500 nm to 3 μm; these sizes are further confirmed with atomic force microscopy (AFM, see appendix for details). Conversely, C8S3 nanotube diameters are much smaller than the confocal excitation spot,[32] and imaging revealed structures with diameters ~ 350 nm, a size that corresponds to the spatial resolution limit of the microscope and is reflective of the excitation spot rather than the nanotube size. To examine energy transfer, several regions of interest were selected in each image to position the excitation focus. These included both isolated aggregate structures as well as regions of the sample that exhibit only background fluorescence, denoted as "passive" regions; the coordinates of these regions were recorded, and these points positioned directly in the focal volume of the laser spot using a piezoelectric stage. Emission from the J-aggregates was then directly imaged onto a CDD camera to examine the spatial extent of energy migration along the nanostructures. The difference in size between the aggregate emission and laser excitation profiles roughly approximates the exciton transport distance. To collect the focused laser profile, the stage was used to adjust the placement of a passive sample region onto the fixed laser spot. Various passive regions, where no emissive structures

were apparent, from each confocal image were used to collect multiple reflected laser profiles to ensure the reproducibility of this measurement and stability of the laser.

Figure 4.2a is a confocal fluorescence image of bundles on a glass surface. Fluorescence emission from a ~1 μm diameter bundle was collected from three regions, which are marked with arrows numbered 1-3 in Figure 4.2b, a magnified panel of the full sized confocal image. Circled numbers 4-6 indicate regions near the bundle that were excited and had emission imaged onto the EMCCD chip. Passive sample regions, labeled P1 and P2 (squares), which exhibit background fluorescence levels, were used to collect laser excitation profiles that were compared to the bundle's fluorescence emission profiles.

The eight tiles below the confocal images represent the light collected by the CCD from the bundles (fluorescence emission) or passive sample regions (reflected laser). Tiles P1 and P2 are images of the laser spot used to excite the bundle. Emission profiles collected from the bundle are shown in Tiles 1-3. It is readily apparent that the images of the fluorescence spot from the bundle (Tiles 1-3) are very different than the images of the passive laser spot (Tiles P1 and P2). The fluorescence from the bundles is both broader and strongly asymmetric compared to the size and shape of focused excitation spot. The elongation of the bundle emission collected by the CCD is clearly oriented along the bundle as measured in the confocal image. The two dimensional (2-D) elongation of the bundle emission profile qualitatively shows that excitons generated in the excitation spot are migrating both along and perpendicular to the bundle long axis before emission. Regions 4-6 are located ~ 1 μm from the investigated bundle feature. Tiles 4-6 show that no emission was collected when regions 4-6 were illuminated (using the same power and collection time as regions 1-3). This is an important result that

indicates the excitation is truly localized and that the stage positions the sample accurately.

Similarly, Figures 4.3a is a confocal image of double-walled nanotubes on a glass surface. Tile p1 is an image of the passive spot used to excite the nanotubes imaged in Figure 4.3a; it is nearly identical to the reflected laser spots collected from other passive sample regions, which demonstrates the stability of the laser spot size. The emission from the nanotubes labeled in Figure 4.3a with arrows 2 is imaged in Tiles 1-3. While the emission profile is preferentially elongated along the nanotube long axis, the extent of energy transfer is smaller when compared to that of the bundle and is confined to one dimension by the small size of the nanotube.

4.3.3 Quantifying exciton migration distances in C8S3 J-aggregates

A 2-D Gaussian fitting routine was used to quantitatively compare the reflected excitation beam spot to the emission profile emanating from the C8S3 aggregate structures. Both emission and laser profiles were fit to a bivariate normal distribution, where width parameters σ_x and σ_y were generated for an ellipsoid with fixed major and minor principle axes that match the laboratory EMCCD chip x-y frame. The spatial orientation of the emissive nanostructures varied, and the principal axes of the ellipsoidal emission profiles were rarely aligned along the laboratory x-y axis. The emission profiles were rotated with a coordinate transformation to determine the widths of the distribution along the principal axes of these elliptical density functions, utilizing a linear algebra method detailed in the appendix. This allowed for determination of both the widths along the long and short ellipse axes (σ_{long} and σ_{short}) as well as the rotation angle (θ) of the ellipse in the laboratory x-y frame. The spatial extent of energy transfer along and perpendicular to the aggregate long axis was found by taking the square root of the

difference between the variances of the emission image and of the passive laser spot fits in the relevant coordinate system for each aggregate (see appendix for details).

A quantitative comparison of the collected emission and passive laser spots for the C8S3 bundles data set represented in Figure 4.2 is given in Table 4.1. Analysis reveals consistent emission broadening relative to the laser excitation for the three illuminated bundle regions; average broadening for the long and short bundle axes is 500 nm and 350 nm, respectively. The analogous laser and emission profile comparison for C8S3 nanotubes shown in Figure 4.3 is found in Table 4.2. In contrast to the bundles, the three nanotube regions labeled in Figure 4.3a have average exciton transport distances 120 nm beyond the area excited with the laser.

To verify the angles determined from the fit of the emission images accurately correspond to the spatial orientation of the nanotubes and bundles, the positions of the aggregates in the confocal images were analyzed. Figures 4.4a and 4.4f are confocal images of C8S3 bundles and nanotubes, respectively. The C8S3 structures were illuminated at the locations indicated with an arrow; the corresponding emission profiles are shown in Figures 4.4b and 4.4g. The calculated angles of rotation from fitting the emission profiles are consistent with the angles measured in the confocal images. For all emission profiles collected, the angles from the confocal images and the emission profile fits agree within ± 5°.

With the angles verified, it is possible to quantify the spreading of the emission both along and perpendicular to the long axis of the aggregates. Figures 4.5a and 4.5b illustrate the localized illumination and resultant broadened emission profiles of C8S3 bundles and nanotubes. Overlaid line profiles show the difference between C8S3 J-aggregate emission (black) and laser (green) profile widths. Average exciton transport lengths for C8S3 bundles were found to be 790 ± 90 nm and 600 ± 70 nm for the

respective long and short axes, from the fitting of 37 bundle emission profiles. The disparity between the two bundle axes appears to suggest that transport parallel to the bundle's long axis is more efficient than transport perpendicular to the long axis. However, further image analysis reveals that exciton transport in the perpendicular direction is limited by the physical width of the aggregate. A confocal image and emission profile of a C8S3 bundle are given in Figures 4.4c and 4.4d. Figure 4.4e overlays the line scans marked in the confocal and CCD images. The line scans overlay nearly perfectly, indicating that the spatial energy transfer along the bundle short axis extends completely to the edge of the bundle; this result was observed for many interrogated bundles. Thus, $\overline{\Delta\sigma}_{\text{bundle, long}} > \overline{\Delta\sigma}_{\text{bundle, short}}$ is a result of the limited bundle diameter rather than a clear preference for energy to spread parallel to the long axis.

Figures 4.4h and 4.4i are confocal and CCD images of an isolated nanotube. Rather than the near-perfect overlap seen for the bundles, Figure 4.4j reveals that the width of the short-axis nanotube emission is defined by the CCD-collected emission profile rather than the confocal image. This expected result holds for all emission profiles collected from nanotube samples, since the beam diameter is larger than the nanotube short axis. The distances of energy migration along the nanotubes are significantly shorter than those observed for the bundles. An average 1-D exciton migration length of 140 ± 40 nm was measured for C8S3 nanotubes from the fits of 24 nanotube emission profiles; this result is illustrated in Figure 4.5b.

4.4 CONCLUSIONS

The shorter distances for exciton transport in the isolated double-walled nanotubes compared to the bundles is somewhat unexpected. C8S3 nanotubes have previously been found to have excellent structural nanotube uniformity.[34, 39] While the

bundles are thought to be larger assemblies of double-walled nanotubes,[33] there is no detailed understanding of their supramolecular structure. The bundle absorption spectrum exhibits a sharp J-band, which is red-shifted further than the lowest energy exciton transition for the nanotubes. The spectral shift to even lower energy upon bundling suggests stronger electronic coupling between the monomers in the bundles compared to the individual nanotubes. However, unlike linear aggregates, there is not a direct correlation between the energy of the lowest J-band and the electronic coupling in the cylindrical aggregates. Conversely, the remainder of the bundle spectrum is a broad, featureless peak, which indicates substantially more disorder than predicted for the double-walled nanotubes, the absorption of which is defined by multiple narrow transitions.[32, 37-38]

Average exciton migration in C8S3 nanotubes is on the order of 150 nm, but was measured to be 600 nm and 800 nm in bundled structures (long and short axis, respectively). Estimates of the 1-D energy transport in C8S3 nanotubes yields very different limits depending on the transport mechanism. In a weak-coupling regime, exciton transport proceeds incoherently (via hopping) and is described with a diffusive, Förster model. Previously, a lower limit of 30 nm[34] was estimated for C8S3 exciton diffusion based on the transition line widths,[40] hopping rate and intermolecular spacing.[39, 41-43] An upper bound of ~ 1 μm was estimated based on purely coherent exciton transport, which depends on intermolecular interaction strength, exciton lifetime and exciton jump time.[34, 44] On the surface, the result for the average migration length in nanotubes, 140 nm, aligns more closely with the incoherent hopping mechanism. The longer distances in the bundles suggest that the migration has some component of coherent motion. Moreover, the results for C8S3 bundles indicate broadening of the emission profile beyond the illuminated area in the directions of the long *and* short bundle axes. This

suggests that the energy transfer in the bundles is not confined to a single dimension, and that there is strong coupling both along and between the nanotubes in the bundle system.

While the energy transfer may result from some coherent transport, it is unlikely, particularly at room temperature, that the migration is entirely coherent.[34, 45] Therefore to quantify the differences in migration, the spreading of the excitation spots was modeled as arising from diffusion. In the simplest limit, the spot size of the emission ($\sigma^2_{emission}$) can be approximated as the sum of the variance without diffusion (σ^2_{laser}) and the mean square displacement from diffusion at a time equal to the exciton lifetime, $\sigma^2_{emission} = \sigma^2_{laser} + 2D\tau$, where D is the diffusion coefficient and τ is the exciton lifetime. Using the previously defined notation, this results in $\Delta\sigma = (2D\tau)^{1/2}$. From this expression, the broadening for the nanotubes, $\overline{\Delta\sigma}_{nanotubes}$ = 140 nm, yields a diffusion coefficient of approximately 100 $nm^2\ ps^{-1}$, assuming a lifetime of 100 ps.[25, 46] The exciton lifetime in the bundles has not been previously reported, but it was measured to be 200 ps. (see appendix). In the diffusive regime, this longer lifetime would result in a $\sqrt{2}$ increase in diffusion length for the bundles. However, the distances measured in the bundles are more than a factor of 5 larger than the nanotubes indicating that the longer distances cannot be solely attributed the increased lifetime. Using the same expression and a 200 ps lifetime, the broadening in the bundles, $\overline{\Delta\sigma}_{bundles}$ = 790 nm, yields an estimated diffusion coefficient of 1500 $nm^2\ ps^{-1}$.

A better measure of the diffusion coefficient can be determined by modeling the spreading of the exciton based on a steady-state, one dimensional diffusion model.[47-48] In the limit of low exciton density, the number of excitons n(x,t) as a function of both time and position can be found from the diffusion equation,

$$\frac{\partial n(x,t)}{\partial t} = \frac{n(x,t)}{-\tau} + D\frac{\partial^2 n(x,t)}{\partial x^2} + pI(x) \qquad (1)$$

where D is the diffusion coefficient, τ is the exciton lifetime, p is the probability of absorption, and I(x) is the spatial profile of the excitation. Assuming a Gaussian excitation profile with a standard deviation of σ_0, the solution to equation 1 yields

$$n(x,t) \propto \frac{1}{(2\sigma_0^2 + 4Dt)^{\frac{1}{2}}} exp\left(\frac{-x^2}{(2\sigma_0^2 + 4Dt)}\right) exp\left(\frac{-t}{\tau}\right) \qquad (2)$$

Unlike measurements in which the diffusion profile is measured as function of time after pulsed excitation,[48-52] the emission profile imaged in the current experiment is the steady-state distribution. This steady-state profile can be modeled by numerically integrating equation 2 over time. This results in a profile that can be compared with the experimental data to extract a diffusion coefficient if the exciton lifetime is known. For simplicity, the one-dimensional steady-state diffusion profile was compared with a Gaussian that represented the average profile along the long-axis of the emission spot. Using 100 ps as the exciton lifetime of the nanotubes yielded a diffusion coefficient of 120 ± 20 nm^2 ps^{-1}, which is in line with the simple estimate from the variance. This is similar to what has been observed in previous measurements on other J-aggregate systems,[29] but is still larger than the lower limit estimate based simply on the line widths.

The steady-state image profile predicted for diffusion in the bundle system is slightly different as the diffusion is two-dimensional. For simplicity, the average image profile was projected onto the long-axis and the diffusion modeled in one dimension. This projection was modeled as a Gaussian profile and compared again to the steady-state one dimensional diffusion profile. While the parameters for the nanotubes yields steady-state profiles that remain Gaussian, the larger diffusion coefficients required to fit the bundles results in profiles that began to deviate from a Gaussian shape. As a result,

parameters were selected with the criterion that the data and the model have the same full-width half maximum. Using an exciton lifetime of 200 ps, the diffusion coefficient was found to 7000 ± 2000 nm^2 ps^{-1} in the bundles. The deviation between the experimental Gaussian shape of the data and the steady-state profile suggests that the transport is not well modeled as a purely incoherent process. The magnitude of the diffusion coefficient is agrees with recent calculations of the diffusion coefficient in J-aggregates based on both coherent and incoherent motion. In this model for exciton transport in cyanine J-aggregate thin films, exciton mobility is initially ($t < 30$ fs) high and the dynamics are best described by coherent motion; at longer times, diffusive transport dominates.[28] From the diffusion portion of the transport, this model gives diffusion coefficients ranging between 100 - 700 nm^2 ps^{-1} depending on the static and dynamic disorder.[28] The diffusion coefficient from the nanotubes is consistent with this result, while the bundles pushes beyond the upper limit. This suggests that the bundle system has a larger component of coherent transport, along with a larger diffusion coefficient, as compared with the nanotubes. Finally, the transport may be limited by environmental fluctuations and surface traps caused by immobilization of the aggregates. This may be the cause of the shorter distances in the nanotubes compared with the bundles, as the dye molecules that comprise the bundles are effectively protected by the outer layers of the bundle system and may experience fewer disruptive interactions. Furthermore, 2-D systems have many more hopping pathways than 1-D systems[43], which favors the increased mobility we observe for the bundles.

The ET differences in bundles and nanotubes suggest future work on the temperature dependence of the energy migration is of great interest. Low temperature studies of J-aggregates indicate that the fluorescence lifetime decreases as temperature is lowered, suggesting stronger coupling as the disorder in the system is reduced.[53-54]

Furthermore, low temperature exciton transport imaging of the aggregates and bundles will shed light on the exciton transport process, as distances would be expected to increase as temperature is lowered for coherent exciton motion while incoherent exciton motion should diminish at low temperatures.[39, 55]

An alternative explanation for the spreading of the excitation spot is waveguiding of the emission within the nanostructure. Some organic molecular aggregates have exhibited spatially extended photoluminescence (PL), with measured PL distances up to 250 μm, due to waveguiding effects.[56-59] Most of these waveguiding materials are H-aggregates, where the constituent monomers are strongly coupled, but the dominant exciton state(s) lies at the upper edge of the exciton band and the resulting aggregate absorption spectrum is blue shifted with respect to the monomer.[21, 60] The large Stokes shift observed for H-aggregates is deemed crucial to their waveguiding behavior.[58] In contrast, the J-aggregate systems have essentially zero Stokes shift; this creates an enormous loss mechanism from the overlap of the emission spectrum and the absorption. If the C8S3 aggregates were operating as waveguides, we would expect strong self-absorption. As the ratio of the two J-aggregate peaks in the emission spectrum is inverted compared to that in the absorption spectrum, if there was self-absorption one would expect to see a change in the shape of the emission spectrum from the sample on the substrate compared with aggregates in the solution. Emission from individual immobilized nanotubes (deposited on a glass surface) is identical to the bulk nanotube solution fluorescence (see appendix). Additionally, the waveguiding properties should be dependent on the size and shape of the aggregates.[58] While the nanotubes and bundles are clearly different, there is only a slight correlation between the size of the extended PL measured for the C8S3 J-aggregate bundles of different sizes (Supporting Information, Section 5); most bundles exhibit the average long axis ET distances of ~ 800 nm

regardless of the short axis ET distance (which corresponds to short axis physical size). Finally, one would expect the waveguiding parallel and perpendicular to the bundle's long axis to be very different, and yet the extension of the PL in the short and long bundle axes directions appears to be nearly identical.

Direct measure of exciton transport in cylindrical carbocyanine dye aggregates demonstrates the energy transport capability of two different structures: nanotubes and bundles. The average 1-D exciton transport length of 140 nm in the nanotubes is more than 4 times greater than diffusion lengths measured in common organic semiconductor thin films.[61] While 1-D exciton propagation in nanotubes makes them promising materials for optical devices, the enhancement of exciton migration upon increasing the C8S3 aggregate structural hierarchy is extraordinary. C8S3 nanotube bundles, which form spontaneously without the need for complex patterning, exhibit long-range 2-D energy migration with average transport distances reaching over 600 nm. These exciting results motivate the increased investigation of these super-structures, not just the nanotubes, as materials for use in energy transport devices.

4.5 APPENDIX

4.5.1 Quantitative determination of C8S3 J-aggregate exciton transport distances

a. Modeling aggregate emission profiles with a bivariate normal distribution

A 2-D Gaussian fitting routine was used to quantitatively compare the reflected excitation beam spot to the emission profile emanating from the C8S3 aggregate structures. The multivariate normal density function for the random vector $\underline{X} = (X_1, X_2, \ldots, X_n)$, can be written with matrices:

$$f_{\underline{X}}(\underline{x}) = \frac{1}{(2\pi)^{n/2}\sqrt{|\Sigma|}} exp\left(-\frac{1}{2}(\underline{X}-\underline{\mu})^T \Sigma^{-1}(\underline{X}-\underline{\mu})\right) \qquad (1)$$

where Σ is a symmetric, positive definite real matrix and $\underline{\mu} = (\mu_1\ \mu_2\ \ldots\ \mu_n)^T$ is a column vector. For the case that n=2, the above equation becomes a bivariate normal distribution function in x and y:

$$f(x,y) = \frac{1}{2\pi\sigma_x\sigma_y\sqrt{1-\rho^2}}\,exp\left(-\frac{1}{2(1-\rho^2)}\left[\frac{(x-\mu_x)^2}{\sigma_x^2}+\frac{(y-\mu_y)^2}{\sigma_y^2}-\frac{2\rho(x-\mu_x)(y-\mu_y)}{\sigma_x\sigma_y}\right]\right) \qquad (2)$$

where σ^2_x and σ^2_y are the variance of the peak in the x and y directions, respectively. The ρ coefficient ($-1 < \rho < 1$) is a cross correlation term, which designates the relative asymmetry of the density function; $\rho = 0$ would generate a distribution with contours consisting of concentric circles. Additionally, the sign of the correlation parameter ρ designates the orientation of the ellipsoid.[62] All J-aggregate emission profiles and reflected passive laser spots were fit to a bivariate normal distribution using IGOR Pro. The fit parameters ρ, σ^2_x and σ^2_y were generated for an ellipsoid with fixed major and minor principle axes that match the laboratory EMCCD chip x-y frame.

The spatial orientation of the aggregates varied, and the principal axes of the ellipsoidal emission profiles were rarely aligned along the laboratory x-y axis. To determine the widths of the distribution along the principal axes (x´ and y´, where x´ designates the C8S3 long axis and y´ is the perpendicular short axis), the emission profiles were rotated with a coordinate transformation to determine the widths of the distribution along the major and minor axes of these elliptical density functions using the following linear algebra method, which is illustrated in Figure 4.6. The real, symmetric matrix Σ was diagonalized and the eigenvalues and eigenvectors were calculated. The eigenvalues of Σ are the variances (σ^2) in x´ and y´ denoted respectively σ^2_{long} and σ^2_{short}. The widths of the ellipsoidal C8S3 nanostructure emission distributions were found by

taking the square root of the variances along the unique principal axes for each ellipsoidal distribution.

b. Rotation angle of ellipsoid emission profiles

The angle of rotation (θ) in the lab x-y frame for each emissive nanostructure was determined by the following method. The matrix Σ represents the emission profile widths along the X-Y laboratory frame:

$$\Sigma = \begin{bmatrix} \sigma_x^2 & \rho\sigma_x\sigma_y \\ \rho\sigma_x\sigma_y & \sigma_y^2 \end{bmatrix} \qquad (3)$$

A 2x2 rotation matrix, R, represents an in-plane ellipsoid rotation by the angle θ about the origin, and has the following property:

$$R = \begin{bmatrix} \cos\theta & -\sin\theta \\ \sin\theta & \cos\theta \end{bmatrix} \text{ where } R^{-1}\Sigma R = \begin{bmatrix} \sigma_x^2 & 0 \\ 0 & \sigma_y^2 \end{bmatrix} \qquad (4)$$

To determine the constraint on the angle θ, the matrix algebra is expanded:

$$R^{-1}\Sigma R = \begin{bmatrix} \sigma_x^2 & 0 \\ 0 & \sigma_y^2 \end{bmatrix} \qquad (5)$$

$$= \begin{bmatrix} \sigma_x^2 \cos^2\theta + 2\rho\sigma_x\sigma_y \cos\theta \sin\theta + \sigma_y^2 \sin^2\theta & \left(\sigma_y^2 - \sigma_x^2\right)\cos\theta \sin\theta + \rho\sigma_x\sigma_y\left(\cos^2\theta - \sin^2\theta\right) \\ \left(\sigma_y^2 - \sigma_x^2\right)\cos\theta \sin\theta + \rho\sigma_x\sigma_y\left(\cos^2\theta - \sin^2\theta\right) & \sigma_x^2 \sin^2\theta - 2\rho\sigma_x\sigma_y \cos\theta \sin\theta + \sigma_y^2 \cos^2\theta \end{bmatrix} \qquad (6)$$

Since the off-diagonal elements both go to zero, we can write:[63]

$$\tan 2\theta = \frac{2\rho\sigma_x\sigma_y}{\sigma_x^2 - \sigma_y^2} \qquad (7)$$

The value of θ was computed for each ellipsoid emission profile. Laser profiles were collected by imaging laser reflection from a passive sample area. Before directly comparing the C8S3 emission profile to laser profile, corresponding laser excitation spot was rotated (by the computed angle θ) to align along the ellipsoid major axis eigenvector.

The spatial extent of energy transfer along and perpendicular to the aggregate long axis was found by taking the square root of the difference between the calculated C8S3 nanostructure and rotated laser variances:

$$\Delta\sigma_{long} = \sqrt{\sigma^2_{\text{C8S3, long}} - \sigma^2_{\text{rotated laser, long}}} \qquad (8)$$

$$\Delta\sigma_{short} = \sqrt{\sigma^2_{\text{C8S3, short}} - \sigma^2_{\text{rotated laser, short}}} \qquad (9)$$

4.5.2 Stability of laser excitation profile

To limit sample photodegradation, all confocal images of C8S3 aggregates were collected using a lower laser power (~ 10X less) than used for collection of emission profiles onto the CCD camera. To ensure that long collection times and varying laser powers did not artificially broaden reflected laser or emission profiles imaged onto the EMCCD, the following control tests were conducted.

a. Effect of integration (collection) time

EMCCD collection times of 10 s were necessary to C8S3 aggregate emission profiles with good signal to noise ratios. To test the stability of the laser and collection camera, laser profiles reflected from passive surfaces were collected at varying integration times. These time-control experiments were performed for three different laser profiles where the integration time was increased by a factor of 10. Broadening of

the reflected laser profile was found to be 5% for the integration times used in C8S3 experiments. Results are given in Tables 4.3, 4.4 and 4.5.

b. Effect of laser power (neutral density filter)

The power used to collect reflected laser profiles was always equal to the power used to excite the C8S3 aggregates. Owing to these excitation laser powers, an absorptive neutral density filter was placed into the emission path only when laser profiles were collected to protect the EMCCD from overexposure. To ensure this did not affect reflected laser beam shape/size, a control experiment was performed where a focused laser spot was reflected from a clean glass coverslip with and without the filter in the emission path. Laser profiles were fit to a bivariate normal distribution, and the profile widths indicate that the neutral density filter does not affect the size or shape of collected laser profiles. Fit results are found in Table 4.6.

4.5.3 Energy migration control experiments

a. Fluorescent spheres

Confocal images of 100 nm diameter fluorescent spheres (Polysciences, Inc. YO Carboxylate Microspheres) were collected using 532 nm laser excitation. Laser beam profiles reflected from passive sample areas and images of bead emission were collected using an EMCCD camera, as in previously described collection scheme. Fluorescent spheres do not exhibit energy transfer; thus, emission spots from these spheres should reflect the point spread function of the excitation. Results from 2-D Gaussian fits indicate no broadening of the emission profile as compared to the reflected focused laser spot. Table 4.7 lists fit results to a bivariate normal distribution for reflected laser and fluorescent sphere emission profiles.

b. Rhodamine 6G / Poly(methyl methacrylate) films

1 mg of Rhodamine 6G (Exciton) and 0.21 g of Poly(methyl methacrylate), PMMA (Aldrich, analytical grade) was dissolved in 5 mL of toluene (Fischer Scientific, ACS grade). 20 μL of this solution was spin cast at 2000 RPM to produce a ~ 200 nm film. Films were imaged in the confocal microscope using; a 532 nm Coherent Compass 215M continuous wave laser was used for excitation. While there were no passive regions in the collected images, emission profiles from multiple illuminated sample regions were acquired. R6G molecules should not exhibit energy transfer, and the collected emission profiles exhibit nearly identical sizes as laser excitation profiles reflected from passive surfaces. Table 4.8 lists fit results to a bivariate normal distribution for an average of six R6G in PMMA and an average of 16 reflected laser emission profiles.

4.5.4 C8S3 bundles: size dependent energy migration

Figure 4.7 shows a confocal image of C8S3 bundles of varying sizes. Tiles labeled p1 and p2 are reflected laser excitation profiles used to illuminate the bundles; tiles numbered 1-4 are EMCCD-collected emission profiles from bundles illuminated with localized laser excitation. Line profile overlays indicate that the spatial energy transfer along the bundle short axis extends to the edge of the bundle (discussed above and shown Figure 4.4).

We compared the parallel and perpendicular (long and short axes, respectively) diffusion lengths for the 37 interrogated bundles, shown in Figure 4.8. This plot shows that most bundles exhibit the average long axis ET distances of ~ 800 nm. There is a slight correlation between the long axis distance and that of the short axis (which corresponds to short axis physical size).

4.5.5 C8S3 J-aggregate size distribution

C8S3 J-aggregates were deposited from solution onto a glass substrate using a drop flow method before imaging. A detailed scanning force microscopy analysis for the C8S3 nanotubes (deposited on quartz using the same technique) has shown that the isolated nanotubes exhibit a uniform diameter of 13 nm.[34] The nanotubes agglomerate into bundles over time, and the size, specifically the diameter, of the bundles varies within a single sample. Atomic force microscopy (AFM) was used to measure the size of C8S3 J-aggregate bundles deposited on a surface using the method described in the main text. The bundles are many microns in length. The average aggregate diameter is ~ 600 nm, but the sizes ranged from 300 nm to over 3 microns for the largest bundle agglomerations. These dimensions for width and length correspond well with the bundle dimensions measured in the confocal microscope. AFM images and line scans showing the height and width of C8S3 bundles are shown in Figure 4.9. The sizes in the AFM indicate that while the larger bundles consist of several nanotubes in the vertical direction from the surface that they are significantly larger in the lateral direction (more ribbon-like).

4.5.6 C8S3 fluorescence lifetime measurements

The fluorescence lifetimes for C8S3 monomer (in methanol), nanotubes and bundles was acquired using a Horiba Scientific FluoroLog®-3 spectrofluorometer with time correlated single photon counting (TCSPC) capability. The J-aggregates and bundles were excited using 561 nm NanoLED excitation with a pulse width less than 1.5 ns; emission was collected at 603 nm (bundles) and 599 nm (nanotubes). All lifetime data was fit using DAS6 software.

C8S3 J-aggregate nanotube decay could not be distinguished from the instrument response, but has been previously reported to be on the order of 100 ps at room

temperature.[25, 46, 64] C8S3 bundle lifetime was found to be double-exponential (Figure 4.10), with decay constants of 2 ns (12% relative amplitude) and 200 ps (88% relative amplitude). However, the fast time component is not clearly resolved with the time resolution of the instrument. Therefore it could easily be faster. For the simplicity in the modeling the lifetime was assumed to be 200 ps. This upper limit was chosen in an effort to not over estimate the diffusion coefficient. The necessity of a double-exponential decay indicates that two unique bundle architectures, or even sizes, could exist within the sample. Alternatively, a portion of the emission may result from an ill-formed aggregate layer on the outside of the bundle that has a longer lifetime. However, the fact that the majority of the decay is not drawn out to long times suggests that there is no significant absorption and re-emission in the sample.

4.5.7 C8S3 nanotube emission: bulk solution vs. immobilized aggregate

After confocal images of C8S3 nanotubes isolated on a glass substrate were acquired, regions of interest, with well-separated aggregates, were located. Those regions were probed with a focused laser beam (532 nm Coherent Compass 215M continuous wave laser), and emission was imaged onto a spectrograph (Acton SpectraPro 150) equipped with a LN2-cooled CCD detector (Princeton Instruments SPEC10). A representative emission spectrum from an isolated nanotube is overlaid with the bulk solution spectrum (acquired using a fluorometer) in Figure 4.11. There is little difference between the two emission ratios, indicating minimal self-absorption prior to emission in the isolated nanotubes on the substrate.

4.5.8 One-dimensional diffusion model

The one dimensional diffusion steady-state profile was found by first considering the distribution of excitons, n(x,t), that would be found as a function of time and space

after an instantaneous delta function pulse.[65] The distribution should satisfy the following differential equation:

$$\frac{\partial n(x,t)}{\partial t} = \frac{n(x,t)}{-\tau} + D\frac{\partial^2 n(x,t)}{\partial x^2} + pI(x) \qquad (10)$$

where τ is the exciton lifetime, D is the diffusion coefficient, p is the probability of absorption, and I(x) is the spatial distribution of the excitation.

For I(x) as a delta function centered at x = 0, the solution to this equation is given as:

$$n(x,t) \propto \frac{1}{(4Dt)^{1/2}} exp\left(\frac{-x^2}{4Dt}\right) exp\left(\frac{-t}{\tau}\right) \qquad (11)$$

For an initial Gaussian excitation with a standard deviation of σ_0, the result is

$$n(x,t) \propto \frac{1}{(2\sigma^2 + 4Dt)^{1/2}} exp\left(\frac{-x^2}{2\sigma^2 + 4Dt}\right) exp\left(\frac{-t}{\tau}\right) \qquad (12)$$

To get the steady-state result for the size of the emission spot measured in the experiment, this expression should be integrated over all times and then convolved with a Gaussian that represents the increase in the width that results from the diffraction of the collection optics. However, if the initial spot and the effect of the optics are treated as being Gaussian, then the entire effect can be wrapped into the initial width σ_0. Therefore, the σ_0 was taken to be the size of the passive spot with any additional width resulting from diffusion.

The steady-state profile for the bundles should be modeled slightly differently as now the diffusion can occur in two dimensions (both along and perpendicular to the long axis of the bundle). However, for simplicity the diffusion was again modeled as one-dimensional by projecting the data onto the long axis of the system. In the case of both the nanotubes and bundles, rather than fitting each individual spot, diffusion coefficients

were estimated by fitting Gaussian profiles. These Gaussian profiles were generated based upon the average Gaussian fits to all of individual spots measured in the lab. This worked well for the nanotubes, as shown in Figure 4.12. Since the profiles and the model were both essentially Gaussian, they overlay exactly. However, the larger diffusion coefficients and distances in the bundle system lead to a model profile that was starting to deviate from Gaussian shape. To simply the fitting, parameters were chosen such that the model and the Gaussian data profile had the same full-width at half maximum.

4.6 FIGURES

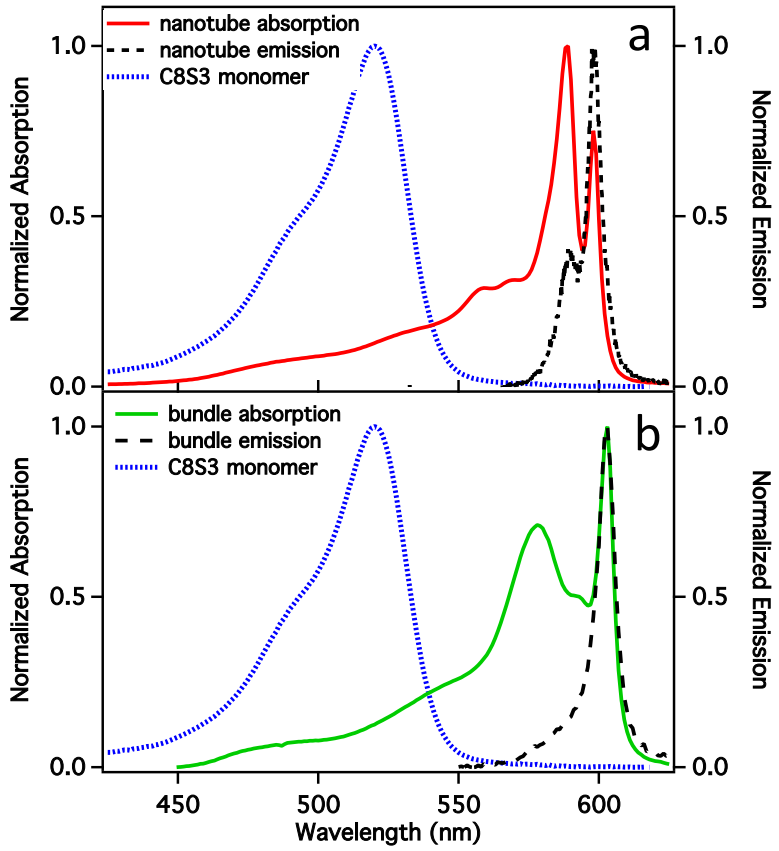

Figure 4.1 C8S3 absorption and emission spectra

Double walled nanotubes self assemble when C8S3 monomer is introduced to aqueous solution. After months of storage, C8S3 J-aggregate nanotubes clump together to form bundles and undergo a spectral transformation. (a) Normalized absorption spectrum of monomeric C8S3 in methanol (blue, dotted) and the red-shifted spectrum of the nanotubes (red, solid) in a mixture of water/methanol. The nanotubes emit from two states (black, dotted), corresponding to the inner and outer cylinder walls. (b) Normalized absorption (green, solid) and emission (blacked, dashed) spectra of C8S3 bundles. The emission spectra of both C8S3 aggregates overlay with the absorption, indicating a negligible Stokes shift.

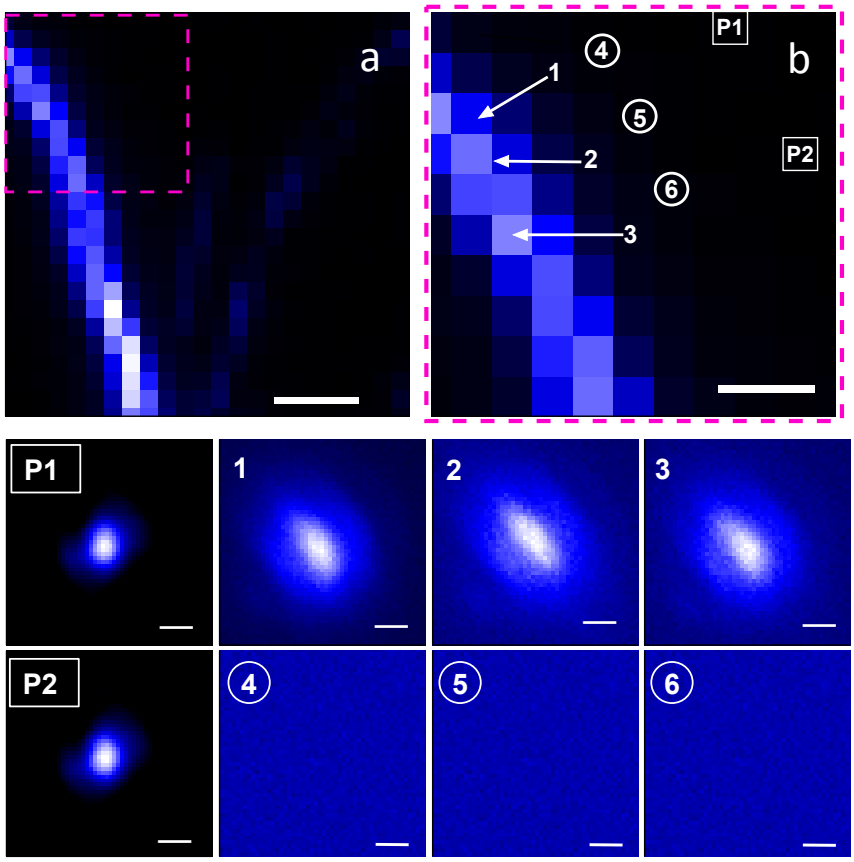

Figure 4.2 C8S3 bundle imaging

(a) Confocal fluorescence image of C8S3 J-aggregate bundles. Scale bar = 2 μm. (b) Zoomed-in panel of bundle. Scale bar = 1 μm. The eight tiles below the confocal images represent the light collected by the CCD from the bundles (fluorescence emission) or passive sample regions (reflected laser); labels correspond to areas marked in Fig. 2b. Tiles P1 and P2 show the reflected laser excitation beam used to excite the bundles. Tiles 1-3 represent emission profiles emanating from the bundle excited at locations marked by numbered arrows in Fig 2b. Tiles 4-6 represent the light collected by the EMCCD when regions 4-6 in the confocal image were illuminated. Scale bar = 0.5 μm for all tiles.

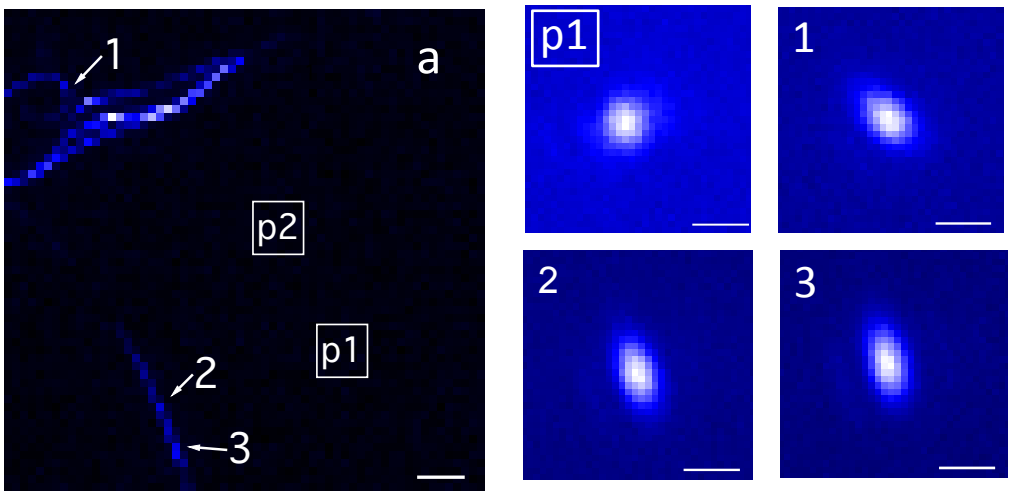

Figure 4.3 C8S3 nanotube imaging

(a) Confocal fluorescence image of C8S3 J-aggregate nanotubes. Scale bar = 2 μm. The four tiles beside the confocal image represent the light collected by the CCD from the J-aggregates (fluorescence emission) or passive sample regions (reflected laser); labels correspond to areas marked with arrows in the confocal image. Tile P1 shows the reflected laser excitation beam used to excite the J-aggregates. Tiles 1-3 represent emission profiles emanating from the aggregate. Scale bar = 0.5 μm for all tiles.

Region	σ^2_{long} (μm^2)	σ^2_{short} (μm^2)	$\Delta\sigma_{long}$ (μm)	$\Delta\sigma_{short}$ (μm)	θ (°)
C8S3 bundles					
Reflected Laser, P1	0.067	0.048	–	–	–
Reflected Laser, P2	0.067	0.048	–	–	–
Bundle 1	0.28	0.18	0.47	0.36	-34
Bundle 2	0.35	0.18	0.53	0.37	-39
Bundle 3	0.29	0.18	0.48	0.36	-37

Table 4.1 C8S3 J-aggregate bundles emission broadening fit results

The reflected laser and C8S3 J-aggregate emission profiles were fit to bivariate normal distributions. For each emission profile, the variances along the major (long) and minor (short) ellipsoidal axis and angle of rotation, θ, from the laboratory X-Y frame were determined. To calculate the difference between the illumination spot and each emission profile widths ($\Delta\sigma$), the passive spot was rotated by the respective angle to lie on the major axis of each ellipsoidal emission profile, and $\Delta\sigma = \sqrt{(\sigma^2_{C8S3} - \sigma^2_{LASER,\ ROTATED})}$. Emission regions 1-3 all lie on the same C8S3 bundle feature, shown in Figure 4.2. Average broadening along and perpendicular to the bundle long axis is ~ 500 nm and 350 nm, respectively. Furthermore, the angular analysis is consistent for all three regions probed by localized laser excitation.

Region	σ^2_{long} (μm^2)	σ^2_{short} (μm^2)	$\Delta\sigma_{long}$ (μm)	$\Delta\sigma_{short}$ (μm)	θ (°)
C8S3 nanotubes					
Reflected Laser, p1	0.029	0.025	–	–	–
Nanotube 1	0.038	0.016	0.10	–	- 43
Nanotube 2	0.048	0.013	0.14	–	- 13
Nanotube 3	0.044	0.014	0.13	–	- 17

Table 4.2 C8S3 J-aggregate nanotubes emission broadening fit results

The reflected laser and C8S3 J-aggregate emission profiles were fit to bivariate normal distributions. For each emission profile, the variances along the major (long) and minor (short) ellipsoidal axis and angle of rotation, θ, from the laboratory X-Y frame were determined. To calculate the difference between the illumination spot and each emission profile widths ($\Delta\sigma$), the passive spot was rotated by the respective angle to lie on the major axis of each ellipsoidal emission profile, and $\Delta\sigma = \sqrt{(\sigma^2_{C8S3} - \sigma^2_{LASER,\ ROTATED})}$. Emission regions 1-3 are shown in Figure 4.3. While the emission profile is broadened compared to the laser excitation, it is considerably smaller than what is measured in the bundled samples. Smaller widths for the nanotube short axis compared to the laser indicate the emissive object probed is smaller than the excitation spot.

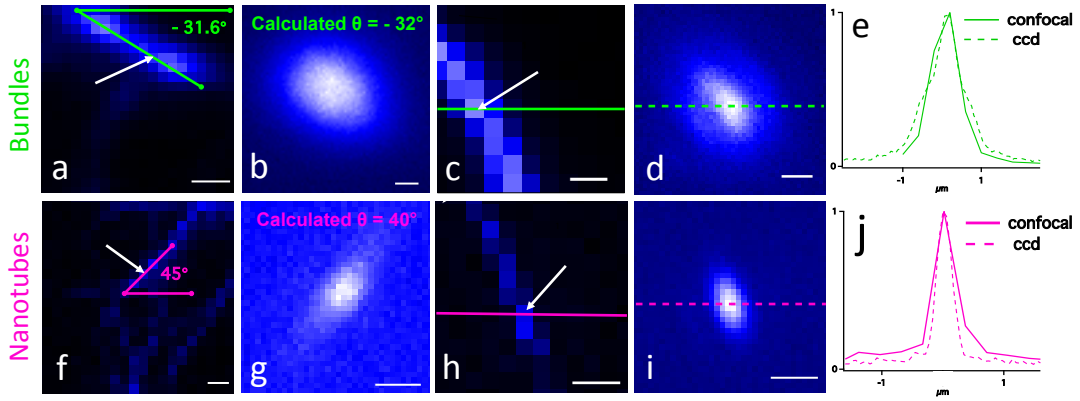

Figure 4.4 Confocal and EMCCD emission profile images of C8S3 aggregates

(a,f) False color confocal fluorescence image of C8S3 (a) bundle and (f) nanotubes. Scale bars = 1 μm (b,g) Emission profiles from C8S3 (b) bundle and (g) nanotube . Scale bars = 0.5 μm. The calculated rotation angle of the ellipsoidal emission profiles corresponds well to the spatial arrangement of the C8S3 aggregates measured in the confocal images. (c) Confocal fluorescence image of C8S3 bundle. Scale bar = 1 μm. (d) C8S3 bundle emission profile from excitation spot marked by the arrow in Fig 3c. Scale bar = 0.5 μm. (e) Overlay of normalized line scans from the bundle confocal (3c) and CCD (3d) images. The profiles are nearly identical. (h) Confocal fluorescence image of C8S3 nanotube. Scale bar = 1 μm. (i) C8S3 nanotube emission profile from excitation spot marked by the arrow in Fig 3h. Scale bar = 0.5 μm .(j) Overlay of normalized line scans from the nanotube confocal (3h) and CCD (3i) images. The line profiles are larger than the nanotube due to convolution of the small nanotube and laser excitation; the confocal line profile width is roughly $\sqrt{2}$ the CCD line profile width.

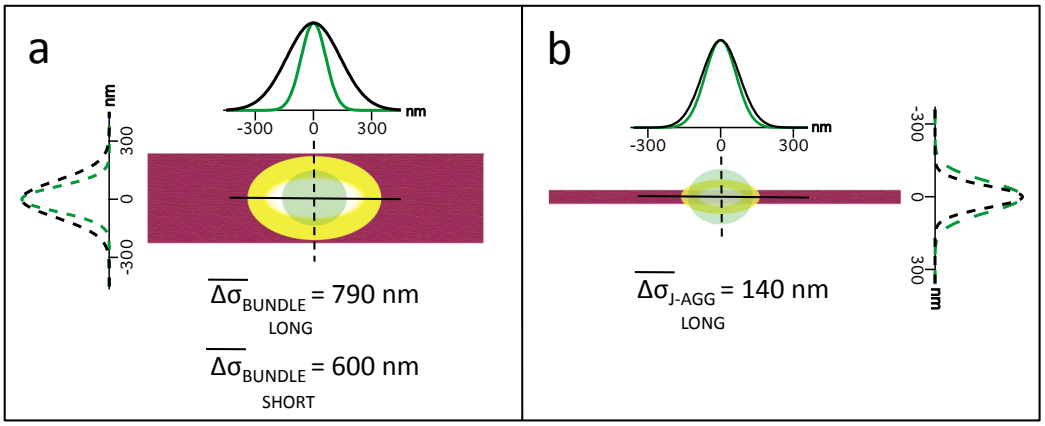

Figure 4.5 Average ET in C8S3 bundles and nanotubes

Schematic illustration of the average energy migration extent in C8S3 (a) bundles and (b) nanotubes upon laser excitation. Exciton transport distances were directly measured by collecting emission profiles (yellow gradient ellipse) from the aggregates illuminated with a localized laser spot (green circle); these profiles were fit to a bivariate normal distribution. (a) The average difference in width between the laser (green, solid/dashed) and emission profiles is 790 ± 90 nm and 600 ± 70 nm for the long (black, solid) and short bundle axes (black, dashed), respectively. (b) The average difference in width between the laser (green, solid/dashed) and emission profiles is 140 ± 40 nm for the long (black, solid) nanotube axis. The laser beam diameter is much larger than the nanotube short axis (~15 nm) diameter. The laser line width (green, dashed) is greater than the emission nanotube emission profile (black, dashed), which is broadened due to convolution of the small J-aggregate and laser beam.

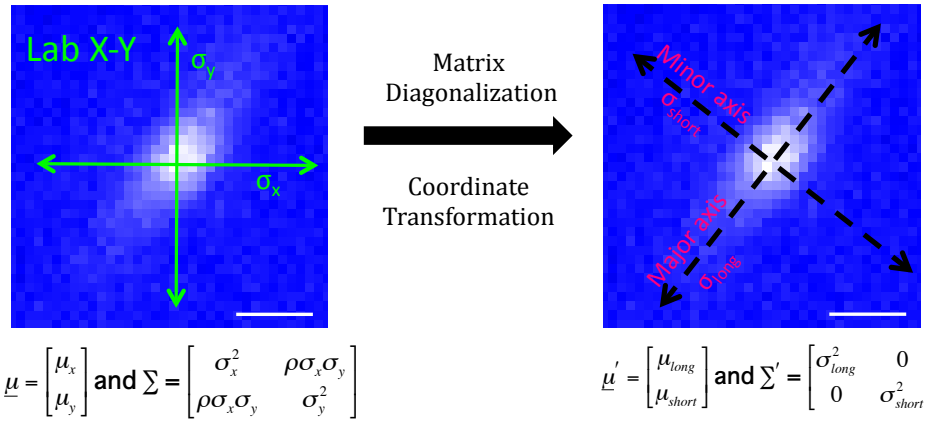

$$\underline{\mu} = \begin{bmatrix} \mu_x \\ \mu_y \end{bmatrix} \text{ and } \sum = \begin{bmatrix} \sigma_x^2 & \rho\sigma_x\sigma_y \\ \rho\sigma_x\sigma_y & \sigma_y^2 \end{bmatrix}$$

$$\underline{\mu}' = \begin{bmatrix} \mu_{long} \\ \mu_{short} \end{bmatrix} \text{ and } \sum' = \begin{bmatrix} \sigma_{long}^2 & 0 \\ 0 & \sigma_{short}^2 \end{bmatrix}$$

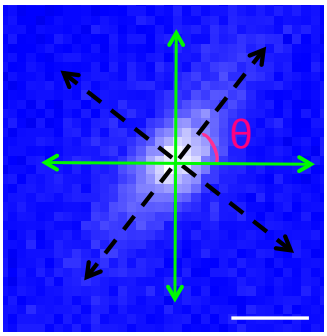

$$R = \begin{bmatrix} \cos\theta & -\sin\theta \\ \sin\theta & \cos\theta \end{bmatrix} \textit{ where } R^{-1}\Sigma R = \begin{bmatrix} \sigma_x^2 & 0 \\ 0 & \sigma_y^2 \end{bmatrix}$$

$$\tan 2\theta = \frac{2\rho\sigma_x\sigma_y}{\sigma_x^2 - \sigma_y^2}$$

Figure 4.6 Illustration of density function coordinate transformation

Ellipsoidal aggregate emission profiles were initially fit to a bivariate normal distribution function in the laboratory X-Y frame. After matrix diagonalization, the widths along the ellipsoid major and minor axes were used to determine the rotation angle for each emission profile.

spot	Average σ_{long} (μm)	Average σ_{short} (μm)
Passive laser reflection (0.1 s collection)	0.162	0.131
Passive laser reflection (1 s collection)	0.172	0.137
% difference	6 %	5 %

Table 4.3 Laser Reflection Profile (0.1 s and 1 s integration) Fit Results

spot	Average σ_{long} (μm)	Average σ_{short} (μm)
Passive laser reflection (0.5 s collection)	0.23	0.22
Passive laser reflection (5 s collection)	0.22	0.21
% difference	5 %	5 %

Table 4.4 Laser Reflection Profile (0.5 s and 5 s integration) Fit Results

spot	Average σ_{long} (μm)	Average σ_{short} (μm)
Passive laser reflection (1 s collection)	0.23	0.22
Passive laser reflection (10 s collection)	0.23	0.23
% difference	--	4 %

Table 4.5 Laser Reflection Profile (1 s and 10 s integration) Fit Results

spot	σ_{long} (μm)	σ_{short} (μm)
Passive laser reflection (OD = 0.9 neutral density)	0.161	0.127
Passive laser reflection (No filter)	0.163	0.130
% difference	2 %	2 %

Table 4.6 Effect of Neutral Density Filter on Laser Profile

spot	Average σ_{long} (μm)	Average σ_{short} (μm)
100 nm fluorescent spheres (5 spots)	0.31	0.22
Passive laser reflection (3 spots)	0.31	0.22

Table 4.7 Fluorescent Sphere Control Test Fit Results

spot	Average σ_{long} (μm)	Average σ_{short} (μm)
R6G in PMMA (8 spots)	0.27	0.23
Passive laser reflection (16 spots)	0.28	0.24

Table 4.8 R6G in PMMA Control Test Fit Results

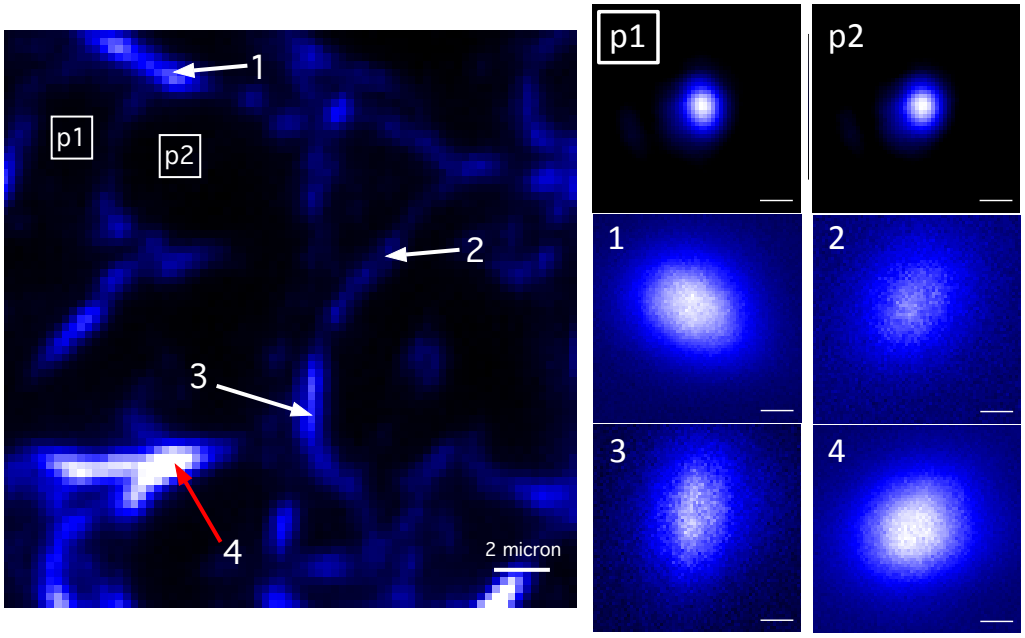

Figure 4.7 Confocal fluorescence image of C8S3 J-aggregate bundles

The six tiles to the right of the confocal image represent the light collected by the CCD from the bundles (fluorescence emission) or passive sample regions (reflected laser); labels correspond to areas marked with arrows in the confocal image. Tiles P1 and P2 show the reflected laser excitation beam used to excite the bundles. Tiles 1-4 represent emission profiles emanating from the bundle excited at locations marked by numbered arrows. Scale bar = 0.5 μm for all tiles.

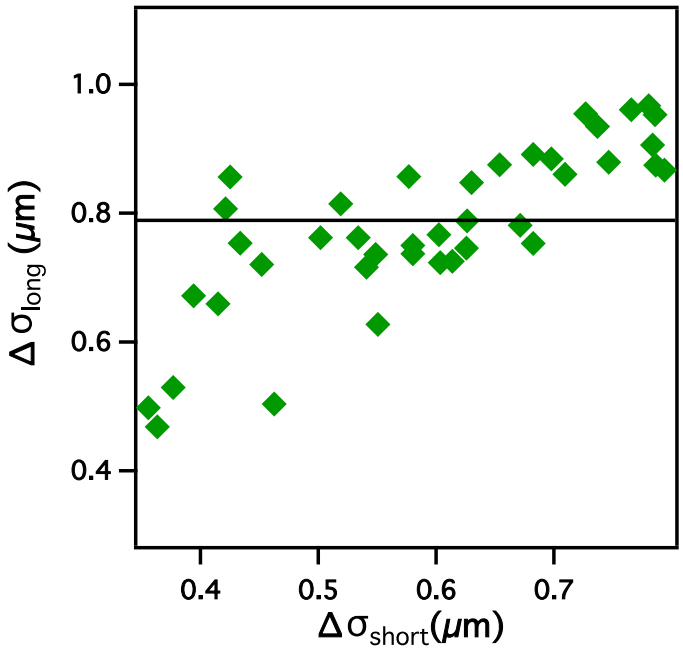

Figure 4.8 C8S3 bundle exciton migration size dependence

The size dependence of C8S3 bundle exciton transport (ET) was investigated by comparing the long and short axis ET widths. The black line indicates the average bundle long axis ET distance of 790 nm.

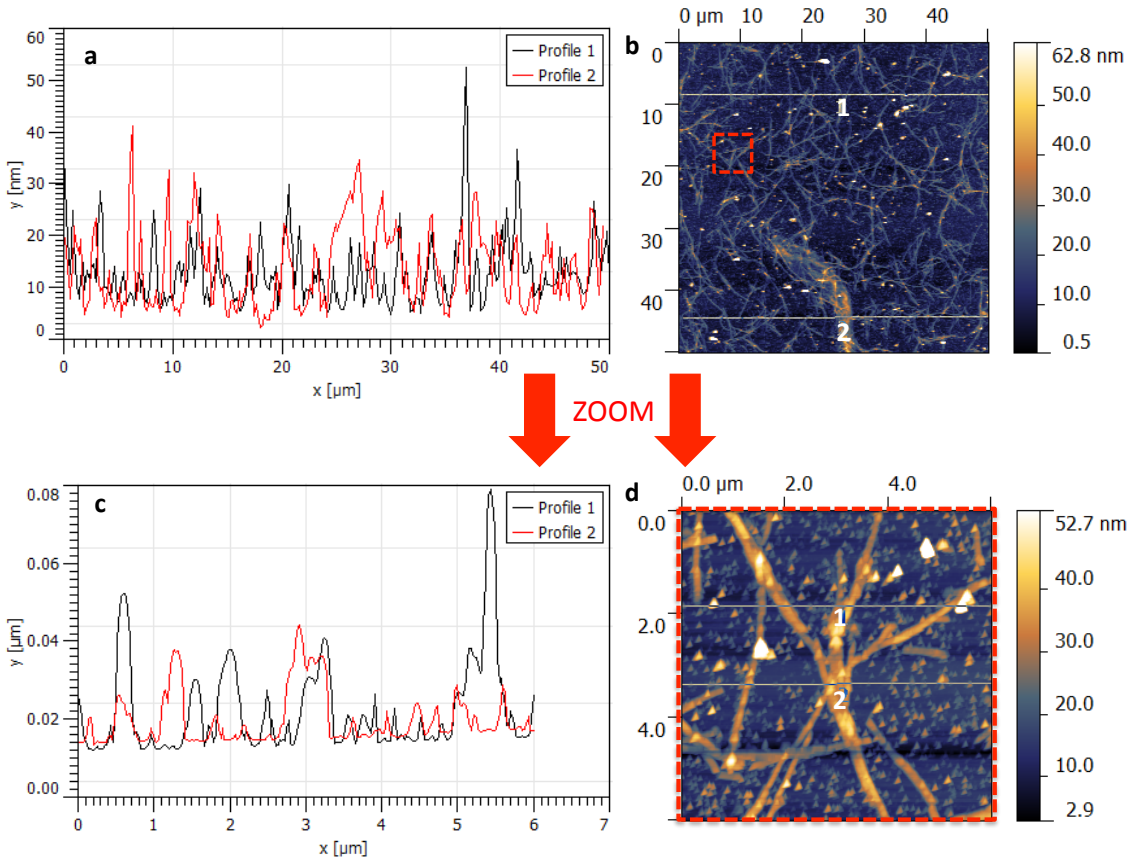

Figure 4.9 AFM images of immobilized C8S3 bundles

AFM images (b, 50 x 50 µm^2) and (d, 5 x 5 µm^2) and corresponding line scans (a) and (c) of C8S3 J-aggregate bundles immobilized on a glass substrate. Average bundle heights of ~ 30 nm indicate that the nanotubular building blocks agglomerate both beside and atop each other. AFM images were collected using an Asylum MFP-3D microscope operating in tapping mode.

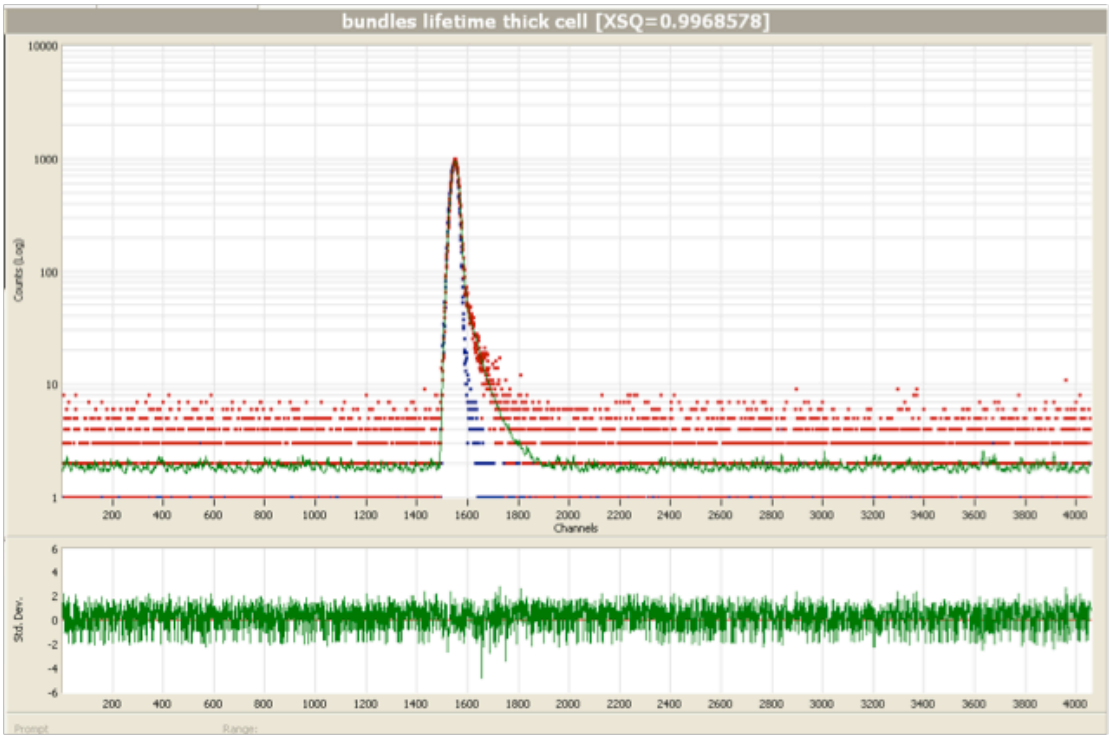

Figure 4.10 C8S3 bundle fluorescence lifetime

Time resolved fluorescence decay of C8S3 bundles in solution (red dots), fit (green line), and instrument response function (blue dots). The residuals from the double exponential fit are shown at the bottom. The fit is a double exponential with a time constant of 200 ps (88% amplitude) and 2 ns (12% amplitude).

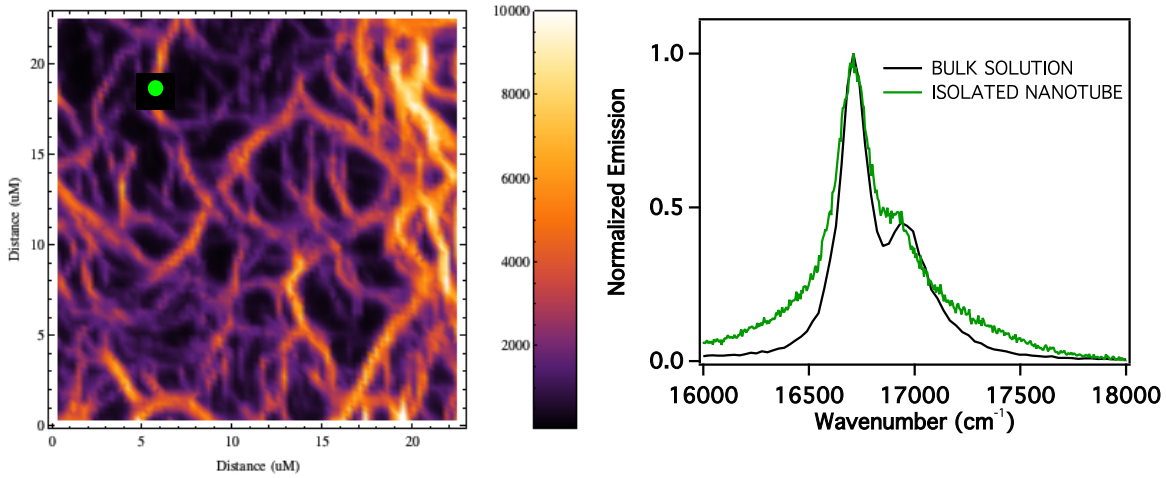

Figure 4.11 Emission from isolated C8S3 nanotubes

Emission spectra from C8S3 nanotubes are overlaid. The bulk solution spectrum (black) is nearly identical to the emission spectrum collected from a nanotube isolated on a glass substrate (green). The isolated emission spectrum corresponds to the region marked with a green dot in the confocal image (left image).

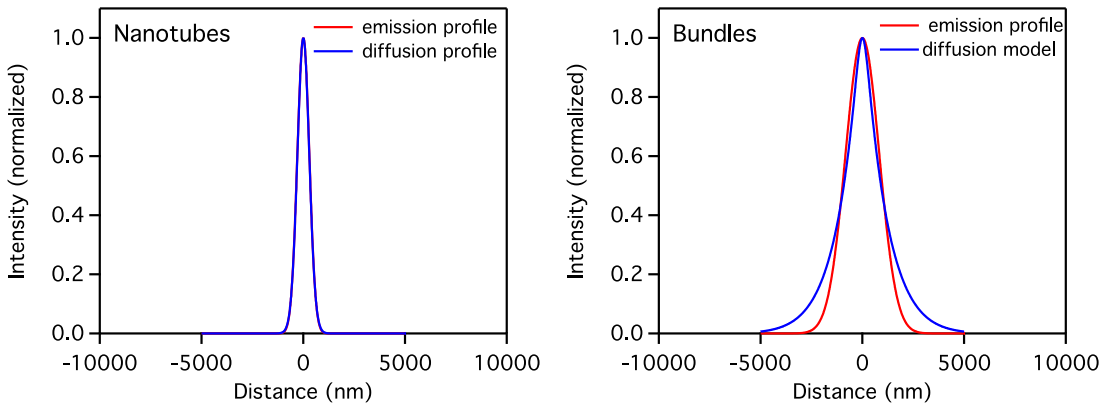

Figure 4.12 C8S3 J-aggregate diffusion model

Left: Nanotube emission profile (red) and 1-D steady-state diffusion profile (blue). Right: Bundles emission profile (red) and 1-D steady-state diffusion profile (blue). For both, the standard deviation without diffusion was set at 260 nm to correspond with the average passive spot. For the nanotubes the model is calculated with a lifetime of 100 ps and a diffusion coefficient of 120 nm^2 ps^{-1}. For the bundles the lifetime was set to 200 ps and the diffusion coefficient is 7000 nm^2 ps^{-1}.

4.7 REFERENCES

1. Ruban, A. V., *The Photosynthetic Membrane: Molecular Mechanisms and Biophysics of Light Harvesting*. Wiley: Chichester, U.K., 2013.
2. Staehelin, L. A.; Golecki, J. R.; Drews, G., Supramolecular Organization of Chlorosomes (Chlorobium Vesicles) and of Their Membrane Attachment Sites in Chlorobium-Limicola. *Biochim. Biophys. Acta* **1980,** *589*, 30-45.
3. Holzwarth, A. R.; Schaffner, K., On the Structure of Bacteriochlorophyll Molecular Aggregates in the Chlorosomes of Green Bacteria - a Molecular Modeling Study. *Photosynth. Res.* **1994,** *41*, 225-233.
4. Buck, D. R.; Struve, W. S., Tubular Exciton Models for Bchl C Antennae in Chlorosomes from Green Photosynthetic Bacteria. *Photosynth. Res.* **1996,** *48*, 367-377.
5. Psencik, J.; Ikonen, T. P.; Laurinmaki, P.; Merckel, M. C.; Butcher, S. J.; Serimaa, R. E.; Tuma, R., Lamellar Organization of Pigments in Chlorosomes, the Light Harvesting Complexes of Green Photosynthetic Bacteria. *Biophys. J.* **2004,** *87*, 1165-1172.
6. Oostergetel, G. T.; Reus, M.; Chew, A. G. M.; Bryant, D. A.; Boekema, E. J.; Holzwarth, A. R., Long-Range Organization of Bacteriochlorophyll in Chlorosomes of Chlorobium Tepidum Investigated by Cryo-Electron Microscopy. *FEBS Letters* **2007,** *581*, 5435-5439.
7. Krauß, N., Mechanisms for Photosystems I and II. *Curr. Opin. Chem. Biol.* **2003,** *7*, 540-550.
8. Balaban, T. S., Tailoring Porphyrins and Chlorins for Self-Assembly in Biomimetic Artificial Antenna Systems. *Acc. Chem. Res.* **2005,** *38*, 612-623.
9. McDermott, G.; Prince, S. M.; Freer, A. A.; Hawthornthwaitelawless, A. M.; Papiz, M. Z.; Cogdell, R. J.; Isaacs, N. W., Crystal-Structure of an Integral Membrane Light-Harvesting Complex from Photosynthetic Bacteria. *Nature* **1995,** *374*, 517-521.
10. Linnanto, J. M.; Korppi-Tommola, J. E. I., Investigation on Chlorosomal Antenna Geometries: Tube, Lamella and Spiral-Type Self-Aggregates. *Photosynth. Res.* **2008,** *96*, 227-245.
11. Novoderezhkin, V.; Razjivin, A., Exciton States of the Antenna and Energy Trapping by the Reaction Center. *Photosynth. Res.* **1994,** *42*, 9-15.
12. Oellerich, S.; Köhler, J., Low-Temperature Single-Molecule Spectroscopy on Photosynthetic Pigment–Protein Complexes from Purple Bacteria. *Photosynth. Res.* **2009,** *101*, 171-179.

13. Escalante, M.; Lenferink, A.; Zhao, Y.; Tas, N.; Huskens, J.; Hunter, C. N.; Subramaniam, V.; Otto, C., Long-Range Energy Propagation in Nanometer Arrays of Light Harvesting Antenna Complexes. *Nano Letters* **2010,** *10*, 1450-1457.

14. Olsen, J. D.; Tucker, J. D.; Timney, J. A.; Qian, P.; Vassilev, C.; Hunter, C. N., The Organization of Lh2 Complexes in Membranes from Rhodobacter Sphaeroides. *J. Biol. Chem.* **2008,** *283*, 30772-30779.

15. Pawlik, A.; Ouart, A.; Kirstein, S.; Abraham, H. W.; Daehne, S., Synthesis and Uv/Vis Spectra of J-Aggregating 5,5 ',6,6 '-Tetrachlorobenzimidacarbocyanine Dyes for Artificial Light-Harvesting Systems and for Asymmetrical Generation of Supramolecular Helices. *Eur. J. Org. Chem.* **2003**, 3065-3080.

16. Bednarz, M.; Knoester, J., The Linear Absorption and Pump-Probe Spectra of Cylindrical Molecular Aggregates. *J. Phys. Chem. B* **2001,** *105*, 12913-12923.

17. Kirstein, S.; Daehne, S., J-Aggregates of Amphiphilic Cyanine Dyes: Self-Organization of Artificial Light Harvesting Complexes. *Int. J. Photoenergy* **2006**.

18. Ganapathy, S.; Oostergetel, G. T.; Wawrzyniak, P. K.; Reus, M.; Gomez Maqueo Chew, A.; Buda, F.; Boekema, E. J.; Bryant, D. A.; Holzwarth, A. R.; de Groot, H. J. M., Alternating Syn-Anti Bacteriochlorophylls Form Concentric Helical Nanotubes in Chlorosomes. *PNAS* **2009,** *106*, 8525-8530.

19. Saikin, S. K.; Eisfeld, A.; Valleau, S.; Guzik, A. A., Photonics Meets Excitonics: Natural and Artificial Molecular Aggregates. *Nanophotonics* **2013,** *2*, 21-38.

20. Scholes, G. D.; Rumbles, G., Excitons in Nanoscale Systems. *Nat Mater* **2006,** *5*, 683-696.

21. Spano, F. C., The Spectral Signatures of Frenkel Polarons in H- and J-Aggregates. *Acc. Chem. Res.* **2009,** *43*, 429-439.

22. Knoester, J., Modeling the Optical Properties of Excitons in Linear and Tubular J-Aggregates. *Int. J. Photoenergy* **2006**.

23. Lang, E.; Sorokin, A.; Drechsler, M.; Malyukin, Y. V.; Köhler, J., Optical Spectroscopy on Individual Amphi-Pic J-Aggregates. *Nano Letters* **2005,** *5*, 2635-2640.

24. Knoester, J.; Daehne, S., Prospects of Artificial Light Harvesting Systems: An Introduction. *Int. J. Photoenergy* **2006**, 1-3.

25. Pugzlys, A.; Augulis, R.; van Loosdrecht, P. H. M.; Didraga, C.; Malyshev, V. A.; Knoester, J., Temperature-Dependent Relaxation of Excitons in Tubular Molecular Aggregates: Fluorescence Decay and Stokes Shift. *J. Phys. Chem. B* **2006,** *110*, 20268-20276.

26. Didraga, C.; Malyshev, V. A.; Knoester, J., Excitation Energy Transfer between Closely Spaced Multichromophoric Systems: Effects of Band Mixing and Intraband Relaxation. *J. Phys. Chem. B* **2006,** *110*, 18818-18827.

27. Sundström, V.; Gillbro, T.; Gadonas, R. A.; Piskarskas, A., Annihilation of Singlet Excitons in J Aggregates of Pseudoisocyanine (Pic) Studied by Pico- and Subpicosecond Spectroscopy. *J. Chem. Phys.* **1988,** *89*, 2754-2762.

28. Valleau, S.; Saikin, S. K.; Yung, M.-H.; Guzik, A. A., Exciton Transport in Thin-Film Cyanine Dye J-Aggregates. *J. Chem. Phys.* **2012,** *137*, 034109: 1-13.

29. Akselrod, G. M.; Tischler, Y. R.; Young, E. R.; Nocera, D. G.; Bulovic, V., Exciton-Exciton Annihilation in Organic Polariton Microcavities. *Phys. Rev. B* **2010,** *82*, 113106.

30. Spitz, C.; Daehne, S., Low Temperature Exciton-Exciton Annihilation in Amphi-Pipe J-Aggregates. *Int. J. Photoenergy* **2006**.

31. Spitz, C.; Knoester, J.; Ouart, A.; Daehne, S., Polarized Absorption and Anomalous Temperature Dependence of Fluorescence Depolarization in Cylindrical J-Aggregates. *Chem. Phys.* **2002,** *275*, 271-284.

32. Didraga, C.; Pugzlys, A.; Hania, P. R.; von Berlepsch, H.; Duppen, K.; Knoester, J., Structure, Spectroscopy, and Microscopic Model of Tubular Carbocyanine Dye Aggregates. *J. Phys. Chem. B* **2004,** *108*, 14976-14985.

33. von Berlepsch, H.; Kirstein, S.; Hania, R.; Pugzlys, A.; Böttcher, C., Modification of the Nanoscale Structure of the J-Aggregate of a Sulfonate-Substituted Amphiphilic Carbocyanine Dye through Incorporation of Surface-Active Additives. *J. Phys. Chem. B* **2007,** *111*, 1701-1711.

34. Eisele, D. M.; Knoester, J.; Kirstein, S.; Vanden Bout, D. A., Uniform Exciton Fluorescence from Individual Molecular Nanotubes Immobilized on Solid Substrates. *Nat Nano* **2009,** *4*, 658-663.

35. Adams, D. M.; Kerimo, J.; O'Connor, D. B.; Barbara, P. F., Spatial Imaging of Singlet Energy Migration in Perylene Bis(Phenethylimide) Thin Films. *J. Phys. Chem. A* **1999,** *103*, 10138-10143.

36. Dubin, F.; Melet, R.; Barisien, T.; Grousson, R.; Legrand, L.; Schott, M.; Voliotis, V., Macroscopic Coherence of a Single Exciton State in an Organic Quantum Wire. *Nat Phys* **2006,** *2*, 32-35.

37. Eisele, D. M.; Cone, C. W.; Bloemsma, E. A.; Vlaming, S. M.; van der Kwaak, C. G. F.; Silbey, R. J.; Bawendi, M. G.; Knoester, J.; Rabe, J. P.; Vanden Bout, D. A., Utilizing Redox-Chemistry to Elucidate the Nature of Exciton Transitions in Supramolecular Dye Nanotubes. *Nat Chem* **2012,** *4*, 655-662.

38. Clark, K. A.; Cone, C. W.; Vanden Bout, D. A., Quantifying the Polarization of Exciton Transitions in Double-Walled Nanotubular J-Aggregates. *J. Phys. Chem. C* **2013,** *117*, 26473-26481.

39. Kobayashi, T., Ed., *J-Aggregates (Volume 2)*. World Scientific Publishing Company: Singapore, 2012.

40. Knox, R. S., Excitation Energy Transfer and Migration: Theoretical Considerations. In *Bioenergetics of Photosynthesis*, Govindjee, Ed. Academic Press: New York, 1975.

41. Kenkre, V. M., Reineker, P., *Exciton Dynamics in Molecular Crystals and Aggregates*. Springer-Verlag: Berlin, 1982.

42. Schein, L. B.; McGhie, A. R., Band-Hopping Mobility Transition in Naphthalene and Deuterated Naphthalene. *Phys. Rev. B* **1979,** *20*, 1631-1639.

43. Shuai, Z., Wang, L., Song, C., *Theory of Charge Transport in Carbon Electronic Materials*. Springer: Heidelberg, 2012.

44. Kopelman, R.; Monberg, E. M.; Ochs, F. W., Exciton Percolation. Ii: Naphthalene $^{1}B_{2u}$ Supertransfer. *Chem. Phys.* **1977,** *21*, 373-383.

45. Silinsh, E. A., *Organic Molecular Crystals: Their Electronic States*. Springer-Verlag: Berlin, 1980.

46. Al-Khatib, O. Structure and Optical Properties of Complex Aggregate-Structures of Amphiphilic Dye Systems. Ph.D. Dissertation, Humboldt University of Berlin, Berlin, 2012.

47. Kenkre, V. M.; Wong, Y. M., Theory of Exciton Migration Experiments with Imperfectly Absorbing End Detectors. *Phys. Rev. B* **1980,** *22*, 5716-5722.

48. Smith, L. M.; Wake, D. R.; Wolfe, J. P.; Levi, D.; Klein, M. V.; Klem, J.; Henderson, T.; Morkoç, H., Picosecond Imaging of Photoexcited Carriers in Quantum Wells: Anomalous Lateral Confinement at High Densities. *Phys. Rev. B* **1988,** *38*, 5788-5791.

49. Müller, A. M.; Bardeen, C. J., Using a Streak Camera to Resolve the Motion of Molecular Excited States with Picosecond Time Resolution and 150 Nm Spatial Resolution. *J. Phys. Chem. C* **2007,** *111*, 12483-12489.

50. Akselrod, G. M.; Deotare, P. B.; Thompson, N. J.; Lee, J.; Tisdale, W. A.; Baldo, M. A.; Menon, V. M.; Bulović, V., Visualization of Exciton Transport in Ordered and Disordered Molecular Solids. *Nat Commun* **2014,** *5*.

51. Ruzicka, B. A.; Wang, R.; Lohrman, J.; Ren, S.; Zhao, H., Exciton Diffusion in Semiconducting Single-Walled Carbon Nanotubes Studied by Transient Absorption Microscopy. *Phys. Rev. B* **2012,** *86*, 205417.

52. Kumar, N.; Cui, Q.; Ceballos, F.; He, D.; Wang, Y.; Zhao, H., Exciton Diffusion in Monolayer and Bulk MoSe2. *Nanoscale* **2014,** *6*, 4915-4919.

53. Lindrum, M.; Glismann, A.; Moll, J.; Daehne, S., Fluorescence Lifetime Measurements and Hole-Burning Experiments on J-Aggregates of a Benzimidocarbocyanine Dye. *Chem. Phys.* **1993,** *178*, 423-432.

54. Scheblykin, I. G.; Bataiev, M. M.; Van der Auweraer, M.; Vitukhnovsky, A. G., Dimensionality and Temperature Dependence of the Radiative Lifetime of J-Aggregates with Davydov Splitting of the Exciton Band. *Chem. Phys. Lett.* **2000,** *316*, 37-44.

55. Silinsh, E. A., Capek, V., *Organic Molecular Crystals: Interaction, Localization, and Transport Phenomena*. American Institute of Physics: New York, 1994.

56. Balzer, F.; Bordo, V. G.; Simonsen, A. C.; Rubahn, H. G., Optical Waveguiding in Individual Nanometer-Scale Organic Fibers. *Phys. Rev. B* **2003,** *67*, 115408.

57. Chaudhuri, D.; Li, D.; Che, Y.; Shafran, E.; Gerton, J. M.; Zang, L.; Lupton, J. M., Enhancing Long-Range Exciton Guiding in Molecular Nanowires by H-Aggregation Lifetime Engineering. *Nano Letters* **2010,** *11*, 488-492.

58. Takazawa, K.; Kitahama, Y.; Kimura, Y.; Kido, G., Optical Waveguide Self-Assembled from Organic Dye Molecules in Solution. *Nano Letters* **2005,** *5*, 1293-1296.

59. Lebedenko, A. N.; Guralchuk, G. Y.; Sorokin, A. V.; Yefimova, S. L.; Malyukin, Y. V., Pseudoisocyanine J-Aggregate to Optical Waveguiding Crystallite Transition: Microscopic and Microspectroscopic Exploration. *J. Phys. Chem. B* **2006,** *110*, 17772-17775.

60. Eisfeld, A.; Briggs, J. S., The J- and H-Bands of Organic Dye Aggregates. *Chem. Phys.* **2006,** *324*, 376-384.

61. Lunt, R. R.; Giebink, N. C.; Belak, A. A.; Benziger, J. B.; Forrest, S. R., Exciton Diffusion Lengths of Organic Semiconductor Thin Films Measured by Spectrally Resolved Photoluminescence Quenching. *J. Appl. Phys.* **2009,** *105*, 053711.

62. Miller, G. K., Probability: Modeling and Applications to Random Processes. John Wiley & Sons, Inc.: Hoboken, New Jersey, 2006.

63. Haber, H. Diagonalization of a 2 X 2 Real Symmetric Matrix. University of California Santa Cruz Physics 116a Web Page. http://scipp.ucsc.edu/~haber/ph116A/diag2x2_11.pdf (accessed October 15 2013).

64. Augulis, R. Molecular Aggregates, Dendrimers, and Motors: Optical Dynamics and Control. Ph.D. Thesis, University of Groningen, Groningen, Netherlands, 2008.

65. Yoon, H. W.; Wake, D. R.; Wolfe, J. P.; Morkoç, H., In-Plane Transport of Photoexcited Carriers in GaAs Quantum Wells. *Phys. Rev. B* **1992,** *46*, 13461-13470.

Bibliography

1. Nathan, F. L.; Paul, V.; Tony, J. P., The State of the Art in Biomimetics. *Bioinspiration & Biomimetics* **2013**, *8*, 013001.
2. Gust, D.; Moore, T. A.; Moore, A. L., Mimicking Photosynthetic Solar Energy Transduction. *Acc. Chem. Res.* **2000**, *34*, 40-48.
3. LaVan, D. A.; Cha, J. N., Approaches for Biological and Biomimetic Energy Conversion. *Proceedings of the National Academy of Sciences* **2006**, *103*, 5251-5255.
4. Ciamician, G., The Photochemistry of the Future. *Science* **1912**, *36*, 385-394.
5. Gust, D.; Moore, T. A., Mimicking Photosynthesis. *Science* **1989**, *244*, 35-41.
6. Sarikaya, M.; Askay, I. A., *Biomimetics: Design and Processing of Materials*. AIP Press: Woodbury, NY, 1995.
7. Bhushan, B., Biomimetics: Lessons from Nature–an Overview. *Philosophical Transactions of the Royal Society A: Mathematical, Physical and Engineering Sciences* **2009**, *367*, 1445-1486.
8. Bar-Cohen, Y., Biomimetics : Biologically Inspired Technologies. Taylor and Francis: Hoboken, 2005.
9. Large, M., *Optical Biomimetics: Materials and Applications*. Woodhead Publishing: Philadelphia, 2012.
10. Nash, M., *Biomimetics. Encyclopedia of Nanoscience and Society. Sage Publications, Inc*. SAGE Publications, Inc.: Thousand Oaks, CA, 2010.
11. Sykora, M.; Maxwell, K. A.; DeSimone, J. M.; Meyer, T. J., Mimicking the Antenna-Electron Transfer Properties of Photosynthesis. *Proceedings of the National Academy of Sciences* **2000**, *97*, 7687-7691.
12. Gratzel, M., Photoelectrochemical Cells. *Nature* **2001**, *414*, 338-334.
13. Rochford, J.; Chu, D.; Hagfeldt, A.; Galoppini, E., Tetrachelate Porphyrin Chromophores for Metal Oxide Semiconductor Sensitization: Effect of the Spacer Length and Anchoring Group Position. *J. Am. Chem. Soc.* **2007**, *129*, 4655-4665.
14. Harriman, A., Unusually Slow Charge Recombination in Molecular Dyads. *Angew. Chem. Int. Ed.* **2004**, *43*, 4985-4987.
15. Orf, G.; Blankenship, R., Chlorosome Antenna Complexes from Green Photosynthetic Bacteria. *Photosynth. Res.* **2013**, *116*, 315-331.

16. Balaban, T. S.; Tamiaki, H.; Holzwarth, A. R., Chlorins Programmed for Self-Assembly. In *Top. Curr. Chem.: Supermolecular Dye Chemistry*, 2005; Vol. 258, pp 1-38.

17. Blankenship, R. E., Matsuura, K., Antenna Complexes from Green Photsynthetica Bacteria. In *Light-Harvesting Antennas in Photosynthesis*, Govindjee, Ed. Kluwer: Dordrecht, 2003; Vol. 13, pp 195-217.

18. Olson, J. M., Chlorophyll Organization in Green Photosynthetic Bacteria. *Biochimica et Biophysica Acta (BBA) - Reviews on Bioenergetics* **1980**, *594*, 33-51.

19. Oostergetel, G. T.; Reus, M.; Chew, A. G. M.; Bryant, D. A.; Boekema, E. J.; Holzwarth, A. R., Long-Range Organization of Bacteriochlorophyll in Chlorosomes of Chlorobium Tepidum Investigated by Cryo-Electron Microscopy. *FEBS Letters* **2007**, *581*, 5435-5439.

20. Renger, T.; May, V.; Kühn, O., Ultrafast Excitation Energy Transfer Dynamics in Photosynthetic Pigment–Protein Complexes. *Physics Reports* **2001**, *343*, 137-254.

21. Psencik, J.; Ikonen, T. P.; Laurinmaki, P.; Merckel, M. C.; Butcher, S. J.; Serimaa, R. E.; Tuma, R., Lamellar Organization of Pigments in Chlorosomes, the Light Harvesting Complexes of Green Photosynthetic Bacteria. *Biophys. J.* **2004**, *87*, 1165-1172.

22. Jelley, E. E., Spectral Absorption and Fluorescence of Dyes in the Molecule State. *Nature* 1936, *138*, 1009-1010.

23. Jelley, E. E., Molecular, Nematic and Crystal States of I:I'-Diethyl-Psi-Cyanine Chloride. *Nature* **1937**, *139*, 631-632.

24. Scheibe, G., Über Die Veränderlichkeit Der Absorptionsspektren in Lösung Und Die Nebenvalenzen Als Ihre Ursache. *Angew. Chem.* **1937**, *50*, 212-219.

25. Scheibe, G., Variability of the Absorption Spectra of Some Sensitizing Dyes and Its Cause. *Angewandte Chemie* **1936**, *1936*, 563.

26. Franck, J.; Teller, E., Migration and Photochemical Action of Excitation Energy in Crystals. *J. Chem. Phys.* **1938**, *6*, 861-872.

27. Scholes, G. D.; Rumbles, G., Excitons in Nanoscale Systems. *Nature Materials* **2006**, *5*, 683-696.

28. Möbius, D., Scheibe Aggregates. *Advanced Materials* **1995**, *7*, 437-444.

29. Davydov, A. S., *Theory of Molecular Excitons*. Plenum Press: New York, 1971.

30. Würthner, F.; Kaiser, T. E.; Saha-Möller, C. R., J-Aggregates: From Serendipitous Discovery to Supramolecular Engineering of Functional Dye Materials. *Angew. Chem. Int. Ed.* **2011**, *50*, 3376-3410.

31. Kobayashi, T., *J-Aggregates*. World Scientific, Singapore: 1996.

32. Frenkel, J., On the Transformation of Light into Heat in Solids. I. *Phys. Rev.* **1931**, *37*, 17-44.

33. Bloemsma, E. A. Exciton Localization and and Optical Spectroscopy of Linear and Tubular J-Aggregates. Dissertation, University of Groningen, Groningen, 2013.

34. De Rossi, U.; Moll, J.; Spieles, M.; Bach, G.; Dähne, S.; Kriwanek, J.; Lisk, M., Control of the J-Aggregation Phenomenon by Variation of the N-Alkyl-Substituents. *J. Prakt. Chem.* **1995**, *337*, 203-208.

35. Pawlik, A.; Ouart, A.; Kirstein, S.; Abraham, H. W.; Daehne, S., Synthesis and Uv/Vis Spectra of J-Aggregating 5,5 ',6,6 '-Tetrachlorobenzimidacarbocyanine Dyes for Artificial Light-Harvesting Systems and for Asymmetrical Generation of Supramolecular Helices. *Eur. J. Org. Chem.* **2003**, 3065-3080.

36. Mishra, A.; Behera, R. K.; Behera, P. K.; Mishra, B. K.; Behera, G. B., Cyanines During the 1990s: A Review. *Chem. Rev.* **2000**, *100*, 1973-2011.

37. Kirstein, S.; Daehne, S., J-Aggregates of Amphiphilic Cyanine Dyes: Self-Organization of Artificial Light Harvesting Complexes. *Int. J. Photoenergy* **2006**.

38. Hamanaka, Y.; Kawasaki, O.; Yamauchi, T.; Nakamura, A., Morphology of Self-Assembled Merocyanine J-Aggregates in Films Studied by Scanning near-Field Optical Microscope. *Chem. Phys. Lett.* **2003**, *378*, 47-54.

39. von Berlepsch, H.; Kirstein, S.; Hania, R.; Pug≈ælys, A.; B√∂ttcher, C., Modification of the Nanoscale Structure of the J-Aggregate of a Sulfonate-Substituted Amphiphilic Carbocyanine Dye through Incorporation of Surface-Active Additives. *J. Phys. Chem. B* **2007**, *111*, 1701-1711.

40. von Berlepsch, H.; Bottcher, C.; Ouart, A.; Regenbrecht, M.; Akari, S.; Keiderling, U.; Schnablegger, H.; Dahne, S.; Kirstein, S., Surfactant-Induced Changes of Morphology of J-Aggregates: Superhelix-to-Tubule Transformation. *Langmuir* **2000**, *16*, 5908-5916.

41. Vacha, M.; Saeki, M.; Hashizume, K.; Tani, T., Micro-Spectroscopy of Individual Nanostructures of Molecular Aggregates: Relationship between Morphology and Optical Properties. *Chemical Physics* **2002**, *285*, 149-155.

42. Kobayashi, T., Ed., *J-Aggregates (Volume 2)*. World Scientific Publishing Company: Singapore, 2012.

43. Mees, C. E. K., *The Theory of the Photographic Provess*. The MacMillan Company: New York, 1942.

44. Herz, A. H., Aggregation of Sensitizing Dyes in Solution and Their Adsorption onto Silver Halides. *Adv. Colloid Interface Sci.* **1977**, *8*, 237-298.

45. McDermott, G.; Prince, S. M.; Freer, A. A.; Hawthornthwaitelawless, A. M.; Papiz, M. Z.; Cogdell, R. J.; Isaacs, N. W., Crystal-Structure of an Integral Membrane Light-Harvesting Complex from Photosynthetic Bacteria. *Nature* **1995**, *374*, 517-521.

46. Holzwarth, A. R.; Schaffner, K., On the Structure of Bacteriochlorophyll Molecular Aggregates in the Chlorosomes of Green Bacteria - a Molecular Modeling Study. *Photosynth. Res.* **1994**, *41*, 225-233.

47. Knoester, J.; Daehne, S., Prospects of Artificial Light Harvesting Systems: An Introduction. *Int. J. Photoenergy* **2006**.

48. von Berlepsch, H.; Bottcher, C.; Ouart, A.; Burger, C.; Dahne, S.; Kirstein, S., Supramolecular Structures of J-Aggregates of Carbocyanine Dyes in Solution. *J. Phys. Chem. B* **2000**, *104*, 5255-5262.

49. von Berlepsch, H.; Kirstein, S.; Hania, R.; Pugzlys, A.; Böttcher, C., Modification of the Nanoscale Structure of the J-Aggregate of a Sulfonate-Substituted Amphiphilic Carbocyanine Dye through Incorporation of Surface-Active Additives. *J. Phys. Chem. B* **2007**, *111*, 1701-1711.

50. Eisele, D. M.; Arias, D. H.; Fu, X.; Bloemsma, E. A.; Steiner, C. P.; Jensen, R. A.; Rebentrost, P.; Eisele, H.; Tokmakoff, A.; Lloyd, S.; Nelson, K. A.; Nicastro, D.; Knoester, J.; Bawendi, M. G., Robust Excitons Inhabit Soft Supra-Molecular Nanotubes. *Proc. Natl. Acad. Sci. USA*, submitted for publication.

51. Saikin, S. K.; Eisfeld, A.; Valleau, S.; Guzik, A. A., Photonics Meets Excitonics: Natural and Artificial Molecular Aggregates. *Nanophotonics* **2013**, *2*, 21-38.

52. Kasha, M.; Rawls, H. R.; Ashraf El-Bayoumi, M., The Exciton Model in Molecular Spectroscopy. *Pure Appl. Chem.* **1965**, *11*, 371-392.

53. Kasha, M., Relation between Exciton Bands and Conduction Bands in Molecular Lamellar Systems. *Reviews of Modern Physics* **1959**, *31*, 162-169.

54. Spano, F. C., The Spectral Signatures of Frenkel Polarons in H- and J-Aggregates. *Acc. Chem. Res.* **2009**, *43*, 429-439.

55. Knoester, J., Modeling the Optical Properties of Excitons in Linear and Tubular J-Aggregates. *Int. J. Photoenergy* **2006**.

56. Didraga, C.; Klugkist, J. A.; Knoester, J., Optical Properties of Helical Cylindrical Molecular Aggregates: The Homogeneous Limit. *J. Phys. Chem. B* **2002**, *106*, 11474-11486.

57. Didraga, C.; Pugzlys, A.; Hania, P. R.; von Berlepsch, H.; Duppen, K.; Knoester, J., Structure, Spectroscopy, and Microscopic Model of Tubular Carbocyanine Dye Aggregates. *J. Phys. Chem. B* **2004**, *108*, 14976-14985.

58. Didraga, C.; Knoester, J., Optical Spectra and Localization of Excitons in Inhomogeneous Helical Cylindrical Aggregates. *J. Chem. Phys.* **2004**, *121*, 10687-10698.

59. Heijs, D. J. Optical Dynamics in Multichromophore Systems. Dissertation, University of Groningen, Groningen, 2006.

60. Fidder, H.; Terpstra, J.; Wiersma, D. A., Dynamics of Frenkel Excitons in Disordered Molecular Aggregates. *J. Chem. Phys.* **1991**, *94*, 6895-6907.

61. Lyon, J. L.; Eisele, D. M.; Kirstein, S.; Rabe, J. P.; Vanden Bout, D. A.; Stevenson, K. J., Spectroelectrochemical Investigation of Double-Walled Tubular J-Aggregates of Amphiphilic Cyanine Dyes. *J. Phys. Chem. C* **2008**, *112*, 1260-1268.

62. Eisele, D. M.; Knoester, J.; Kirstein, S.; Vanden Bout, D. A., Uniform Exciton Fluorescence from Individual Molecular Nanotubes Immobilized on Solid Substrates. *Nat Nano* **2009**, *4*, 658-663.

63. Augulis, R.; Pugžlys, A.; van Loosdrecht, P. H. M., Exciton Dynamics in Molecular Aggregates. *Phys. Status Solidi C* **2006**, *3*, 3400-3403.

64. Milota, F.; Sperling, J.; Nemeth, A.; Kauffmann, H. F., Two-Dimensional Electronic Photon Echoes of a Double Band J-Aggregate: Quantum Oscillatory Motion Versus Exciton Relaxation. *Chemical Physics* **2009**, *357*, 45-53.

65. Milota, F.; Sperling, J.; Nemeth, A.; Abramavicius, D.; Mukamel, S.; Kauffmann, H. F., Excitonic Couplings and Interband Energy Transfer in a Double-Wall Molecular Aggregate Imaged by Coherent Two-Dimensional Electronic Spectroscopy. *J. Chem. Phys.* **2009**, *131*, 054510-23.

66. Sperling, J.; Nemeth, A.; Hauer, J.; Abramavicius, D.; Mukamel, S.; Kauffmann, H. F.; Milota, F., Excitons and Disorder in Molecular Nanotubes: A 2d Electronic Spectroscopy Study and First Comparison to a Microscopic Model. *J. Phys. Chem. A* **2010**, *114*, 8179-8189.

67. Womick, J. M.; Miller, S. A.; Moran, A. M., Correlated Exciton Fluctuations in Cylindrical Molecular Aggregates. *J. Phys. Chem. B* **2009**, *113*, 6630-6639.

68. Womick, J. M.; Miller, S. A.; Moran, A. M., Probing the Dynamics of Intraband Electronic Coherences in Cylindrical Molecular Aggregates. *J. Phys. Chem. A* **2009**, *113*, 6587-6598.

69. Eisele, D. M.; Cone, C. W.; Bloemsma, E. A.; Vlaming, S. M.; van der Kwaak, C. G. F.; Silbey, R. J.; Bawendi, M. G.; Knoester, J.; Rabe, J. P.; Vanden Bout, D.

A., Utilizing Redox-Chemistry to Elucidate the Nature of Exciton Transitions in Supramolecular Dye Nanotubes. *Nat Chem* **2012**, *4*, 655-662.

70. Vlaming, S. M.; Bloemsma, E. A.; Nietiadi, M. L.; Knoester, J., Disorder-Induced Exciton Localization and Violation of Optical Selection Rules in Supramolecular Nanotubes. *J. Chem. Phys.* **2011**, *134*, 114507-11.

71. Scheblykin, I. G.; Sliusarenko, O. Y.; Lepnev, L. S.; Vitukhnovsky, A. G.; Van der Auweraer, M., Strong Nonmonotonous Temperature Dependence of Exciton Migration Rate in J Aggregates at Temperatures from 5 to 300 K. *J. Phys. Chem. B* **2000**, *104*, 10949-10951.

72. Kaiser, T. E.; Scheblykin, I. G.; Thomsson, D.; Wu¨rthner, F., Temperature-Dependent Exciton Dynamics in J-Aggregates—When Disorder Plays a Role. *J. Phys. Chem. B* **2009**, *113*, 15836-15842.

73. Scheblykin, I. G.; Sliusarenko, O. Y.; Lepnev, L. S.; Vitukhnovsky, A. G.; Van der Auweraer, M., Excitons in Molecular Aggregates of 3,3‘-Bis-[3-Sulfopropyl]-5,5‘-Dichloro-9- Ethylthiacarbocyanine (Thiats): Temperature Dependent Properties. *J. Phys. Chem. B* **2001**, *105*, 4636-4646.

74. Dorn, H.-P.; Müller, A., Scheibe-Aggregates of Pseudoisocyanine in Solution and in Molecular Monolayers. *Appl. Phys. B* **1987**, *43*, 167-172.

75. Fidder, H.; Knoester, J.; Wiersma, D. A., Superradiant Emission and Optical Dephasing in J-Aggregates. *Chemical Physics Letters* **1990**, *171*, 529-536.

76. Scheblykin, I. G.; Bataiev, M. M.; Van der Auweraer, M.; Vitukhnovsky, A. G., Dimensionality and Temperature Dependence of the Radiative Lifetime of J-Aggregates with Davydov Splitting of the Exciton Band. *Chemical Physics Letters* **2000**, *316*, 37-44.

77. Pugzlys, A.; Augulis, R.; van Loosdrecht, P. H. M.; Didraga, C.; Malyshev, V. A.; Knoester, J., Temperature-Dependent Relaxation of Excitons in Tubular Molecular Aggregates: Fluorescence Decay and Stokes Shift. *J. Phys. Chem. B* **2006**, *110*, 20268-20276.

78. Knoester, J.; Daehne, S., Prospects of Artificial Light Harvesting Systems: An Introduction. *Int. J. Photoenergy* **2006**, 1-3.

79. Knoester, J.; Agranovich, V. M., Frenkel and Charge-Transfer Excitons in Organic Solids. In *Electronic Excitations in Organic Based Nanostructures*, Agranovich, V. M. B., G.F., Ed. Elsevier: Amsterdam, 2003; Vol. 31, pp 1-96.

80. Sundström, V.; Gillbro, T.; Gadonas, R. A.; Piskarskas, A., Annihilation of Singlet Excitons in J Aggregates of Pseudoisocyanine (Pic) Studied by Pico- and Subpicosecond Spectroscopy. *J. Chem. Phys.* **1988**, *89*, 2754-2762.

81. Silinsh, E. A., Capek, V., *Organic Molecular Crystals: Interaction, Localization, and Transport Phenomena*. American Institute of Physics: New York, 1994.

82. Spitz, C.; Knoester, J.; Ouart, A.; Daehne, S., Polarized Absorption and Anomalous Temperature Dependence of Fluorescence Depolarization in Cylindrical J-Aggregates. *Chemical Physics* **2002**, *275*, 271-284.

83. Valleau, S.; Saikin, S. K.; Yung, M.-H.; Guzik, A. A., Exciton Transport in Thin-Film Cyanine Dye J-Aggregates. *J. Chem. Phys.* **2012**, *137*, 034109: 1-13.

84. Akselrod, G. M.; Tischler, Y. R.; Young, E. R.; Nocera, D. G.; Bulovic, V., Exciton-Exciton Annihilation in Organic Polariton Microcavities. *Physical Review B* **2010**, *82*, 113106.

85. Adams, D. M.; Kerimo, J.; O'Connor, D. B.; Barbara, P. F., Spatial Imaging of Singlet Energy Migration in Perylene Bis(Phenethylimide) Thin Films. *J. Phys. Chem. A* **1999**, *103*, 10138-10143.

86. Kumar, N.; Cui, Q.; Ceballos, F.; He, D.; Wang, Y.; Zhao, H., Exciton Diffusion in Monolayer and Bulk $MoSe_2$. *Nanoscale* **2014**, *6*, 4915-4919.

87. Dubin, F.; Melet, R.; Barisien, T.; Grousson, R.; Legrand, L.; Schott, M.; Voliotis, V., Macroscopic Coherence of a Single Exciton State in an Organic Quantum Wire. *Nat Phys* **2006**, *2*, 32-35.

88. Escalante, M.; Lenferink, A.; Zhao, Y.; Tas, N.; Huskens, J.; Hunter, C. N.; Subramaniam, V.; Otto, C., Long-Range Energy Propagation in Nanometer Arrays of Light Harvesting Antenna Complexes. *Nano Letters* **2010**, *10*, 1450-1457.

89. Pawlik, A.; Kirstein, S.; DeRossi, U.; Daehne, S., Structural Conditions for Spontaneous Generation of Optical Activity in J-Aggregates. *J. Phys. Chem. B* **1997**, *101*, 5646-5651.

90. Aida, T.; Meijer, E. W.; Stupp, S. I., Functional Supramolecular Polymers. *Science* **2012**, *335*, 813-817.

91. Linnanto, J. M.; Korppi-Tommola, J. E. I., Investigation on Chlorosomal Antenna Geometries: Tube, Lamella and Spiral-Type Self-Aggregates. *Photosynth. Res.* **2008**, *96*, 227-245.

92. Balaban, T. S., Tailoring Porphyrins and Chlorins for Self-Assembly in Biomimetic Artificial Antenna Systems. *Acc. Chem. Res.* **2005**, *38*, 612-623.

93. Psencik, J.; Ma, Y.-Z.; Arellano, J. B.; Hala, J.; Gillbro, T., Excitation Energy Transfer Dynamics and Excited-State Structure in Chlorosomes of Chlorobium Phaeobacteroides. *Biophys. J.* **2003**, *84*, 1161-1179.

94. Milota, F.; Prokhorenko, V. I.; Mancal, T.; von Berlepsch, H.; Bixner, O.; Kauffmann, H. F.; Hauer, J., Vibronic and Vibrational Coherences in Two-Dimensional Electronic Spectra of Supramolecular J-Aggregates. *J. Phys. Chem. A* **2013**, *117*, 6007-6014.

95. Eisele, D. M.; von Berlepsch, H.; Bottcher, C.; Stevenson, K. J.; Vanden Bout, D. A.; Kirstein, S.; Rabe, J. P., Photoinitiated Growth of Sub-7 Nm Silver Nanowires within a Chemically Active Organic Nanotubular Template. *J. Am. Chem. Soc.* **2010**, *132*, 2104-2105.

96. von Berlepsch, H.; Kirstein, S.; Bottcher, C., Effect of Alcohols on J-Aggregation of a Carbocyanine Dye. *Langmuir* **2002**, *18*, 7699-7705.

97. Spano, F. C., Modeling Disorder in Polymer Aggregates: The Optical Spectroscopy of Regioregular Poly(3-Hexylthiophene) Thin Films. *J. Chem. Phys.* **2005**, *122*, 234701-15.

98. Scholes, G. D.; Rumbles, G., Excitons in Nanoscale Systems. *Nat Mater* **2006**, *5*, 683-696.

99. Abrahams, E.; Anderson, P. W.; Licciardello, D. C.; Ramakrishnan, T. V., Scaling Theory of Localization: Absence of Quantum Diffusion in Two Dimensions. *Phys. Rev. Lett.* **1979**, *42*, 673-676.

100. Hofrichter, J.; Eaton, W. A., Linear Dichroism of Biological Chromophores. *Annu. Rev. Biophys. Bio.* **1976**, *5*, 511-560.

101. Nordén, B., Applications of Linear Dichroism Spectroscopy. *Appl. Spectrosc. Rev.* **1978**, *14*, 157-248.

102. Nordén, B.; Rodger, A.; Dafforn, T., *Linear Dichroism and Circular Dichroism: A Textbook on Polarized-Light Spectroscopy*. Royal Society of Chemistry: Cambridge, 2010.

103. von Berlepsch, H.; Kirstein, S.; Hania, R.; Didraga, C.; Pugzlys, A.; Bottcher, C., Stabilization of Individual Tubular J-Aggregates by Poly(Vinyl Alcohol). *J. Phys. Chem. B* **2003**, *107*, 14176-14184.

104. v. Berlepsch, H.; Böttcher, C., Supramolecular Structure of Ttbc J-Aggregates in Solution and on Surface. *Langmuir* **2013**, *29*, 4948-4958.

105. Dafforn, T. R.; Rodger, A., Linear Dichroism of Biomolecules: Which Way Is Up? *Curr. Opin. Struc. Biol.* **2004**, *14*, 541-546.

106. Cone, C. W.; Cho, S.; Lyon, J. L.; Eisele, D. r. M.; Rabe, J. r. P.; Stevenson, K. J.; Rossky, P. J.; Vanden Bout, D. A., Singular Value Decomposition Analysis of Spectroelectrochemical Redox Chemistry in Supramolecular Dye Nanotubes. *J. Phys. Chem. C* **2011**, *115*, 14978-14987.

107. Spano, F. C.; Clark, J.; Silva, C.; Friend, R. H., Determining Exciton Coherence from the Photoluminescence Spectral Line Shape in Poly(3-Hexylthiophene) Thin Films. *J. Chem. Phys.* **2009**, *130*, 074904-16.

108. Spano, F. C.; Yamagata, H., Vibronic Coupling in J-Aggregates and Beyond: A Direct Means of Determining the Exciton Coherence Length from the Photoluminescence Spectrum. *J. Phys. Chem. B* **2011**, *115*, 5133-5143.

109. Eisfeld, A.; Schulz, G.; Briggs, J., The Influence of Geometry on the Vibronic Spectra of Quantum Aggregates. *J. Lumin.* **2011**, *131*, 2555-2564.

110. Bednarz, M.; Knoester, J., The Linear Absorption and Pump-Probe Spectra of Cylindrical Molecular Aggregates. *J. Phys. Chem. B* **2001**, *105*, 12913-12923.

111. Würthner, F.; Kaiser, T. E.; Saha-Möller, C. R., J-Aggregates: From Serendipitous Discovery to Supramolecular Engineering of Functional Dye Materials. *Angew. Chem. Int. Ed.*, **2011**, *50*, 3376-3410.

112. von Berlepsch, H.; Bottcher, C., The Morphologies of Molecular Cyanine Dye Aggregates as Revealed by Cryogenic Transmission Electron Microscopy. In *J-Aggregates (Volume 2)*, Kobayashi, T., Ed. World Scientific Publishing Co. : Singapore, 2012.

113. Clark, K. A.; Krueger, E. L.; Vanden Bout, D. A., Direct Measurement of Energy Migration in Supramolecular Carbocyanine Dye Nanotubes. *J. Phys. Chem. Lett.***2014**, *5*, 2274-2282.

114. Makio, S.; Kanamaru, N.; Tanaka, J., The J-Aggregate 5,5″,6,6″-Tetrachloro-1,1″-Diethyl-3,3″-Bis(4-Sulfobutyl)Benzimidazolocarbocyanine Sodium Salt in Aqueous Solution. *Bull. Chem. Soc. Jpn.* **1980**, *53*, 3120-3124.

115. Saga, Y.; Tamiaki, H., Transmission Electron Microscopic Study on Supramolecular Nanostructures of Bacteriochlorophyll Self-Aggregates in Chlorosomes of Green Photosynthetic Bacteria. *Journal of Bioscience and Bioengineering* **2006**, *102*, 118-123.

116. Clark, K. A.; Cone, C. W.; Vanden Bout, D. A., Quantifying the Polarization of Exciton Transitions in Double-Walled Nanotubular J-Aggregates. *J. Phys. Chem. C* **2013**, *117*, 26473-26481.

117. Lyon, J. L.; Eisele, D. M.; Kirstein, S.; Rabe, J. P.; Vanden Bout, D. A.; Stevenson, K. J., Spectroelectrochemical Investigation of Double-Walled Tubular J-Aggregates of Amphiphilic Cyanine Dyes. *J. Phys. Chem. C* **2008**, *112*, 1260-1268.

118. Cooper, W., Multiplet Structure of Aggregated States in 1,1′-Diethyl-2,2′-Cyanine Dye. *Chemical Physics Letters* **1970**, *7*, 73-77.

119. Murata, S., On the Stability of the J Aggregates of Pseudoisocyanine Formed in Low Temperature Glasses. *J. Soc. Photogr. Sci. Technol. Japan* **1989**, *52*, 24-26.

120. Drobizhev, M. A.; Sapozhnikov, M. N.; Scheblykin, I. G.; Varnavsky, O. P.; Auweraer, M. V. d.; Vitukhnovsky, A. G., Exciton Dynamics and Trapping in J-Aggregates of Carbocyanine Dyes. *Pure and Applied Optics: Journal of the European Optical Society Part A* **1996**, *5*, 569.

121. de Boer, S.; Vink, K. J.; Wiersma, D. A., Optical Dynamics of Condensed Molecular Aggregates: An Accumulated Photon-Echo and Hole-Burning Study of the J-Aggregate. *Chemical Physics Letters* **1987**, *137*, 99-106.

122. Pugzlys, A.; Hania, P. R.; Augulis, R.; Duppen, K.; van Loosdrecht, P. H. M., Cylindrical Aggregates of 5,5 ',6,6 '-Tetrachlorobenzimidacarbocyanine Amphiphilic Derivatives: Structure-Related Optical Properties and Exciton Dynamics. *Int. J. Photoenergy* **2006**.

123. Al-Khatib, O. Structure and Optical Properties of Complex Aggregate-Structures of Amphiphilic Dye Systems. Ph.D. Dissertation, Humboldt University of Berlin, Berlin, 2012.

124. Potma, E. O.; Wiersma, D. A., Exciton Superradiance in Aggregates: The Effect of Disorder, Higher Order Exciton-Phonon Coupling and Dimensionality. *J. Chem. Phys.* **1998**, *108*, 4894-4903.

125. Kamalov, V. F.; Struganova, I. A.; Yoshihara, K., Temperature Dependent Radiative Lifetime of J-Aggregates. *The Journal of Physical Chemistry* **1996**, *100*, 8640-8644.

126. Fidder, H.; Wiersma, D. A., Collective Optical Response of Molecular Aggregates. *physica status solidi (b)* **1995**, *188*, 285-295.

127. Feldmann, J.; Peter, G.; Göbel, E. O.; Dawson, P.; Moore, K.; Foxon, C.; Elliott, R. J., Linewidth Dependence of Radiative Exciton Lifetimes in Quantum Wells. *Phys. Rev. Lett.* **1987**, *59*, 2337-2340.

128. Moll, J.; Daehne, S.; Durrant, J. R.; Wiersma, D. A., Optical Dynamics of Excitons in J Aggregates of a Carbocyanine Dye. *J. Chem. Phys.* **1995,** *102*, 6362-6370.

129. Bednarz, M.; Malyshev, V. A.; Knoester, J., Temperature Dependent Fluorescence in Disordered Frenkel Chains: Interplay of Equilibration and Local Band-Edge Level Structure. *Phys. Rev. Lett.* **2003**, *91*, 217401.

130. Kenkre, V. M., Reineker, P., *Exciton Dynamics in Molecular Crystals and Aggregates*. Springer-Verlag: Berlin, 1982.

131. Ruban, A. V., *The Photosynthetic Membrane: Molecular Mechanisms and Biophysics of Light Harvesting*. Wiley: Chichester, U.K., 2013.

132. Staehelin, L. A.; Golecki, J. R.; Drews, G., Supramolecular Organization of Chlorosomes (Chlorobium Vesicles) and of Their Membrane Attachment Sites in Chlorobium-Limicola. *Biochimica Et Biophysica Acta* **1980**, *589*, 30-45.

133. Buck, D. R.; Struve, W. S., Tubular Exciton Models for Bchl C Antennae in Chlorosomes from Green Photosynthetic Bacteria. *Photosynth. Res.* **1996**, *48*, 367-377.

134. Krauß, N., Mechanisms for Photosystems I and II. *Curr. Opin. Chem. Biol.* **2003**, *7*, 540-550.

135. Novoderezhkin, V.; Razjivin, A., Exciton States of the Antenna and Energy Trapping by the Reaction Center. *Photosynth. Res.* **1994**, *42*, 9-15.

136. Oellerich, S.; Köhler, J., Low-Temperature Single-Molecule Spectroscopy on Photosynthetic Pigment–Protein Complexes from Purple Bacteria. *Photosynth. Res.* **2009**, *101*, 171-179.

137. Olsen, J. D.; Tucker, J. D.; Timney, J. A.; Qian, P.; Vassilev, C.; Hunter, C. N., The Organization of Lh2 Complexes in Membranes from Rhodobacter Sphaeroides. *J. Biol. Chem.* **2008**, *283*, 30772-30779.

138. Ganapathy, S.; Oostergetel, G. T.; Wawrzyniak, P. K.; Reus, M.; Gomez Maqueo Chew, A.; Buda, F.; Boekema, E. J.; Bryant, D. A.; Holzwarth, A. R.; de Groot, H. J. M., Alternating Syn-Anti Bacteriochlorophylls Form Concentric Helical Nanotubes in Chlorosomes. *Proceedings of the National Academy of Sciences* **2009**.

139. Lang, E.; Sorokin, A.; Drechsler, M.; Malyukin, Y. V.; Köhler, J., Optical Spectroscopy on Individual Amphi-Pic J-Aggregates. *Nano Letters* **2005**, *5*, 2635-2640.

140. Didraga, C.; Malyshev, V. A.; Knoester, J., Excitation Energy Transfer between Closely Spaced Multichromophoric Systems: Effects of Band Mixing and Intraband Relaxation. *J. Phys. Chem. B* **2006**, *110*, 18818-18827.

141. Spitz, C.; Daehne, S., Low Temperature Exciton-Exciton Annihilation in Amphi-Pipe J-Aggregates. *Int. J. Photoenergy* **2006**.

142. Knox, R. S., Excitation Energy Transfer and Migration: Theoretical Considerations. In *Bioenergetics of Photosynthesis*, Govindjee, Ed. Academic Press: New York, 1975.

143. Schein, L. B.; McGhie, A. R., Band-Hopping Mobility Transition in Naphthalene and Deuterated Naphthalene. *Physical Review B* **1979**, *20*, 1631-1639.

144. Shuai, Z., Wang, L., Song, C., *Theory of Charge Transport in Carbon Electronic Materials*. Springer: Heidelberg, **2012**.

145. Kopelman, R.; Monberg, E. M.; Ochs, F. W., Exciton Percolation. Ii: Naphthalene 1b2u Supertransfer. *Chemical Physics* **1977**, *21*, 373-383.

146. Silinsh, E. A., *Organic Molecular Crystals: Their Electronic States*. Springer-Verlag: Berlin, 1980.

147. Kenkre, V. M.; Wong, Y. M., Theory of Exciton Migration Experiments with Imperfectly Absorbing End Detectors. *Physical Review B* **1980**, *22*, 5716-5722.

148. Smith, L. M.; Wake, D. R.; Wolfe, J. P.; Levi, D.; Klein, M. V.; Klem, J.; Henderson, T.; Morkoç, H., Picosecond Imaging of Photoexcited Carriers in Quantum Wells: Anomalous Lateral Confinement at High Densities. *Physical Review B* **1988**, *38*, 5788-5791.

149. Müller, A. M.; Bardeen, C. J., Using a Streak Camera to Resolve the Motion of Molecular Excited States with Picosecond Time Resolution and 150 Nm Spatial Resolution. *J. Phys. Chem. C* **2007**, *111*, 12483-12489.

150. Akselrod, G. M.; Deotare, P. B.; Thompson, N. J.; Lee, J.; Tisdale, W. A.; Baldo, M. A.; Menon, V. M.; Bulović, V., Visualization of Exciton Transport in Ordered and Disordered Molecular Solids. *Nat Commun* **2014**, *5*.

151. Ruzicka, B. A.; Wang, R.; Lohrman, J.; Ren, S.; Zhao, H., Exciton Diffusion in Semiconducting Single-Walled Carbon Nanotubes Studied by Transient Absorption Microscopy. *Physical Review B* **2012**, *86*, 205417.

152. Lindrum, M.; Glismann, A.; Moll, J.; Daehne, S., Fluorescence Lifetime Measurements and Hole-Burning Experiments on J-Aggregates of a Benzimidocarbocyanine Dye. *Chemical Physics* **1993**, *178*, 423-432.

153. Balzer, F.; Bordo, V. G.; Simonsen, A. C.; Rubahn, H. G., Optical Waveguiding in Individual Nanometer-Scale Organic Fibers. *Physical Review B* **2003**, *67*, 115408.

154. Chaudhuri, D.; Li, D.; Che, Y.; Shafran, E.; Gerton, J. M.; Zang, L.; Lupton, J. M., Enhancing Long-Range Exciton Guiding in Molecular Nanowires by H-Aggregation Lifetime Engineering. *Nano Letters* **2010**, *11*, 488-492.

155. Takazawa, K.; Kitahama, Y.; Kimura, Y.; Kido, G., Optical Waveguide Self-Assembled from Organic Dye Molecules in Solution. *Nano Letters* **2005**, *5*, 1293-1296.

156. Lebedenko, A. N.; Guralchuk, G. Y.; Sorokin, A. V.; Yefimova, S. L.; Malyukin, Y. V., Pseudoisocyanine J-Aggregate to Optical Waveguiding Crystallite Transition: Microscopic and Microspectroscopic Exploration. *J. Phys. Chem. B* **2006**, *110*, 17772-17775.

157. Eisfeld, A.; Briggs, J. S., The J- and H-Bands of Organic Dye Aggregates. *Chemical Physics* **2006**, *324*, 376-384.

158. Lunt, R. R.; Giebink, N. C.; Belak, A. A.; Benziger, J. B.; Forrest, S. R., Exciton Diffusion Lengths of Organic Semiconductor Thin Films Measured by Spectrally Resolved Photoluminescence Quenching. *J. Appl. Phys.* **2009**, *105*, 053711.

159. Miller, G. K., Probability: Modeling and Applications to Random Processes. John Wiley & Sons, Inc.: Hoboken, New Jersey, 2006; pp 399-401.

160. Haber, H. Diagonalization of a 2 X 2 Real Symmetric Matrix. University of California Santa Cruz Physics 116a Web Page. http://scipp.ucsc.edu/~haber/ph116A/diag2x2_11.pdf (accessed October 15 2013).

161. Augulis, R. Molecular Aggregates, Dendrimers, and Motors: Optical Dynamics and Control. Ph.D. Thesis, University of Groningen, Groningen, Netherlands, 2008.

162. Yoon, H. W.; Wake, D. R.; Wolfe, J. P.; Morkoç, H., In-Plane Transport of Photoexcited Carriers in GaAs Quantum Wells. *Physical Review B* **1992**, *46*, 13461-13470.

Vita

Katie Ann Clark was born in Nacogdoches, Texas to Donald and Patricia Clark. She has two wonderful sisters, Heather and Emily, a brother (-in-law), Shane, and a shih tzu, Jax. She graduated from Woden High School in 2003 as the valedictorian of her class, and attended Stephen F. Austin State University, where she majored in chemistry and minored in mathematics. After graduating magna cum laude from SFASU in 2006, she worked briefly in industry before beginning graduate school at the University of Texas at Austin in 2007, where she worked under the supervision of Professor David Vanden Bout.

Permanent email: katieannclark@gmail.com

This dissertation was typed by the author.